COMPLETE ENGINE CFD OF A MICRO GAS TURBINE BY MODELLING COMBUSTION AS A HEAT SOURCE

by

Johan C. Kotzé

Submitted in partial fulfilment of the requirements for the degree

Master in Engineering (Mechanical and Aeronautical Engineering)

In the

Department of Mechanical and Aeronautical Engineering

Faculty of Engineering, Built Environment and Information Technology

UNIVERSITY OF PRETORIA

Supervisor:

Dr G. Snedden

November 2018

ABSTRACT

The design challenges of micro gas turbines, compared to large gas turbines, lies in the size of the components. Firstly, the small components cannot achieve a high-pressure ratio which cause the mass flow rate to be relatively high for the engine size in order to meet the thrust requirements. This leads to a low combustor residence time and a poor turbine inlet temperature profile. Secondly, the small components make achieving the manufacturing tolerances in the tip gaps difficult which can lead to component mismatches.

Complete gas turbine CFD simulations are used to determine component mismatches as a final step before manufacturing an engine by simulating the full flow path of the fluid through the engine. Due to the size and complexity of a gas turbine, the mesh used to model the geometry in CFD packages is large and, consequently, takes a long time to converge. Because time is money, methods to reduce the simulation time are developed and tested. Lower fidelity models than 3D CFD were not considered as they would not be able to provide the required insight into the fluid solution to, if proven to be accurate, determine component mismatches in future projects.

The objective of this study was to develop a CFD model using Numeca to simulate the full, main gas flow path of a micro gas turbine. The key limitation was that the chemical process of combustion would not be modelled and the simulation had to run on a single i7 computer with 32 GB of RAM. Furthermore, the accuracy of the developed method had to be assessed. This was achieved, firstly, by determining how well the performance parameters of the simulated engine compared to experimental results and, secondly, the accuracy of the temperature distributions in the combustor.

This study modelled combustion as a heat source rather than using complex combustion models built into modern CFD packages which are computationally more expensive. Methods used to simulate gas turbines were found in the open literature, but none of them modelled combustion with a heat source. Two methods for applying the heat source to the combustion domain, namely primary zone heating and global heating were investigated. Primary zone heat addition introduced heat only in the primary combustion zone in the inner combustor annulus. Global heating introduced heat throughout the entire combustor domain from its inlet up to its outlet.

The simulated results compare well with experimental results with most variables being within approximately 5% for the BMT 120 KS engine. The mass flow rate results were underpredicted on average by 21%. This should be investigated by, firstly calibrating the bell mouth inlet, limiting the temperature in the combustor and secondly, increasing the distance between the trailing edge of the deswirler and the interface between the domains of the compressor and the combustor.

The results produced by the primary zone heat source model were closer to the experimental results than those produced by the global heat source model, but the former took more than

six times longer to converge. The temperature contours in the combustor were also more realistic when using primary zone heating since this method predicted the location where the inner liner of the combustor was burnt during the experiments. The location of the heating zone was found to be important because the temperature distributions are sensitive to recirculation zones.

It can be concluded that the simulation methods of this study can be used to perform performance predictions when changes are made to engine components. Identifying component mismatches can also be investigated with these methods when the mass flow deficit has been addressed.

Keywords: Gas turbine CFD, micro gas turbine, combustion, heat source

ACKNOWLEDGEMENTS

First and foremost, I give thanks to God the Almighty, Father, Son and Holy Spirit who gave me the ability, knowledge, research environment and perseverance to complete this study successfully.

I would also like to give thanks to Dr Glen Snedden, Dr Dwain I. Dunn and Radeshen Moodley for their help and guidance in the project and the DPSS division of the CSIR for allowing me to use their computers and software.

A special thanks to Numeca for supplying me with an extended student license to run their software and my brother Gert Kotzé for allowing me to run simulations on his personal server.

Finally, I would like to thank my family and friends for their support during the project.

TABLE OF CONTENTS:

ABSTRACT ---- II

ACKNOWLEDGEMENTS ---- IV

TABLE OF CONTENTS: ---- V

LIST OF FIGURES ---- VII

LIST OF TABLES ---- X

NOMENCLATURE ---- XI

CHAPTER 1 INTRODUCTION ---- 1

1.1 BACKGROUND AND MOTIVATION ---- 1
1.2 PROBLEM IDENTIFICATION ---- 2
1.3 RESEARCH OBJECTIVES AND LIMITATIONS ---- 3
1.4 EXPECTED OUTCOME ---- 4
1.5 RESEARCH SCOPE AND REQUIRED INFORMATION ---- 4
1.6 REQUIRED RESOURCES ---- 5
1.7 LITERATURE STUDY SUMMARY ---- 5

CHAPTER 2 LITERATURE STUDY ---- 7

2.1 MICRO GAS TURBINES ---- 7
2.2 ADVANTAGES AND DISADVANTAGES OF MICRO GAS TURBINES ---- 9
2.3 USES OF MICRO GAS TURBINES ---- 12
2.4 MICRO GAS TURBINES VS IC ENGINES ---- 14
2.5 THE NEED FOR CFD ---- 15
2.6 HISTORICAL WORK IN THIS FIELD ---- 18
2.7 MODELLING COMBUSTION ---- 21
2.8 BOUNDARY CONDITIONS ---- 22
2.9 CONCLUSION ---- 23
2.10 ANALYSIS OF SOURCES ---- 24

CHAPTER 3 METHODOLOGY ---- 25

3.1 GAS TURBINE DESIGN METHODOLOGY ---- 25
3.2 GEOMETRY ---- 26
3.3 MESH ---- 29

3.3.1 RAM limitations ---- *31*
3.3.2 Intake and compressor mesh ---- *31*
3.3.3 Combustor mesh ---- *35*
3.3.4 Turbine mesh ---- *37*
3.3.5 Outlet domain mesh ---- *39*
3.3.6 Combustor mesh interfaces ---- *39*
3.3.7 Mesh summary ---- *42*

3.4 SIMULATION SETUP ---- 43
3.4.1 Fluid properties used in the simulation ---- 43
3.4.2 Turbulence model ---- 47
3.4.3 Modelling combustion ---- 48
3.4.4 Boundary conditions ---- 51
3.4.5 Initialising the solution ---- 54
3.4.6 Numerical discretisation schemes ---- 54
3.4.7 Convergence criterion ---- 55

CHAPTER 4 CFD VALIDATION ---- 57

4.1 SIMULATED RESULTS VS EXPERIMENTAL RESULTS ---- 57
4.1.1 Mass flow deficit: Experimental causes ---- 62
4.1.2 Mass flow deficit: Numerical causes ---- 62
4.2 GLOBAL HEAT VS PRIMARY ZONE HEAT ---- 69
4.3 COMPARING THE COMPRESSOR AND TURBINE POWER ---- 70
4.4 CONSTANT GAS CONSTANT "R" ---- 71
4.5 SUMMARY ---- 72

CHAPTER 5 COMBUSTION HEAT SOURCE ---- 74

5.1 EFFECT ON PHYSICS ---- 74
5.2 METHOD OF HEAT ADDITION ---- 75
5.2.1 CFD results when modelling combustion ---- 76
5.2.2 Global heat addition ---- 77
5.2.3 Primary zone heat addition ---- 81
5.3 SUMMARY ---- 85

CHAPTER 6 DISCUSSION OF THE ENGINE PERFORMANCE AND FLUID FLOW 87

6.1 IDENTIFYING COMPONENT MISMATCHES ---- 87
6.2 COMPRESSOR FLOW ---- 88
6.3 TURBINE FLOW ---- 100
6.4 NOZZLE FLOW ---- 106
6.5 SUMMARY ---- 110

CHAPTER 7 CONCLUSION ---- 112

CHAPTER 8 RECOMMENDATIONS ---- 114

REFERENCES ---- 117

APPENDIX A FLUID PROPERTY GRAPHS ---- 122

LIST OF FIGURES

Figure 1-1: Micro gas turbines available on the market (red crosses indicate local turbines). 1
Figure 1-2: Gas turbine layout (Banerjee, 2018). 4
Figure 2-1: Micro gas turbine used for power generation (“Jet Engine Diagram”, n.d.). 8
Figure 2-2: Micro-turbine used as a jet engine (“Mini Gas Turbine Lab | Educational Gas Turbine Jet Engine”, n.d.).....9
Figure 2-3: Comparison between micro gas turbines' and commercial aircraft turbines' thrust to weight ratios (“AMT Netherlands”, n.d.; “PBS - Aircraft Engines”, n.d.). 10
Figure 2-4: Comparing electric efficiencies of different power generation methods (KRUGER et al., 2003). 11
Figure 2-5: Comparison between the electrical efficiencies of gas turbines and IC engines (Grosshauser, 2016).....11
Figure 2-6: Micro gas turbines used as jet engines (“PBS - Aircraft Engines”, n.d.).....13
Figure 2-7: Powered human flight (“Micro jet turbine-powered Jet Vest developers seek a Kickstart”, n.d.; “Science in a can, Yves Rossy: A Modern-Day Daedalus Ovid’s legendary...”, n.d.). 13
Figure 2-8: Power generating micro gas turbine range (“Capstone Turbine Corporation (CPST)”, n.d.). 14
Figure 2-9: Mesh independence study using inlet pressure.....17
Figure 2-10: Combustor terminology (Lefebvre & Ballal, 2010).....22
Figure 3-1: Final BMT 120 KS CAD model. 26
Figure 3-2: Sectioned view of the simplified BMT 120 KS. 27
Figure 3-3: BMT 120 KS Compressor that was simulated.....28
Figure 3-4: BMT 120 KS turbine that was simulated. 28
Figure 3-5: BMT 120 KS combustor. 29
Figure 3-6: BMT 120 KS simulation domain.....30
Figure 3-7: Compressor streamwise flow paths. 32
Figure 3-8: Impeller blade-to-blade view at 50% blade height. 33
Figure 3-9: Wedge diffuser and deswirler blade-to-blade view at 50% blade height.....33
Figure 3-10: 3D impeller blade mesh.....34
Figure 3-11: 3D wedge diffuser and deswirler blade mesh.....34
Figure 3-12: Combustor mesh along the axis. 35
Figure 3-13: Combustor internal mesh element slice and zoomed in section. 36
Figure 3-14: Turbine streamwise flow paths. 37
Figure 3-15: Turbine blade-to-blade view at 50% blade height. 38
Figure 3-16: 3D turbine blade mesh. 38
Figure 3-17: Outlet domain mesh.....39
Figure 3-18: Compressor-combustor mesh interface.....40
Figure 3-20: Turbine rotor-outlet mesh interface. 41
Figure 3-19: Turbine-combustor mesh interface.....41
Figure 3-21: Fluid properties of air. 44

Figure 3-22: Fluid properties of burnt air. 45
Figure 3-23: Pressure and temperature effects on Prandtl number (ÇENGEL & GHAJAR, 2015; "Engineering Toolbox. Air - Prandtl Number", 2018). 46
Figure 3-24: Combustion chamber's fuel delivery components. 49
Figure 3-25: Primary zone heat addition zone. 50
Figure 3-26: Full Mach number plot for different boundary conditions on the outlet domain. 53
Figure 3-27: Limited Mach number plot for different boundary conditions on the outlet domain. 53
Figure 4-1: EGT comparison between simulated and experimental results. 58
Figure 4-2: Air mass flow rate comparison between simulated and experimental results. ...59
Figure 4-3: Total-to-static pressure ratio comparison between simulated and experimental results. 59
Figure 4-4: Thrust comparison between simulated and experimental results. 61
Figure 4-5: Combustor 2500 K iso-surface comparison. 63
Figure 4-6: Comparison between the burnt air material model and experimentally recorded air properties. 64
Figure 4-7: Centrifugal compressor map (Korpela, 2011). 65
Figure 4-8: 2500 K iso-surface for primary zone heating at 80 kRPM. 66
Figure 4-9: Static pressure on compressor outlet and combustor inlet comparison. 67
Figure 4-10: Static pressure in combustor at its inlet. 68
Figure 4-11: The effect of the heat source magnitude on the mass flow rate. 69
Figure 4-12: BMT 120 KS compressor map with simulation and experimental results plotted (Krige, 2013). 70
Figure 5-1: Temperature distribution obtained by modelling combustion (Trebunskikh et al., n.d.; Gonzalez et al., 2007). 76
Figure 5-2: Combustor outlet temperature profile when modelling the combustion process (Gonzalez et al., 2007). 77
Figure 5-3: Global heat: Combustor temperature distribution contours at 120 kRPM. 77
Figure 5-4: Global heat: Recirculating flow along the tangential direction in the combustor. 78
Figure 5-5: Global heat: Temperature distribution in the combustor with recirculation zones identified. 79
Figure 5-6: Primary zone heat: Combustor temperature distribution contours for 120 kRPM. 82
Figure 5-7: Primary zone heat: Extent of the hot zone and streamlines from the secondary and dilution holes. 83
Figure 5-8: Primary zone heat: Hot zone influence on the combustor outlet temperature profile. 84
Figure 5-9: Recirculation zone caused by the flow leaving the vaporiser tube. 85
Figure 0-1: Specific heat plotted against temperature for air. 122
Figure 0-2: Thermal conductivity plotted against temperature for air. 122

Figure 0-3: Dynamic viscosity plotted against temperature for air.....123

LIST OF TABLES

Table 2-1: Micro gas turbine vs. IC engine. 14
Table 3-1: Cells per mesh block. 42
Table 3-2: Y+ considerations for the turbulence model. 48
Table 3-3: Comparing simulation results for outlet domain. 52
Table 4-1: Uncertainty in the experimental results (Krige, 2013). 57
Table 4-2: Impeller and turbine torque comparison. 71
Table 4-3: Gas constant comparison values. 72
Table 5-1: Areas of the inner and outer combustor liner. 81
Table 6-1: Impeller streamlines coloured by velocity in $m.s^{-1}$. 89
Table 6-2: Wedge diffuser streamlines coloured by velocity in $m.s^{-1}$. 91
Table 6-3: Deswirler streamlines coloured by velocity in $m.s^{-1}$. 92
Table 6-4: Compressor pitch average streamlines coloured by velocity in $m.s^{-1}$. 95
Table 6-5: Impeller Mach number iso-surface of M=1. 96
Table 6-6: Impeller and wedge diffuser Mach number iso-surface of M=1. 97
Table 6-7: Wedge diffuser and deswirler Mach number iso-surface of M=1. 99
Table 6-8: NGV streamlines coloured by velocity in $m.s^{-1}$. 101
Table 6-9: Rotor streamlines coloured by velocity in $m.s^{-1}$. 102
Table 6-10: Turbine Mach number iso-surface of M=1. 104
Table 6-11: Nozzle streamlines coloured by velocity in $m.s^{-1}$ 107
Table 6-12: Flow swirl angle in degrees leaving the turbine and entering the nozzle. 108
Table 6-13: Nozzle centre Mach number contour. 109
Table 6-14: TIT for the different heat addition methods at 80, 120 and 140 kRPM 110

NOMENCLATURE

Acronyms and Abbreviations:

AM	Additive Manufacturing
CC	Complex Cycle
CFD	Computational Fluid Dynamics
CFL	Courant-Friedrichs-Lewy
CSIR	Council for Scientific and Industrial Research
DPSS	Defence, Peace, Safety and Security
EGT	Exhaust Gas Temperature
FEA	Finite Element Analysis
GCI	Grid Convergence Index
HD	Heavy Duty
IC	Internal Combustion
LES	Large-Eddy Simulation
LNS	Limited-Numerical Scales
NC	Numerical Controlled
NGV	Nozzle Guide Vane
RAM	Random Access Memory
RANS	Reynolds-Averaged Navier-Stokes
RPM	Revolutions per minute
SC	Simple Cycle
TRL	Technology Readiness Level
TIT	Turbine Inlet Temperature
UAV	Unmanned Aerial Vehicle

Symbols:

γ	Specific heat ratio
τ	Torque [N.m]
ω	Rotational velocity [rad/s]
A	Area [m^2]
C_P	Specific heat at constant pressure [J/kg.K]
c	Speed of sound in fluid [m/s]
F_S	Constant for GCI.
f	User defined variable extracted from CFD solution.
HV	Heating value [J/kg]
M	Mach number
$\dot{m}$	Mass flow rate [kg/s]
P	Pressure [Pa]
	Power [W]
p	Used for substitution
$\dot{Q}$	Heat transfer rate (source or sink) [W]
R	Gas constant [J/kg.K]
r	Mesh refinement factor
T	Temperature [K]
V	Flow velocity magnitude [m/s]
$\dot{W}$	Work [W]

Subscripts:

1	Fine mesh.
2	Medium mesh.
3	Coarse mesh.
in	Into a region.
out	Out of a region.

CHAPTER 1 INTRODUCTION

This chapter introduces the Master Study: Full Engine Computational Fluid Dynamics (CFD) of a Micro Gas Turbine by Modelling Combustion as a Heat Source by providing background information and motivation for the study. Following this, the study will be described by defining the problem statement, research objectives and the expected outcomes thereof. The introduction will be concluded with a summary of the literature study.

1.1 BACKGROUND AND MOTIVATION

A key area in the South African aeronautical industry identified as being deficient is that of propulsion systems. The lack of having local research and development of propulsion systems, specifically gas turbines, means that these has to be acquired from international suppliers. Due to this, it was possible for the international community to control the sales of, amongst others, the Denel Dynamics weapons systems by controlling the number or type of propulsion systems supplied to Denel Dynamics.

The South African defence industry noted that, in the medium term future, they will need a micro gas turbine capable of powering their glider bomb. This gas turbine would have to fit within the tailpipe of the weapon and has to produce 600N thrust together with 600W electrical power for the on-board electronics, according to an internal report written by Snedden (2018) to the DTI. It will then also fill a gap identified by the South African Department of Trade and Industry in the gas turbine market as indicated by the green lines in Figure 1-1. Additionally, this gas turbine could also be used for powering weapons, UAV's, target drones and may even have the capability to power glider sustainers. The possibility exists that this gas turbine could also be used for power generation in remote areas, using biomass fuels.

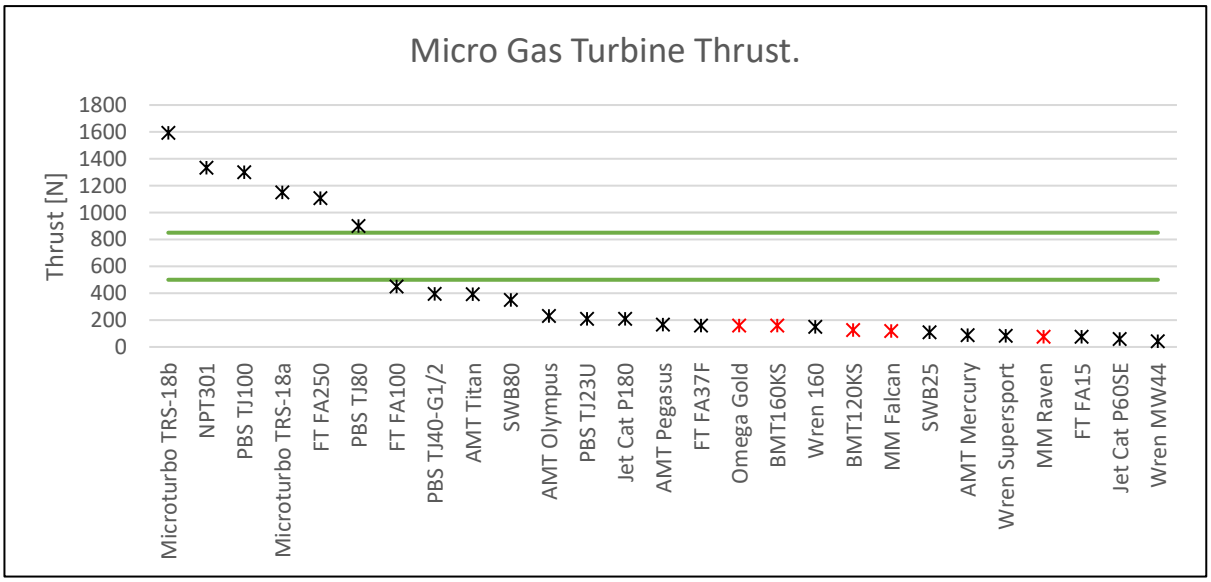

Figure 1-1: Micro gas turbines available on the market (red crosses indicate local turbines).

The information above shows a clear market and strategic need for the South African aeronautical industry to introduce a propulsion sector which would develop a single product with the capability to fulfil the need in multiple markets.

During the design of micro gas turbines, the compressor and turbine are simulated as components. The main aim of these simulations is to improve the geometry of the micro gas turbine components in order to improve its performance. Doing only individual component simulations led to system-level issues when matching the compressor, combustor and turbine. These matching issues have been plaguing the design of micro gas turbines ever since its development commenced.

The move to do full engine CFD analyses was driven by the mentioned component mismatches. It is speculated that the mismatches are caused by the fact that simulating each component individually did not account for the interaction between the different engine components. Doing an advanced CFD analysis on each subcomponent in the engine allows for component optimisation and will give the performance maps of each component. These maps contain the possible operating conditions of each individual component. The maps do, however, not account for the interactions between the different components in the engine and can therefore have an adverse effect on the overall engine performance. The only way to be able to capture these interactions will be to do a full engine CFD analysis on the assembled micro gas turbine.

Full engine CFD is seen as the last stage in the design before manufacturing the engine because these simulations are time-consuming due to the large simulation domain and instability issues. It is thus more efficient to design the individual components using advanced CFD analysis and when these results are satisfactory, the full engine CFD analysis can be conducted (Reed et al., 2003). This may then identify any component mismatches and allow the designer to resolve the issues before manufacturing and testing commence to reduce the development cost (Slagter, 2011; Ando, 2014; Paquin, 2015).

When comparing the differences between the technology readiness levels (TRL) of a micro gas turbine and those of larger gas turbines, it is clear that the former has a lower TRL than its larger counterpart. This is because micro gas turbines have not been in the development process for as long as large gas turbines. To mature the TRL of micro gas turbines, complete CFD simulations of micro gas turbines can be performed with relative ease as these engines are of small and simple design and therefore do not require as many computational resources as large gas turbines would and can run on a single i7 computer with 32 GB of RAM.

1.2 PROBLEM IDENTIFICATION

The problem that had to be addressed, was the long simulation times when investigating component mismatches in a micro gas turbine because the complete engine must be simulated, consequently leading to a large mesh and a high number of equations that have to be solved. Mismatches are caused by simulating components in isolation, resulting in some

components being incompatible and the micro gas turbine failing to meet the design criterion. These component mismatches have, until now, complicated micro gas turbine designs. Typically, either the turbine stator or the jet pipe nozzle of the engine is designed to choke at design flow. However, if the components are not matched correctly, any of the other three main aerodynamic components of the engine, i.e. the compressor, diffuser, or turbine rotor, may choke, severely limiting the performance of the overall engine.

To reduce the simulation time, it was proposed to model the combustion process with a heat source which eliminates the added combustion equations. Therefore, the research question that has to be answered is whether it is possible to accurately simulate the micro gas turbine as an assembly when modelling the combustion process as a heat source.

1.3 RESEARCH OBJECTIVES AND LIMITATIONS

The aim of the research is to determine if it is possible to accurately simulate an assembled micro gas turbine with a heat source. This study requires research into the following:

1. Can suitable boundary conditions be applied to the assembled micro gas turbine so that a full engine CFD is possible?
    a. Assess the accuracy of these boundary conditions by comparing the performance parameters of the simulated engine with experimental results.
    b. Assess the validity of the simulated engine by comparing the power produced by the turbine with the power consumed by the compressor to ensure the power in the engine was balanced.
2. Develop a simplified method to simulate the combustion process in the combustor of the micro gas turbine.
    a. Evaluate the accuracy of and identify the differences in the temperature distribution in the combustor by comparing the results of this study with simulations where the chemical aspects of combustion were modelled.

The limitations of this study as well as their impact on the study are as follows:

1. The chemical process of combustion was not modelled.
2. The simulation had to run on a single computer with an i7 processor and 32 GB of RAM which resulted in the following:
    a. Simplifications in the micro gas turbine geometry.
    b. Using periodic boundary conditions rather than simulating entire components. This also required the use of appropriate non-matching boundary conditions to connect the periodic mesh blocks of the components.
    c. No mesh independence study was done due to the mesh size being limited.
3. Fluid-structure interactions and solid mechanics were not modelled.
    a. This had a negligible effect on the results.

1.4 EXPECTED OUTCOME

The expected outcome of the project will be a method for simulating an assembled micro gas turbine. This assembly will include the diffuser and nozzle before and aft the compressor and turbine, respectively. The simulation method will state the boundary conditions that will be used and how to model the combustor so that it mimics the combustion process without modelling the chemical reactions inside the combustor. Figure 1-2 shows the general configuration of a bypass gas turbine (Banerjee, 2018).

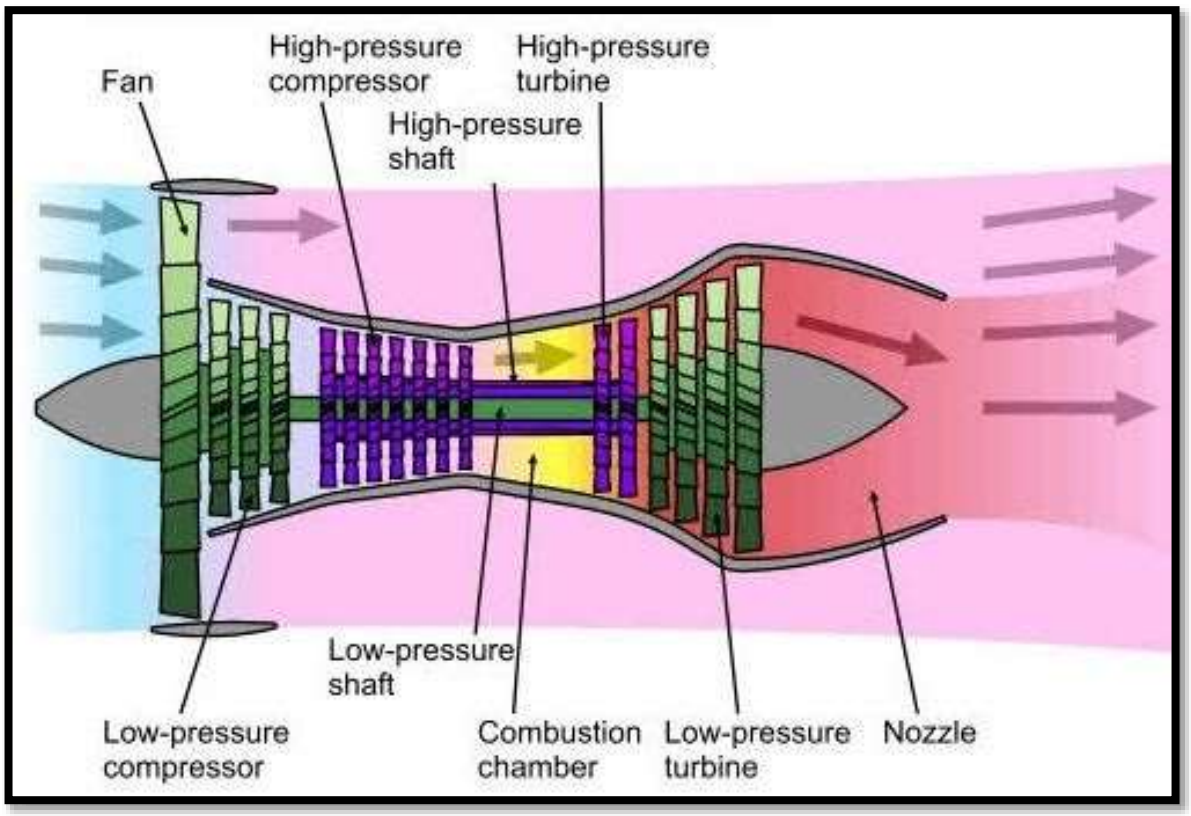

Figure 1-2: Gas turbine layout (Banerjee, 2018).

1.5 RESEARCH SCOPE AND REQUIRED INFORMATION

This section discusses the limitations of the research project and what information is required to complete the project successfully. It was decided that this research project will use the BMT 120 KS micro gas turbine as its base for conducting simulations. The turbine was developed by Baird Micro Turbines for model aircraft applications. This engine was selected to be simulated because of the following:

- It was a working engine without component mismatches.
- The geometry of the engine was available.
- Experimental results were available for the engine (Krige, 2013).

The following is required for the research project:

1. An assembled model of the micro gas turbine.
2. The operating conditions under which the micro gas turbine will have to be simulated.
3. The micro gas turbine thermodynamic cycle information for the specified flight condition.

The following is not expected from the student:

1. Designing the micro gas turbine.
2. Component optimisation.
3. Verification, because only 1 simulation package is available.

1.6 REQUIRED RESOURCES

This section indicates the resources required to successfully complete the project. These resources are:

1. Access to CFD software, NUMECA Fine/Open^{TM}.
2. Suitable computers for performing the CFD analysis.

1.7 LITERATURE STUDY SUMMARY

Micro gas turbines are essentially small gas turbines. These turbines can be either the traditional gas turbines used for power generation or they can be used as jet engines, depending on what they were designed for. Because this research project is about jet engines, this was the main focus of the research with regards to CFD.

From the literature study, it is evident that micro gas turbines will be used more and more in the future for powering missiles, Unmanned Aerial Vehicles (UAV's), experimental vehicles like jetpacks, etc. Micro gas turbines can also be used for power generation where it replaces the conventional diesel-powered generators as they are capable of powering small establishments and large office complexes. In recent times, the fuel to electricity efficiency gap between micro gas turbines and Internal Combustion (IC) engines was reduced by using higher turbine inlet temperatures made possible by the use of ceramic components, resulting in micro gas turbines being more desirable than IC engines. Additionally, the manufacturing of micro gas turbines has an added advantage of providing a platform to develop Additive Manufacturing (AM) techniques that can be applied when manufacturing commercial gas turbines.

Using CFD during the design phase of a micro gas turbine will reduce the development cost and time (Slagter, 2011; Ando, 2014; Paquin, 2015). This is because CFD is used to perform what-if-analysis that will help to eliminate several experimental cycles. It should also be

noted that when using CFD, the solution given is an approximate solution and not the actual solution. This is because simplifying assumptions are being made in the equations describing the physics of the problem. Care should also be taken with the boundary conditions and the mesh used for the simulations as this will affect the accuracy of the solution.

To conclude the introduction, it should be noted that there are three tried and tested methods for simulating a gas turbine (Trebunskikh et al., n.d.; Reed et al., 2003; Turner et al., 2004; Schlüter et al., 2005). These three methods are closely aligned with the objectives of this project but with several differences which make this project unique. The main reason why this project can be seen as being unique is that the combustion process will not be simulated. The claim is strengthened by finding no previous work in the literature describing how to simulate combustion without taking the chemical reactions into account.

CHAPTER 2 LITERATURE STUDY

This chapter contains information from the literature regarding gas turbines. The information in the following sections is required to be able to fully understand the extent of the project and also to learn from existing studies in the field of full engine Computational Fluid Dynamics (CFD). This research will then form the basis of the project regarding the implementation of full engine CFD. Because the research topic relates specifically to micro gas turbines, more research had to be conducted to get a thorough understanding of what is implied by a micro gas turbine.

2.1 MICRO GAS TURBINES

A micro gas turbine has the same components as a gas turbine, but it is smaller. Micro gas turbines generally consist of a compressor, combustor and a turbine("Microturbine - definition of Microturbine by The Free Dictionary", n.d.). Additionally, when the micro gas turbine is used to generate electrical power, it has an alternator (electrical generator) or when it is used as a jet engine, it has a diffuser and a nozzle. Micro gas turbines can use a variety of fuels such as natural gas, hydrogen, propane and diesel.

Generally, gas turbines are able to produce between 4 MW and 450 MW, but micro gas turbines will only be able to generate between 20 kW and 500 kW. This clearly demonstrates the difference in size when referring to a micro gas turbine. Micro gas turbines usually rotate at speeds of 40'000 RPM to 120'000 RPM ("Gas turbines - Power Generation - Siemens Global Website", n.d.; "Microturbines - What is a Microturbine?", n.d.; "Microturbines | WBDG Whole Building Design Guide", n.d.).

Micro gas turbines used as a jet engine should be as light as possible. The heavier the engine, the more lift must be generated by the wings of the air vehicle for steady flight, which increases the lift-induced drag. Increasing the drag will then require more power from the engine for steady flight, reducing the flight range of the air vehicle because of higher fuel consumption rates. This means that micro gas turbines used as jet engines will have a Simple Cycle (SC) i.e. it will not have any additional features to increase its efficiency as this will add weight and reduce the flight range.

Micro gas turbines used for power generation have no limitations set on their weight and their main concern is efficiency. This has led to several components being added to the turbine to increase its efficiency leading to it having a Complex Cycle (CC). A micro gas turbine without any features to improve its efficiency will generally have a fuel to electrical energy efficiency of around 15%. To increase the efficiency of the micro gas turbine, hot exhaust gasses from the turbine outlet can be used to heat cold air from the compressor before combustion. This is called recuperation which will increase the efficiency to between 20 and 30% by reducing the fuel consumption. To achieve the greatest thermal electrical efficiency,

heat recovery should be used in conjunction with recuperation. Heat recovery involves heating water with hot exhaust gasses from the micro gas turbine outlet. The water heated to between 50^0C and 80^0C can be used for several applications, including heating houses, warm water supply for houses or for industrial processes ("Microturbines - What is a Microturbine?", n.d.; "Microturbines | WBDG Whole Building Design Guide", n.d.; Vick et al., 2016).

Additional methods that are used to increase the power output of power generating gas turbines include intercooling and reheating the air. These methods require the gas turbine to have two compressors when using intercooling and two turbines when using reheating. Intercooling refers to cooling the air between the two compressors so that less work is required for compression, thus increasing the power output. Reheating occurs when the air is combusted a second time between the two turbines to extract more power from the gas, thus increasing the power output. The idea behind both methods is to reduce the average compression temperature and increase the average turbine temperature, both increasing the nett power output. These methods do however require a lot of space and will generally not be used on micro gas turbines.

A new method for increasing the efficiency of a micro gas turbine is to use ceramic components. These components are capable of handling higher turbine inlet temperatures which would increase the efficiency of a micro gas turbine. The ceramic components will mainly be the turbine rotor and stator as well as the recuperator. The efficiency that a 12 kW recuperated ceramic micro gas turbine can achieve is predicted to be 21% (Vick et al., 2016).

Figure 2-1 shows a typical micro gas turbine used for power generation.

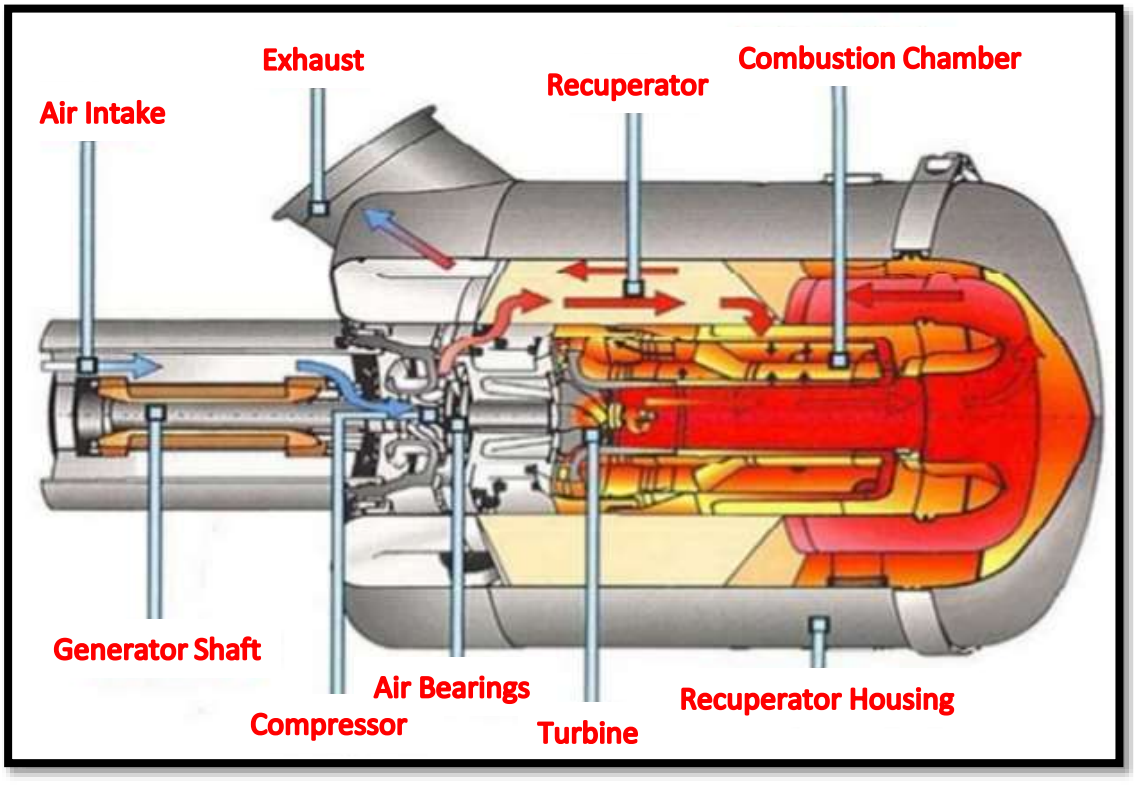

Figure 2-1: Micro gas turbine used for power generation ("Jet Engine Diagram", n.d.).

Figure 2-2 shows a typical micro gas turbine used as a jet engine.

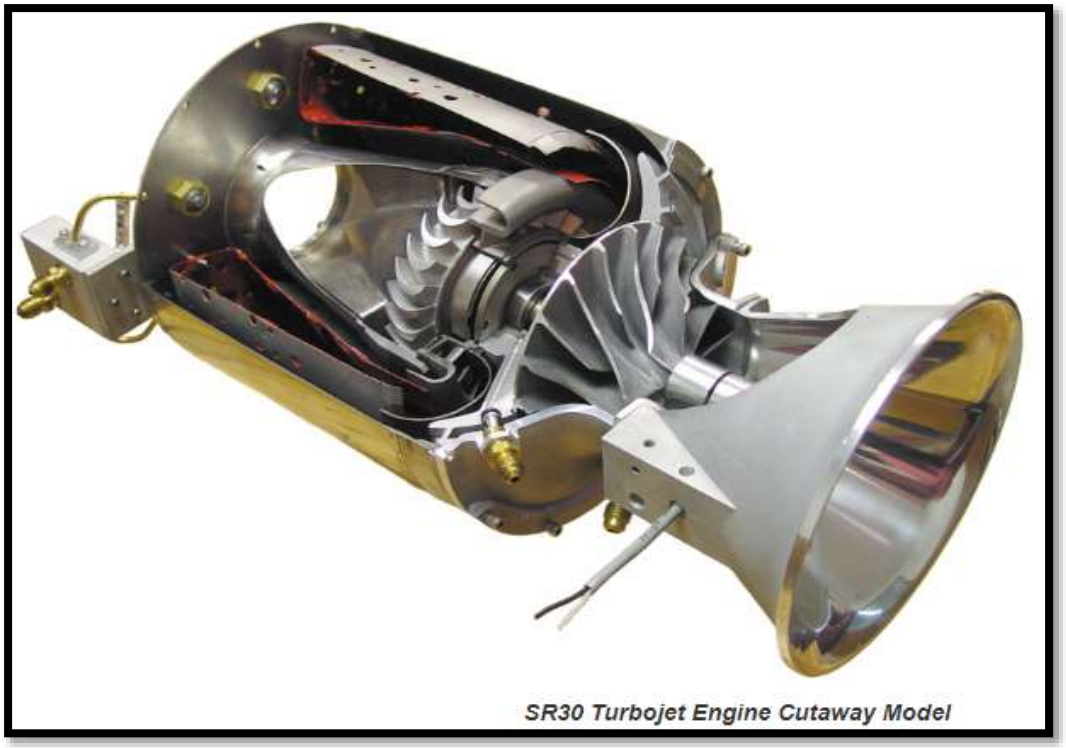

Figure 2-2: Micro-turbine used as a jet engine ("Mini Gas Turbine Lab | Educational Gas Turbine Jet Engine", n.d.).

2.2 ADVANTAGES AND DISADVANTAGES OF MICRO GAS TURBINES

The advantages and disadvantages will be discussed for micro gas turbines used for jet propulsion and for power generation, respectively.

The advantages of micro gas turbines used as jet engines are as follows.

- Compact design.
- Excellent thrust to weight ratios. Figure 2-3 compares the thrust to weight ratios of micro gas turbines with that of commercial aircraft turbines.
- Low fuel consumption.
- Fuel is used as lubrication which enables the micro gas turbine to operate maintenance free.

For small-scale power generation, micro gas turbines have several advantages over other technologies such as wind turbines and petrol or diesel mobile generators. These advantages include:

- A small number of moving parts.
- Longer maintenance intervals.
- Lightweight.
- Compact in size allowing them to be installed on sites where space is limited.

- Capable of delivering power at a high efficiency when using co-generation which then reduces the cost of electricity.
- Environmentally friendly with lower emissions (<9 – 50ppm NOx), compared to other non-renewable power generation methods.
- Exhaust gasses can be used for applications such as heating.

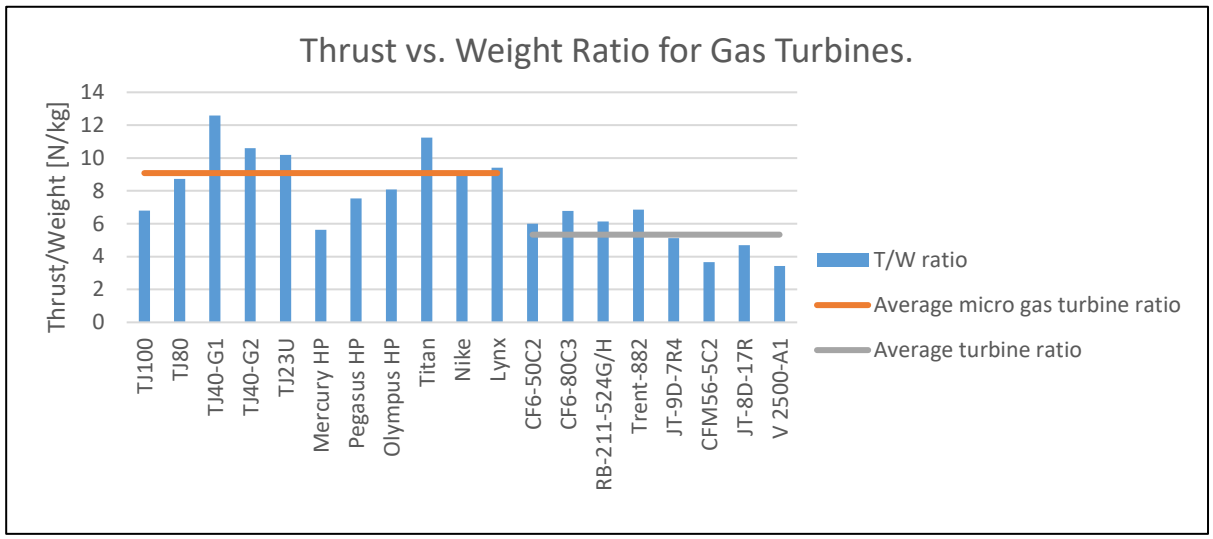

Figure 2-3: Comparison between micro gas turbines' and commercial aircraft turbines' thrust to weight ratios ("AMT Netherlands", n.d.; "PBS - Aircraft Engines", n.d.).

Manufacturing micro gas turbines create the possibility to experiment with Additive Manufacturing (AM) in order to develop new techniques to manufacture commercial gas turbines ("Additive manufacturing revolution for gas turbines", 2016). Experimenting with a commercial jet engine is expensive compared to experimenting with micro gas turbines. The manufacturing methods applied to micro gas turbines can mostly just be scaled up to commercial gas turbines.

The major disadvantage of micro gas turbines is their low fuel to electrical energy efficiency of up to 21% for a 12 kW recuperated ceramic micro gas turbine (Vick et al., 2016). This is not the efficiency when using heat recovery. This low efficiency means that a large amount of fuel is used to generate a small amount of electrical energy. Figure 2-4 contains the expected electrical efficiency ranges of several power generation methods, including that of the micro gas turbine (in blue).

Studying Figure 2-4, using a diesel Internal Combustion (IC) engine will give a much better efficiency when compared to a simple recuperated cycle micro gas turbine. It should, however, be noted that the efficiencies depend on the amount of power output of the power generation methods. Figure 2-5 compares the electrical efficiency of IC engines and gas turbines used for power generation at different power output ratings.

Note that CC, SC and HD in Figure 2-5 refer to Complex Cycle, Simple Cycle and Heavy Duty, respectively. Studying Figure 2-5, IC engines and gas turbines both function optimally in specific ranges. IC engines have a better efficiency at low power outputs of between 15 MW and 70 MW after which the gas turbines have a better efficiency. It is also clear from Figure

2-5 that, for power generation purposes, gas turbines will only be competitive with IC engines when they are used in a complex cycle configuration. This is because gas turbines used in a simple cycle configuration have significantly lower efficiencies than IC engines. The difference between the simple cycle configuration and the complex cycle configuration is that the latter has features like recuperation and heat recovery. As mentioned in Section 2.1, recuperation increases the efficiency of the cycle.

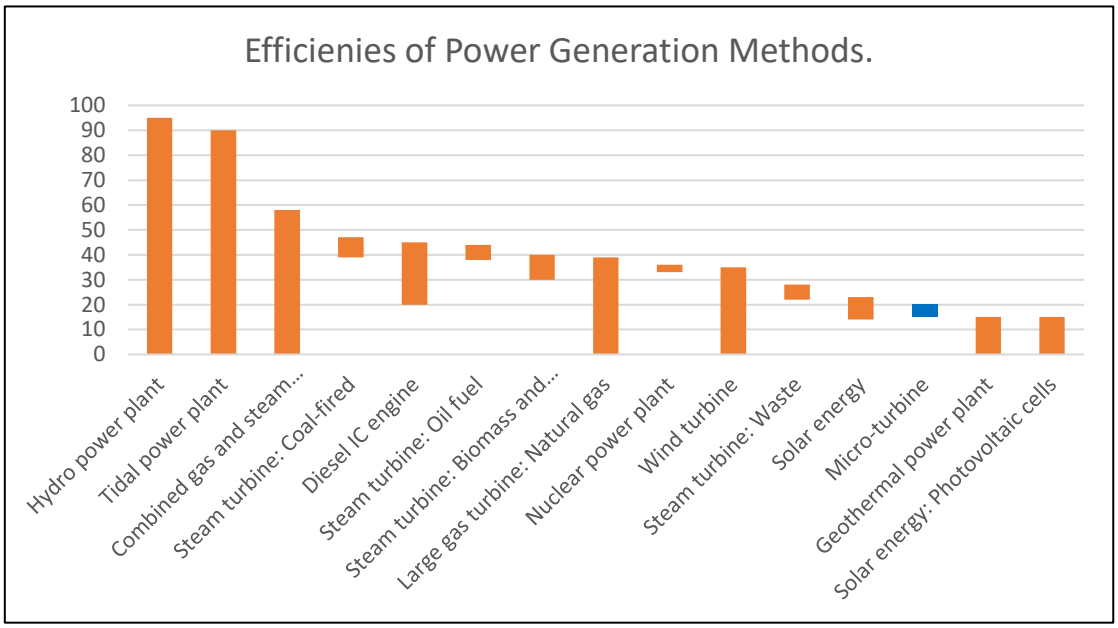

Figure 2-4: Comparing electric efficiencies of different power generation methods (KRUGER et al., 2003).

Taking Figure 2-5 and the fact that ceramic gas turbines are being developed into account, micro gas turbines can possibly surpass IC engines with regard to efficiencies at low power outputs in the future. This makes using micro gas turbines as power generators attractive.

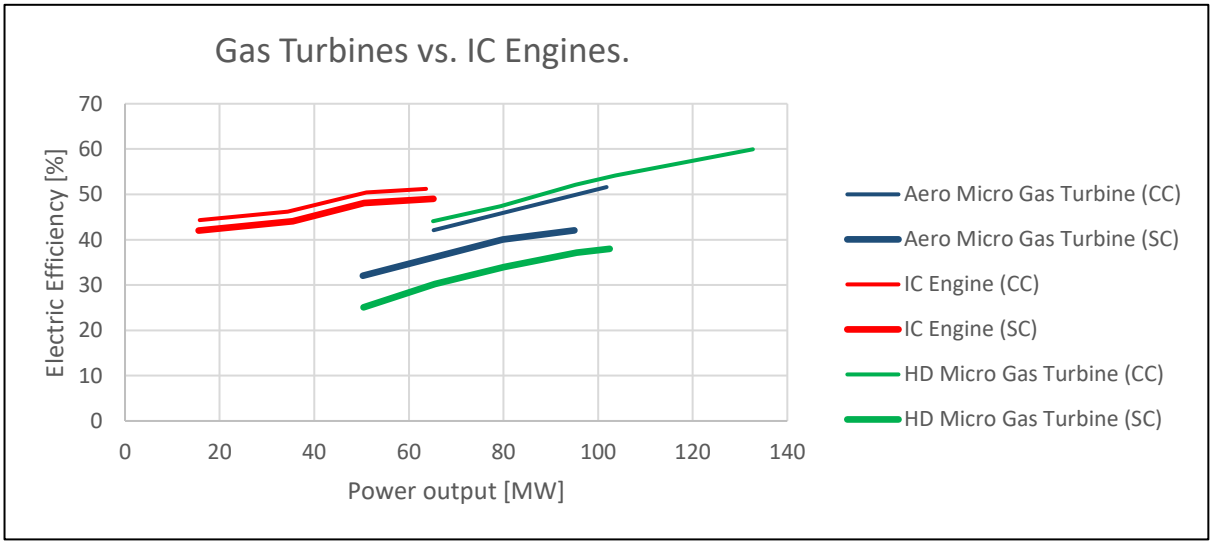

Figure 2-5: Comparison between the electrical efficiencies of gas turbines and IC engines (Grosshauser, 2016).

A disadvantage of the micro gas turbine, independent of its use, is its sensitivity to inlet conditions. As the inlet temperature of a micro gas turbine rises, the density of the inlet air decreases. This decrease in the density prevents the compressor from delivering its design pressure ratio, resulting in a reduced mass flow rate. The reduced mass flow rate lowers the power output of the turbine and, consequently, also the power input to the compressor and the generator (Grosshauser, 2016). If the micro gas turbine is operated at higher elevations, the power output will decrease due to the reduced air density. It should, however, be noted that as the altitude increases, the temperature will decrease. A reduction in temperature will increase the density of the air, thus partially counteracting the reduction in power. A secondary factor that plays a role in both cases where the density is reduced, is the reduction of oxygen present in the combustion chamber.

IC engines are also affected by the inlet pressure and temperature. With an increased inlet temperature and altitude, air density is reduced. This reduced air density results in a smaller mass of oxygen present in the combustion chamber, consequently lowering the power output of the engine.

Another disadvantage of gas turbines is that their combustion chamber does not scale linearly with the size of the engine due to the minimum required residence time of the fuel and air in the combustor. This presents a key challenge for designers regarding the sizing of the combustor since the residence time of fuel should be such that it has enough time to evaporate, mix with air and burn before leaving the combustor. The design is further complicated by the residence time of air in the combustor after burning such that a good turbine inlet temperature profile can be achieved by allowing the burnt air to mix. All of these aspects have an effect on the efficiency of the combustor and directly links to the length of the combustor. In summary, the combustor needs to be long to increase its efficiency and short to be able to fit onto its intended flight structure.

2.3 USES OF MICRO GAS TURBINES

Micro gas turbines are used in several different applications. This section investigates where micro gas turbines are used currently and historically to discover what the future holds for these turbines.

Micro gas turbines are used for several thrust generating applications. These applications are dependent on the thrust produced by the micro gas turbine. The thrust ranges, as well as the application thereof, are listed below:

1. Large micro gas turbines (±1300N thrust) can be used for light and ultralight sports planes, gliders which has an auxiliary engine, some experimental vehicles such as jetpacks and large UAVs.
2. Midsized (900N) micro gas turbines can be used as the propulsion system in missiles, UAVs and targeting drones.

3. Medium to Small micro gas turbines (400N) are generally used for UAVs but can also be used to power lightweight gliders and model aircraft.
4. Small micro gas turbines produce a maximum thrust of 210N at take-off. These micro gas turbines can be used for UAVs and model aircraft ("AMT Netherlands", n.d.; "PBS - TJ80 Turbojet Engine", n.d.).

Figure 2-6 shows the 210N, 395N and 1300N engines produced by PBS Velka Bites.

Figure 2-6: Micro gas turbines used as jet engines ("PBS - Aircraft Engines", n.d.).

In the previous paragraph, it was mentioned that micro gas turbines can be used for experimental vehicles. These experimental vehicles also attempt to achieve powered human flight, as indicated in Figure 2-7.

Figure 2-7: Powered human flight ("Micro jet turbine-powered Jet Vest developers seek a Kickstart", n.d.; "Science in a can, Yves Rossy: A Modern-Day Daedalus Ovid's legendary...", n.d.).

Micro gas turbines can be used for a wide range of power generating applications. These tasks include supplying electrical power to secluded towns, restaurants, office parks and hotels, just to name a few. Other than this, micro gas turbines are being developed to be used on hybrid cars and buses as a source of electrical energy ("The use of Micro turbine

generators in hybrid electric vehicles", 2000; "Jaguar C-X75 Concept", 2010; "Microturbines | WBDG Whole Building Design Guide", n.d.). Figure 2-8 shows the micro gas turbine power generating range of Capstone Turbine Corp.

Figure 2-8: Power generating micro gas turbine range ("Capstone Turbine Corporation (CPST)", n.d.).

2.4 MICRO GAS TURBINES VS IC ENGINES

This section is devoted to comparing micro gas turbines to IC engines for use as propulsion systems. These two technologies are in direct competition in the market for powering flight vehicles and for power generation. Table 2-1 shows a comparison between the micro gas turbine and the IC engine ("Uninhabited Air Vehicles: Enabling Science for Advanced Military Systems", 2000; "UAV Reliability Study", 2003; "AMT Netherlands", n.d.; "PBS - Aircraft Engines", n.d.; Griffis et al., 2009; Marcellan, 2015; Grosshauser, 2016; Vick et al., 2016).

Table 2-1: Micro gas turbine vs. IC engine.

Parameter	Micro Gas Turbine	IC engine
Fuel to electrical efficiency	21% (Ceramic)	34% (Diesel) 27% (Gasoline piston and Wankel engines)
Power/Weight [kW/kg]	Superior	Lacks performance
Maintenance	Little to no maintenance	More than micro gas turbines
Total cost of ownership	Lower	Higher
Engine life	3500 hours	250-1000 hours
Vibration	Low to none	High
Noise	Low	High
Reliability	High	Low
Fuel	Multi-fuel support	One fuel type per engine
Affected by operating conditions	Reduced performance at increased temperature and reduced pressure at inlet	Requires retuning for weather changes

From Table 2-1, micro gas turbines provide a better solution than IC engines for propulsion systems. In 2013, more IC engines (26.5%) than micro gas turbines (8.6%) were used for UAV propulsion when comparing the different propulsion systems used on UAVs. It should be noted that the propulsion systems on 34.4% of UAVs were not known (Marcellan, 2015). A similar conclusion was reached in the Master of Science Thesis: "An exploration into the potential of microturbine based propulsion systems for civil Unmanned Aerial Vehicles" by Anna Marcellan.

2.5 THE NEED FOR CFD

This section discusses the advantages and possible disadvantages of using CFD. Results obtained from this study will not only be applicable to CFD, but also to Finite Element Analysis (FEA).

Traditionally, when designing a micro gas turbine, most of the design iterations will be conducted by manufacturing and testing the prototype. During each of the design and test iterations, the prototype will improve until it meets all the design criterion, producing the final product. All these iterations are time-consuming and costly resulting in an expensive product.

CFD attempts to reduce the cost and time required to reach a final design by eliminating most of the manufacturing and testing phases of traditional design strategies. This is done by running simulations to optimise the design before manufacturing it to produce better prototypes. Simulations allow iterations to be completed timelier than it would take traditionally to complete an iteration by manufacturing and testing. The cost of the simulation package will also be less expensive than the costs involved in manufacturing prototypes traditionally. It is, therefore, clear that CFD reduces the cost of a final design and allow the final design to be completed in less time than traditional design methods (Slagter, 2011; Ando, 2014; Paquin, 2015).

The major disadvantage of CFD is that it is not 100% accurate. The inaccuracies are introduced by the mesh used to represent the simulation domain as being the fluid inside the micro gas turbine. The finer the mesh, the smaller the mesh elements become and the more accurate the simulation is. This is because the mesh elements become much smaller than the flow phenomena present in the micro gas turbine and will, in essence, act like a fluid particle. This means that the mesh should be made as fine as possible to minimise the mesh induced errors. Making the mesh finer will increase the simulation time but can be counteracted to some extent by increasing the computational power to solve the problem. Balancing the mesh induced errors and the simulation time is called a mesh independence study.

A mesh independence study is used to determine the least amount of mesh elements, i.e. the coarsest possible mesh, required to obtain an accurate solution. This is preferable rather than

adding a large number of mesh elements because it will increase the simulation time unnecessarily. A common method used is the Grid Convergence Index (GCI) (Roache, 1998) which requires 3 different mesh densities. According to this method, mesh independence is achieved when the following is true:

$$\frac{GCI_{23}}{r^p GCI_{12}} \approx 1$$

With r being the factor by which the number of mesh elements in each direction is increased. Because r is a constant, it should be the same in both directions. The medium mesh should be r times finer in the x-, y- and z-directions than the coarse mesh and similarly, the fine mesh should be r times finer in the x-, y- and z-directions than the medium mesh. When r is chosen, p can be calculated.

$$p = \ln\left(\frac{f_3 - f_2}{f_2 - f_1}\right) / \ln(r)$$

The variable f is a variable extracted from the CFD simulation of each mesh to indicate the solution accuracy. The variable is chosen by the user and will depend on what is simulated, and which parameters are of importance. The subscripts indicate from which mesh the variable f was extracted from. Subscript 1 indicates the finest mesh, while subscript 3 indicates the coarsest mesh. After p is calculated, the final two variables can be calculated.

$$GCI_{12} = \frac{F_S}{r^p - 1} \times \left|\frac{f_2 - f_1}{f_1}\right|$$

$$GCI_{23} = \frac{F_S}{r^p - 1} \times \left|\frac{f_3 - f_2}{f_2}\right|$$

With:

- $F_S = 1.25$: This is a constant depending on the number of solutions available. This value is valid when using 3 meshes as this will give 3 solutions.

Doing the mesh independence study ensures that the mesh induced error is negligible, compared to the order of magnitude of the solution. The GCI method has 2 shortcomings as listed below and may render it unsuitable.

- It is only applicable to simple flow cases and does not ensure mesh independency when higher order flow phenomena are present, such as separation bubbles.
- It is difficult to control how fine the mesh is for unstructured meshes used for complex geometries, meaning that r cannot be enforced uniformly over the entire simulation domain.

For complex flow fields and geometries, it is, therefore, common practice to monitor a variable of interest when doing a mesh independence study. The variable of interest is often the inlet pressure and any other variables that the user deems important and should be mesh independent. The variable of interest will then typically be plotted against the number of mesh elements. When mesh independency is reached, the variable of interest will stay constant as the mesh is refined further. Figure 2-9 illustrates the results of a mesh independence study performed using the inlet pressure as the variable of interest. It was

found that the inlet pressure only changes by 0.03Pa when the number of mesh elements increased from 95’310 to 353’220. Because of this, the mesh with 95’310 elements would be used rather than the 353’220 mesh because the slightly better result does not justify the drastic increase in simulation time.

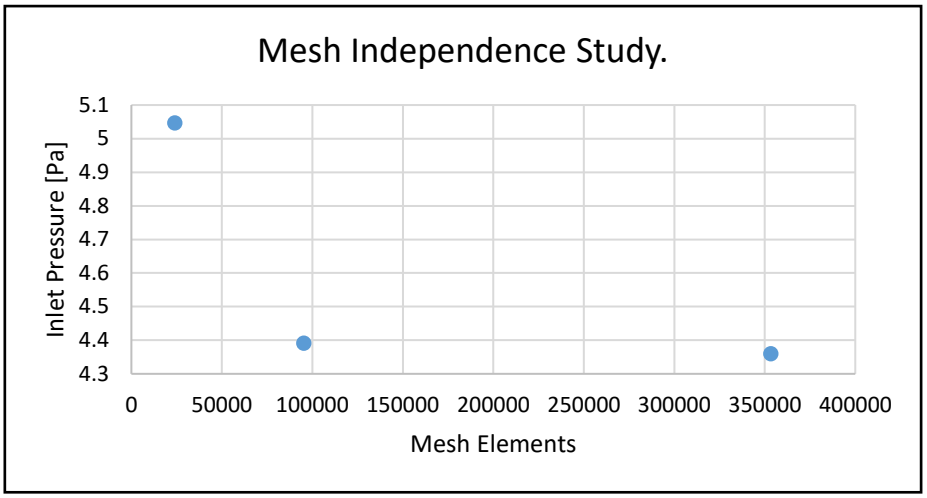

Figure 2-9: Mesh independence study using inlet pressure.

The other main reason why simulation and experimental results differ is the simplifying assumptions used to derive the turbulence models to solve the flow patterns in a simulation. These simplifying assumptions neglect some higher order and complex phenomena present in experiments for various reasons, including to speed up the simulation. Because the turbulence models contain a simplified version of the physics of the problem, the solution will be an approximation of real-life fluid behaviour. For this reason, it is good practice to build a prototype and compare the tested and simulated results. It will allow the user to see what the actual results are, and he can then adapt the turbulence model so that it fits the experimental results more accurately.

Other areas where inaccuracies can be introduced are:

- A skew mesh is less accurate than a square mesh.
- Using the wrong boundary conditions for the simulation.
- Having a boundary too close to the simulation domain can also affect results.
- The turbulence model used for the simulation.
- The method for modelling combustion.
- The mesh around walls in the simulation domain should comply with the y+ criterion. More information about the y+ criterion is presented by Salim & Cheah (2009).

The disadvantages of CFD is thus dependent on the user and his experience in simulating problems and most of them can be avoided or minimised.

2.6 HISTORICAL WORK IN THIS FIELD

This section covers work done previously in CFD simulations of gas turbines. The wider topic of gas turbines, rather than micro gas turbines, was researched because both have similar components, with the only difference being the size of the components.

Due to the complexities in the design of a gas turbine, it goes without saying that all major gas turbine designing companies use CFD to improve on their current designs. However, research papers about the detail design process are scarce because of the competitive nature of the aeronautical industry together with gas turbines being a strictly regulated technology. Despite this, three methods for simulating gas turbines are presented.

The first method consists of several steps executed one after the other. This process is labour intensive if not integrated into a software package which automates these steps. The steps are as follows, noting that it is somewhat simplified (Reed et al., 2003; Turner et al., 2004):

Step 1: Select an operating point at which the full engine performance is determined.
Step 2: Run 3D CFD simulations on each component for various design points concentrated around the engine operating point. These simulations only represent a narrow operating range of the individual components.
Step 3: Use a 1D mean line design program and the 3D CFD results from Step 2 to generate performance maps, i.e. plots of performance parameters against flow variables, for each component. These maps are also referred to as mini-maps because they only represent a small part of the entire performance map of the component.
Step 4: Perform a thermodynamic cycle analysis of the full engine to determine the inlet and outlet conditions for each component. The performance maps are used in this step to ensure that a power balance between the compressors and turbines are achieved. This requires several iterations.
Step 5: The inlet and outlet operating conditions from the cycle analysis serve as the engine inlet and component outlet boundary conditions for the component simulations.
Step 6: The 3D full engine CFD is then performed by simulating each component separately, using an upstream to downstream sequence.
    a. Use the outlet boundary condition as discussed in Step 5 for each component.
    b. If an upstream component is present, use the solution at the outlet of that component as the inlet boundary condition of the current component.
    c. If there is no component upstream of the current component, use the inlet boundary condition of the engine as discussed in Step 5.
    d. The combustor was simulated using software specifically created to simulate the combustor.
Step 7: Repeat these steps to obtain a performance map of the full engine.

This process reduces the setup and simulation time for a full engine CFD simulation, which is advantageous, as it allows the design process to be completed timelier. The results produced

by this technique were within 0.5% of the baseline data obtained through experiments (Reed et al., 2003; Turner et al., 2004).

This simulation method takes the effects of component interaction into account, but it does not simulate the gas turbine as an assembly and simulates the combustion process. The reason for not simulating the gas turbine as an assembly was most likely because simulating a full-scale gas turbine would have an enormous simulation domain which would be computationally expensive as it would simulate for extended periods of time. The advantage of simulating micro gas turbines is that the simulation domain is small. This will consequently not be as computationally expensive as a full-scale gas turbine.

The second method simulated an assembled compressor, combustor and turbine. This method used two different flow solvers which calculated the flow solution in the engine. The flow solvers and where they were active was as follows (Schlüter et al., 2005):

- Reynolds-Averaged Navier-Stokes (RANS) flow solver:
    1. Compressor
    2. Turbine
- Large-Eddy Simulation (LES) flow solver:
    1. Combustor

The RANS flow solver was used to simulate the compressor and turbine because several models were developed to accurately model the flow characteristics in these components of which all are based on the RANS approach to model turbulence. Thus, selecting one of the models developed for simulating the flow in compressors and turbines would automatically result in using a RANS flow solver.

The LES flow solver was used to simulate the combustor because the flow in the combustor is complex, especially when trying to simulate the combustion process. The flow in the combustor contains separated flow, chemical reactions and the release of heat, which is modelled best by LES flow solvers. Although LES simulations are best at capturing flow phenomena such as detached flow and free turbulence, this comes at a cost, since LES simulations are computationally more expensive than RANS flow solvers.

It should be noted that a hybrid approach to combine RANS and LES flow solvers is available. This flow solver is known as the Detached-Eddy Simulation (DES). This hybrid approach is simpler to implement but lacks the distinct validated advantages that were built into the RANS and LES solvers during their development.

The RANS and LES simulations were then conducted in a similar fashion to fluid-structure interaction simulations. The information flowed from the RANS flow solver of the compressor, across a boundary to the LES flow solver in the combustor and then finally across the boundary to the RANS simulation of the turbine. At the component interfaces, the calculated solution had to be transferred while preserving or regenerating the turbulence at the boundaries. This required a special boundary condition at the LES inlet and at the RANS inlet and outlet boundary. Before describing the boundary conditions, the following should be noted:

Firstly, turbulent velocity consists of two parts. The first part is the average turbulent velocity and the second the transient turbulent velocity. At any location in the simulation domain, the average turbulent velocity will stay constant while the transient turbulent velocity is constantly changing. Furthermore, the transient turbulent velocity is insignificant compared to the average turbulent velocity.

Secondly, the RANS simulation only solves the average turbulent velocity, while the LES solves the average turbulent velocity as well as any large-scale transient turbulent velocities.

The LES inlet boundary condition requires average turbulent velocity as well as transient turbulent velocities to be specified for every point on the component interface. The difficulty of this is that the RANS flow solver only gave average turbulent velocities for the points on the component interface. The transient turbulent velocity was generated by using a pipe simulation to obtain turbulent velocity fluctuations which were stored in a database. The data was then used to reconstruct the transient turbulent velocities. The turbulent velocity was created by scaling the data used as the transient turbulent velocity and then adding it to the average turbulent velocity given by the RANS simulation.

The inlet and outlet boundary condition for the RANS simulation was much simpler. The RANS boundary conditions were the time-average of the solution given by the LES simulation.

Finally, to integrate the two different flow solvers with the above-mentioned boundary conditions required coupling software:

1. The coupling software receives the mesh and the solution from one solver at an interface.
2. The coupling software uses the mesh, solution, boundary conditions and the database to generate the output solution to the solver on the other side of the interface.

This method for simulating an assembled micro gas turbine is more in line with the objective of this research project. However, it differs slightly because the project aims to simulate the assembled micro gas turbine without having to simulate the combustion process. This means that using two different flow solvers is unnecessary and overly complicated.

The third and final method found was implemented on a micro gas turbine and was thus closest in size to the engine that will be simulated in this project. This method had the following key features (Trebunskikh et al., n.d.):

1. The combustion process was modelled.
2. The full geometry was simulated without any periodic boundary conditions.
3. Resolving the boundary layer with wall functions.
4. A transient simulation was done.

This approach differed from the one followed in this project when looking at the key features above:

1. The combustion process will not be modelled.
2. Periodic boundary conditions will be used to reduce the mesh size.
3. Boundary layers will be calculated using fine mesh at the walls.
4. A steady-state simulation will be done.

The method used by Trebunskikh, Ivanov and Dumnov delivered accurate results when compared to experimental results for the micro gas turbine which they used for their simulations. This meant that by modelling combustion, a micro gas turbine can be modelled accurately. If the method used in this project also match the experimental results well, a conclusion can be drawn with regards to how important modelling the combustion process is for having an accurate simulation.

2.7 MODELLING COMBUSTION

For gas turbines, non-premixed combustion is modelled using the mixture fraction approach which only adds one additional equation to the governing Navier-Stokes equations. This equation tracks the species concentrations through the domain which is used to model the chemistry by using either the equilibrium equations or steady or unsteady tabulated flamelet data. The turbulence-chemistry interaction is then modelled using assumed-shape PDF models ("USERGUIDE FINE™/Open with OpenLabs™ 6.2", 2018; "FLUENT 6.3 User's Guide - 15. Modeling Non-Premixed Combustion", n.d.).

Modelling combustion using chemistry increases the simulation time due to the added complexities of accounting for the mixture fraction and modelling the chemistry and turbulence-chemistry interactions. This is only one of many possible models to model combustion with and the user has the choice to add additional complexities to the model which will further increase the simulation time (Candel et al., 1999; "USERGUIDE FINE™/Open with OpenLabs™ 6.2", 2018). The one major difference between work in the open literature and this project was how combustion was modelled as mentioned in Section 2.6. The CFD simulation contained in this study will use one of the boundary conditions mentioned in Section 2.8 to model combustion which does not add additional combustion equations to be solved in the domain. Because of this, the increase in simulation time as a result of modelling combustion in this study will be minimal.

In order to effectively discuss how accurately the combustion process was modelled, the combustor terminology is illustrated in Figure 2-10 below (Lefebvre & Ballal, 2010).

Note that the fluid flows from left to right in Figure 2-10 which is in the axial direction and that the section and chapters to follow will refer to these terms without referencing Figure 2-10. In Figure 2-10, the outer annulus was separated from the primary, intermediate and

dilution zone by the outer combustor liner, similarly, the inner annulus was separated from these zones by the inner combustor liner.

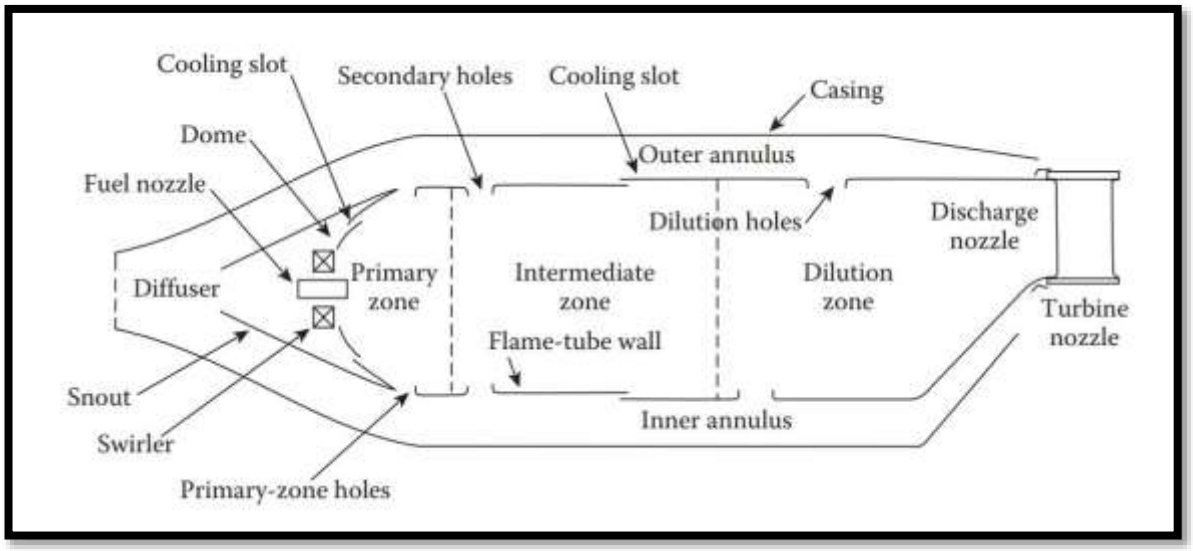

Figure 2-10: Combustor terminology (Lefebvre & Ballal, 2010).

2.8 BOUNDARY CONDITIONS

Boundary conditions are required when performing any simulation. As the name suggests, it is the condition that must be met at the boundaries in the simulation domain. These conditions drive and form the solution because they stay constant during the simulation and are used in the differential equations being solved by the CFD software.

The boundary conditions for the micro gas turbine simulation are:

1. Inlet boundary condition.
2. Outlet boundary condition.
3. Wall boundary condition.
4. Rotating shaft boundary condition.
5. Combustion boundary condition.

Boundary conditions can be used in simulations to mimic or model certain physics inside the simulation domain that is difficult and time-consuming to solve and implement. An example of mimicking physics is heat generated by an electronic component due to the current flowing through it. Rather than trying to model the heat generation of the electronic component, it can be modelled as a block with a specified heat generation rate. A similar strategy would be followed to model the combustion boundary condition since combustion should not be modelled explicitly in the micro gas turbine. This is computationally less expensive.

The combustion process is essentially only a heat addition process that is performed at constant pressure. This means that the combustion process has to be replaced by a heat

addition boundary condition. The possible heat addition boundary conditions are as follows ("Heat Transfer Boundary Conditions", n.d.; Cole, 2003; Reed et al., 2003):

1. Heat generation in the combustor domain.
2. Temperature boundary condition on the combustor walls.
3. Heat transfer rate through the combustor walls.

No past papers describe alternative methods to simulate a combustor. The papers available report on modelled combustion using commercially available CFD software that has the capability to simulate combustion ("Combustion Modeling", n.d.; "Combustion Tools | ANSYS Combustion Simulation", n.d.; "Follow the chemistry to better CFD combustion simulations - SAE International", n.d.; Nusca et al., 2010; Xu et al., 2016).

2.9 CONCLUSION

From the information gathered in the literature study, the development and use of micro gas turbines will increase in the future. With the new ceramic micro gas turbines being developed, the fuel to electrical efficiency of a micro gas turbine is on par with that of IC engines. This, together with the other advantages micro gas turbines have over IC engines, for example, low noise, low vibration, high power/weight ratio's and reliability, micro gas turbines will be able to compete with and replace IC engines in most industries.

For micro gas turbines, the advantages outweigh the disadvantages and industry has a definite need for micro gas turbines. This need arises from the fact that UAV's are being used more and more for reconnaissance and for offensive and defensive military strategies. These are the military-driven motivations for developing micro gas turbines, but there are also civilian applications, for example, power generation, entertainment and for perhaps improving personal transportation by developing powered human flight.

An added advantage of the production of micro gas turbines is that it will give an opportunity to develop Additive Manufacturing technology for commercial gas turbines. Micro gas turbines are the ideal testing platform because they have small parts which will be less expensive to manufacture than the large parts used on commercial gas turbines. The techniques developed for micro gas turbines can then be scaled up for use on commercial gas turbines.

It was also found that using CFD has great advantages in saving time and money during the development of a new product like a micro gas turbine. Care should, however, be taken when simulating the micro gas turbine because poor mesh will lead to inaccurate results.

Three tried and tested CFD methods are described and can be used to simulate a micro gas turbine, however, none of these methods is entirely applicable to this project, with the main difference being the combustor modelling. These three methods all simulated combustion, while an alternative method must be implemented in this project which will reduce the computational time. The reduction in simulation time is dependent on the stability of the

simulation when using a boundary condition to model combustion. An in-depth search for available research to simulate a combustor without modelling chemical reactions yielded no results. This search did, however, lead to three possible boundary conditions which could be implemented to mimic the combustion process. During the execution of the project, one of the three possible boundary conditions will be implemented based on ease of implementation and will be altered if it does not produce the desired results. The three possibilities are:

1. Temperature boundary condition on the combustor walls.
2. Heat transfer rate through the combustor walls.
3. Heat generation in the combustor domain.

It is thus clear that this research is plausible and ought to yield a valuable method for accurately simulating a micro gas turbine. This will be true if the necessary care is taken in the generation of the mesh, set-up of the simulation and implementation of the boundary conditions. This method can then be applied to a newly designed micro gas turbine to identify possible component mismatches prior to manufacturing and testing the engine.

2.10 ANALYSIS OF SOURCES

The resources used to gather the information mentioned in the literature were scrutinised for accuracy, quality and completeness. The information was obtained from reliable sources such as conference papers and official websites of companies. The information from the various sources was cross-checked with several other sources found to ensure their authenticity.

CHAPTER 3 METHODOLOGY

This chapter describes the methodology used to simulate the complete BMT 120 KS micro gas turbine. The mesh and simulation settings are also shown in this chapter to point out important aspects considered when this simulation was performed. The structure of this chapter is similar to the steps that were followed during the simulation setup.

It should be noted that a compressor, combustor and turbine simulation were run separately. This was done to ensure that the mesh generation techniques used for the complete simulation would deliver a mesh that did not cause the solver to crash when they were run together. These simulations do not form part of this write-up as they would distract the reader from the main focus, namely the complete micro gas turbine simulation.

3.1 GAS TURBINE DESIGN METHODOLOGY

The purpose of this section is to inform the reader of the general steps followed to design a micro gas turbine in order to understand where this investigation fits into the current design process.

The design process commences with requirements obtained from the user which are then used to do a cycle analysis of the micro gas turbine. The cycle analysis gives as output the thermodynamic properties at each component interface in the micro gas turbine. These thermodynamic properties are then used as the input to first order design tools from where the geometry of the components are produced and can then be used in CFD simulation software packages to do a more in-depth analysis as well as optimisation studies. The CFD simulations are also used to construct component maps, which are compared to one another to determine if the components match. Lastly, FEA simulations are performed to determine the natural frequencies of the components to ensure that they do not coincide with the operating frequencies of the micro gas turbine and that there is sufficient safety margin based on material strength.

Normally when the above-mentioned steps are executed, a complete micro gas turbine simulation is run which is the purpose of this study. It entails that each component is meshed and linked to one another to produce the simulation domain of the micro gas turbine. This domain is simulated to check that the designed components are matched to prevent engine failure during testing and operation.

The final step in the design process is to ensure that all of the components fit together and that they have adequate tolerances for assembly. This means that the simulated engine components are slightly modified, and some components added to the engine to produce the final components for manufacturing, assembly and operation thus finalising the CAD model of the micro gas turbine. This CAD model was provided to the student for the purpose of this study.

3.2 GEOMETRY

The micro gas turbine geometry, made available to the student, included parts and features that were required for manufacturing, assembly and successful operation of the engine, as mentioned in Section 3.1. Although these parts and features are necessary for the final CAD model, they unnecessarily complicated the simulation model of this study and required a substantial number of mesh elements to fully capture them. This lead to making geometrical modifications to neglect these parts. This section will note these changes with Figure 3-1 showing the final manufacturing and assembly model.

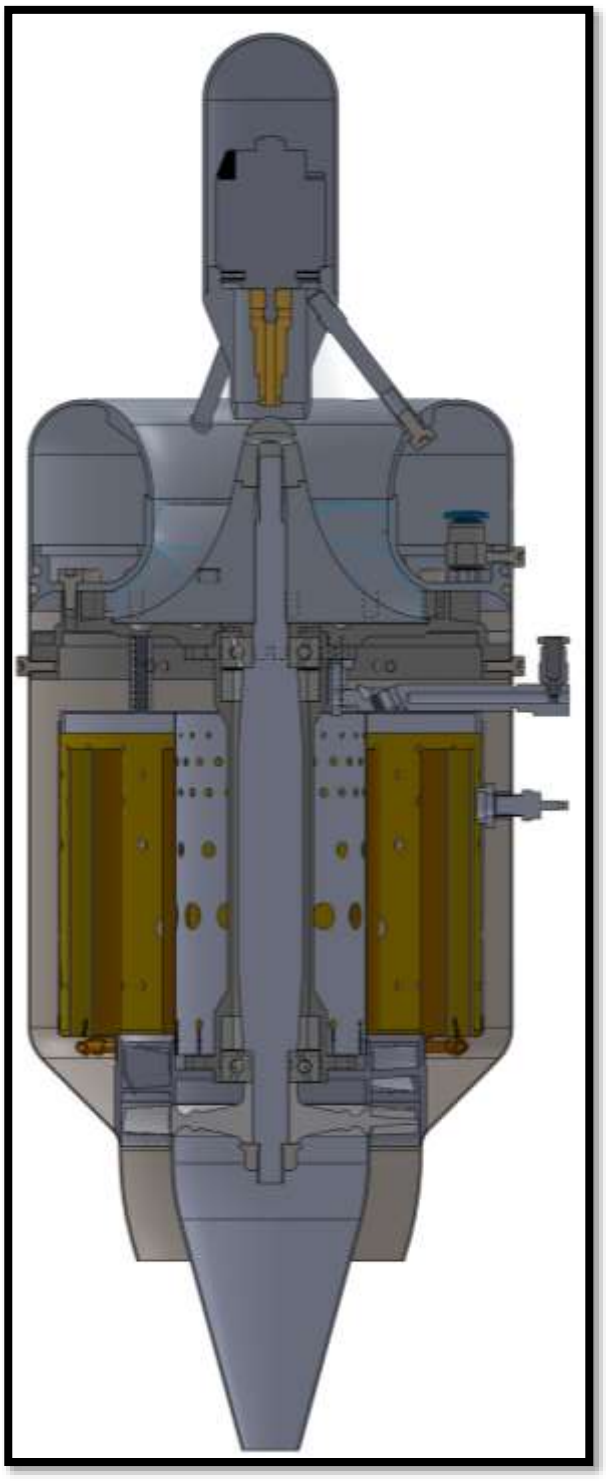

Figure 3-1: Final BMT 120 KS CAD model.

The simplification of the CAD model included removing the starter and fuel delivery system in the combustor, smoothing the annulus of the compressor and turbine while neglecting the cooling flow through the bearings and shaft tunnels. Figure 3-2 to Figure 3-5 show the simplified geometry.

The original geometry files of the micro gas turbine were SolidWorks Part files. These documents were loaded into SolidWorks from which GeomTurbo, .stl and .X_T files were created. These files were required because SolidWorks and the mesh generating platforms of Numeca, AutoGrid5, Hexpress and Hexpress Hybrid were not compatible. The .stl and .X_T files were used to import the combustor and outlet domain of the micro gas turbine into Hexpress and Hexpress Hybrid, while the GeomTurbo files were used to import the compressor and turbine into AutoGrid5.

It can be seen in Figure 3-2 that the deswirler had thicker vanes onto which the combustor outer shell was mounted. This was not included in the simulation because it would require simulating several deswirler flow passages which

would increase the mesh size significantly. The simulated engine deswirler would thus have less blockage but the effect of this is expected to be negligible.

Figure 3-2 to Figure 3-4 shows the simplified BMT 120 KS micro gas turbine geometry that was simulated.

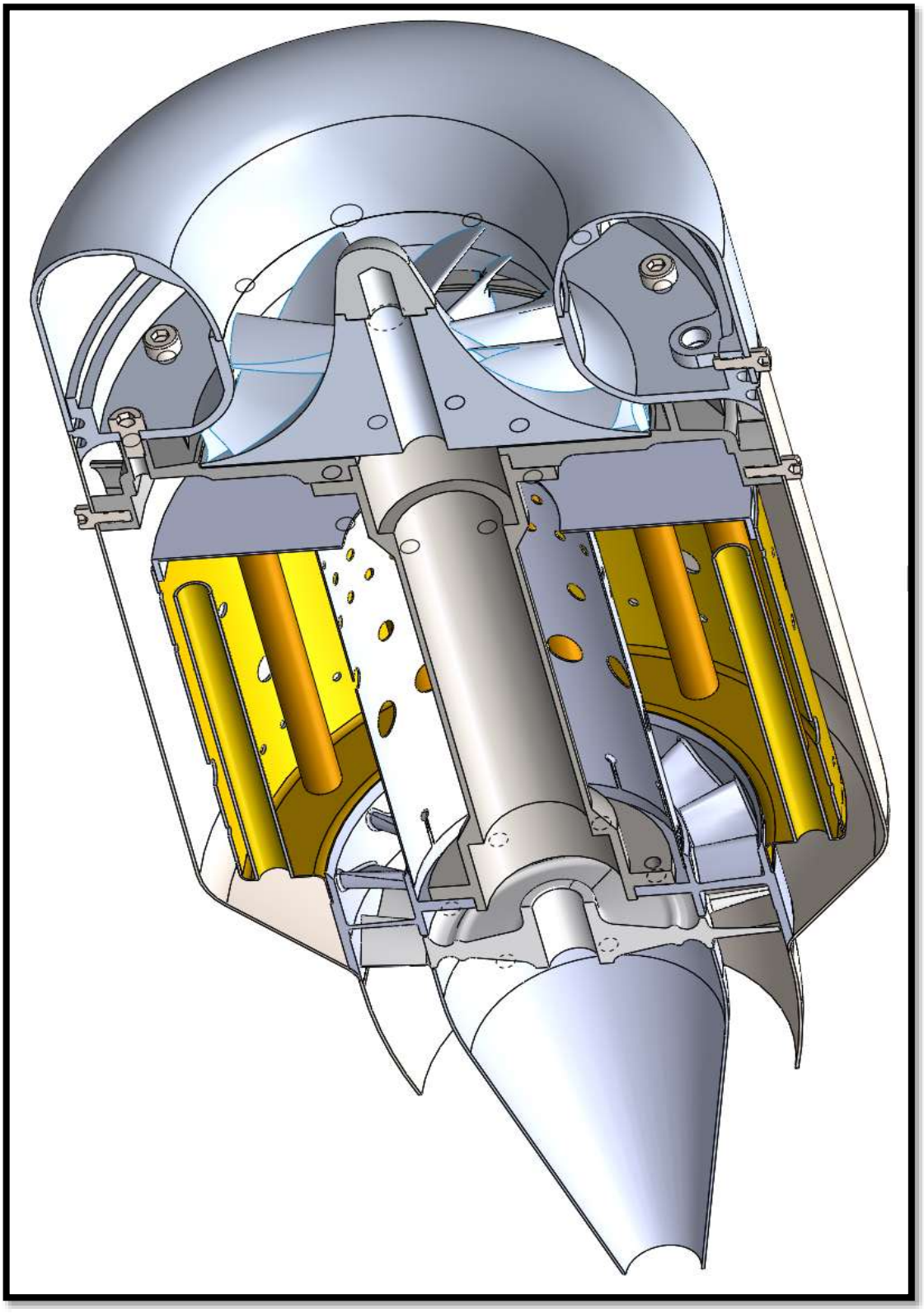

Figure 3-2: Sectioned view of the simplified BMT 120 KS.

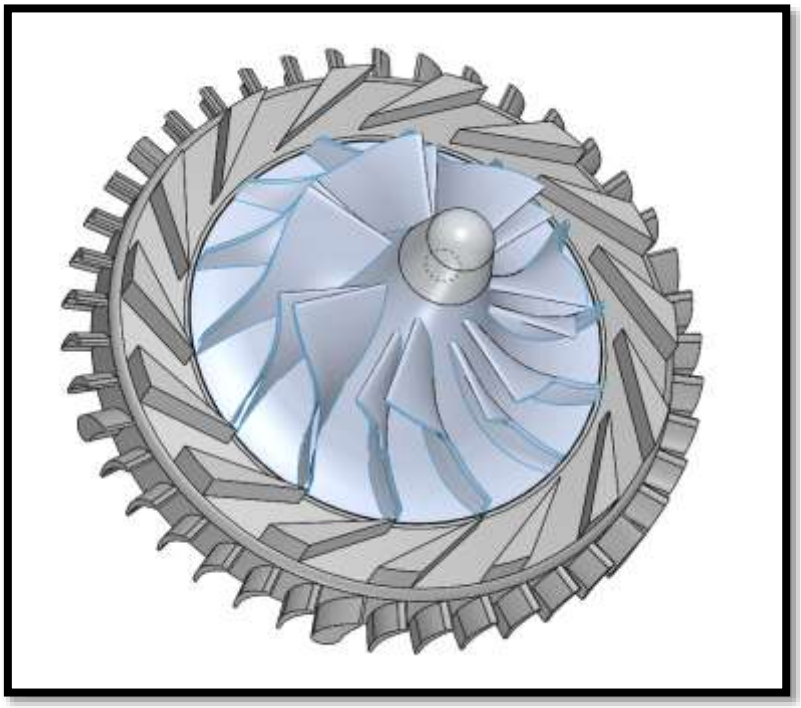

Figure 3-3: BMT 120 KS Compressor that was simulated.

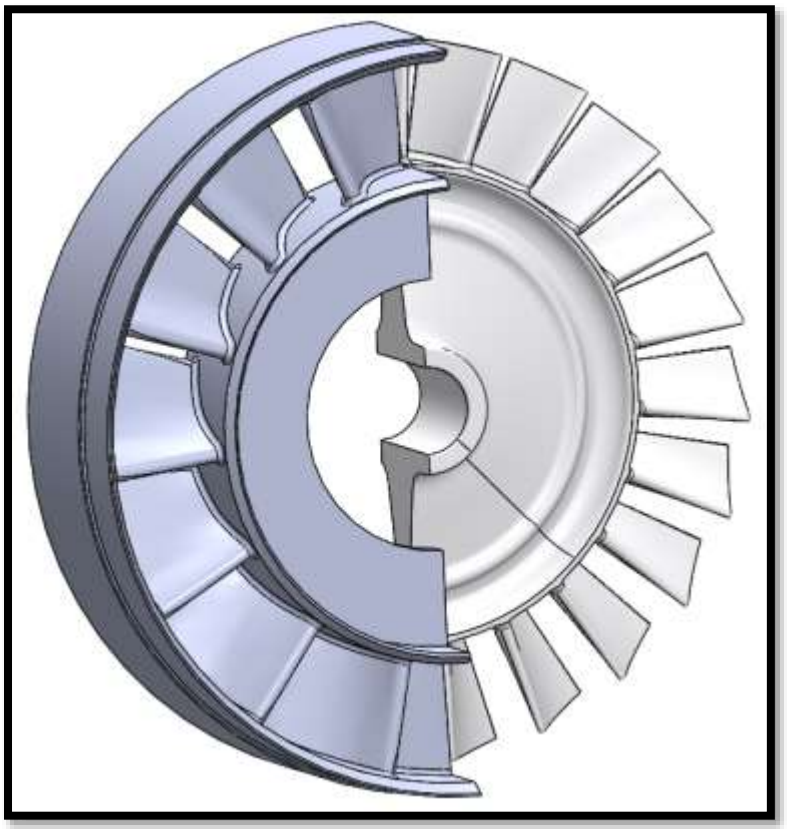

Figure 3-4: BMT 120 KS turbine that was simulated.

The impeller and turbine blades have a 3D profile which was inaccurately represented in the geometry files provided for this study. The turbine blades required smoothing on the pressure side such that it better represented the actual blade profiles of a turbine. Because of this, some deviation from the experimental results could be expected.

Figure 3-5 shows the combustor used for the simulation.

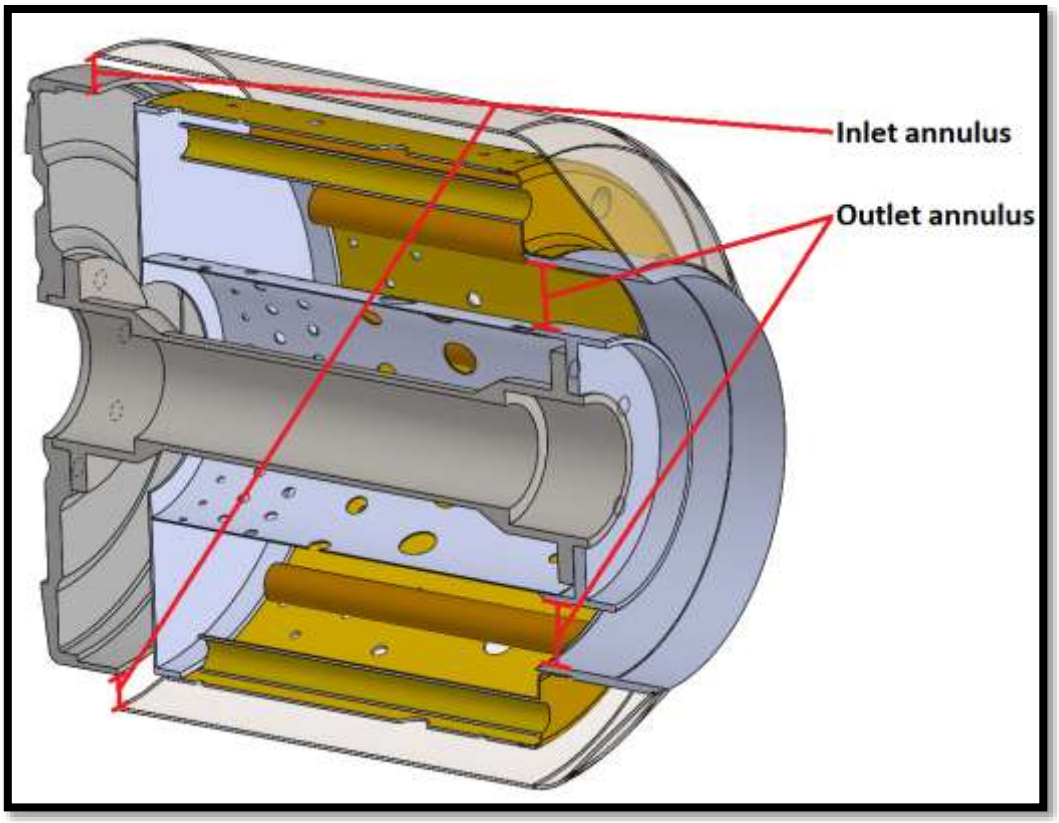

Figure 3-5: BMT 120 KS combustor.

3.3 MESH

This section of the study discusses the mesh used for the complete micro gas turbine simulation. It should be noted that every component of the micro gas turbine was meshed individually and the mesh generated for that component is called a mesh block.

When connecting the domains, each mesh block had to be imported into Hexpress in its correct location in relation to the other mesh blocks. When connecting the mesh blocks to each other, the interface at which the blocks connect had to be in the same plane otherwise the domains would not be connected. Hexpress does have the capability to move mesh blocks but the CAD platform was more suitable for use.

Figure 3-6 shows the general layout of the mesh blocks with air flowing through the domain from the intake to the outlet.

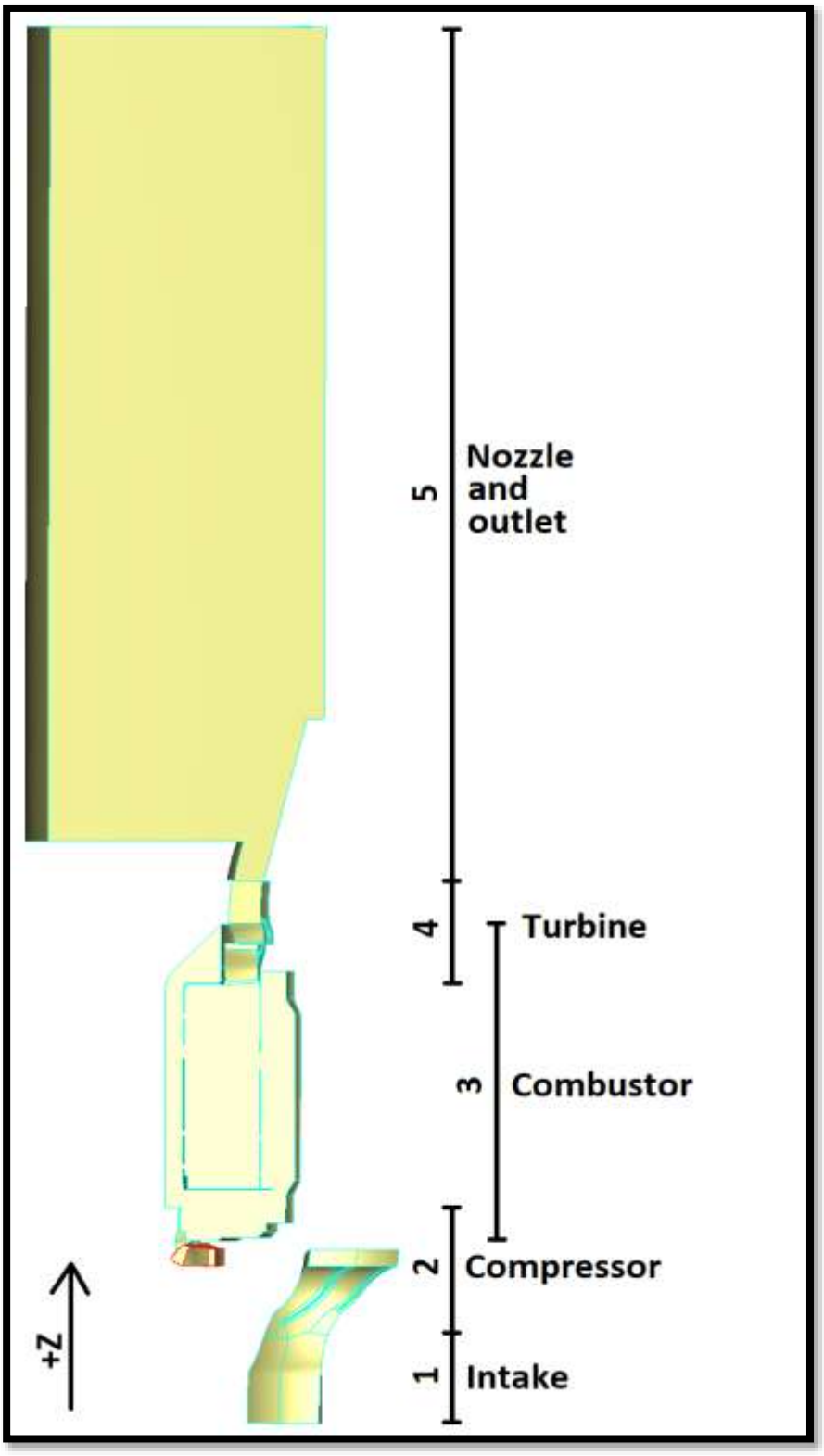

Figure 3-6: BMT 120 KS simulation domain.

Note that the nozzle of the engine is part of both domains 4 and 5 with the nozzle outlet in domain 5. The nozzle guide vane (NGV) and turbine rotor (Figure 3-6) is located in the overlapping section of components 3 and 4. The deswirler can barely be seen in Figure 3-6 as it is mostly behind the combustor.

The domain was oriented such that the fluid flows in the positive Z-direction. This was preferred because the Numeca AutoGrid5 meshing platform requires the input geometry to be rotating around the z-axis and meshes the geometry accordingly. To prevent having to rotate and translate the meshed components when assembling the micro gas turbine mesh blocks, all components were meshed with the fluid flowing in the positive z-direction.

Refer to Subsection 3.3.7 for the summary of the meshed components while the following subsections contain more detail regarding the mesh.

3.3.1 RAM limitations

RAM was an important consideration for the simulation, especially when generating the mesh because a large mesh has a long simulation time and the computer can run out of RAM, forcing the operating system to start paging. Paging drastically increases the simulation time since data stored in RAM is accessed orders of magnitude faster than data stored on the disk (Gilheany, 2003; Leniart, 2017).

The first mesh generated had 13 321 458 mesh elements and required 34GB of RAM because the entire combustor was meshed. This posed a problem because the computer assigned for this study had 32GB of RAM installed of which 2.2GB is used for background processes and leaves 29.8GB of RAM available for the simulation. To resolve this problem, only a twelfth of the combustor was simulated. The new mesh generated had 5 399 768 mesh elements and required 19.4GB of RAM. This mesh did not surpass the RAM limitations of the computer and the operating system did not start paging.

Simulating only a twelfth of the combustor was expected to have a negligibly small effect on the results since the combustor was sliced on its symmetry axis. The slice did split some of the combustor holes in half, but a simple simulation proved that the effects of this were negligible.

For a CFD project, it is custom to have a mesh independence study as discussed in Section 2.5 where the mesh density is doubled for every mesh refinement. Taking the RAM limitations and the RAM required for the new mesh into account it is clear that the number of mesh elements could not be doubled to refine the mesh to perform the independent study.

3.3.2 Intake and compressor mesh

The compressor was meshed in AutoGrid5 which is a dedicated turbomachinery mesh generation platform. The compressor mesh was generated using the automated meshing wizard in this platform according to best practices for turbomachinery as used in industry, except for the number of elements per row for the diffuser and deswirler (Sideroff, n.d.; Visavale, n.d.; Dunham & Meauze, 1998; “Best practice guidelines for turbomachinery CFD”,

2015; "USERGUIDE FINE™/Open with OpenLabs™ 6.2", 2018). According to best practices, the mesh should have between 1 million and 2 million cells in each stator or rotor row with a minimum of 500'000 when not using an extended wall function. This mesh had approximately 550'000 cells in the diffuser and deswirler. This was just above the minimum recommended number of mesh elements per row and was required to reduce the simulation time and RAM requirements of the simulation. From Snedden, (2011) it was clear that this mesh density will be sufficient to capture secondary flow accurately for a complete micro gas turbine simulation since it was proven that 66'000 mesh elements captured the secondary flow in a 1½ stage turbine accurately.

The locations where the mesh was refined, how the mesh at the mesh block interface matched and the 3D mesh can be seen in Figure 3-7 to Figure 3-11.

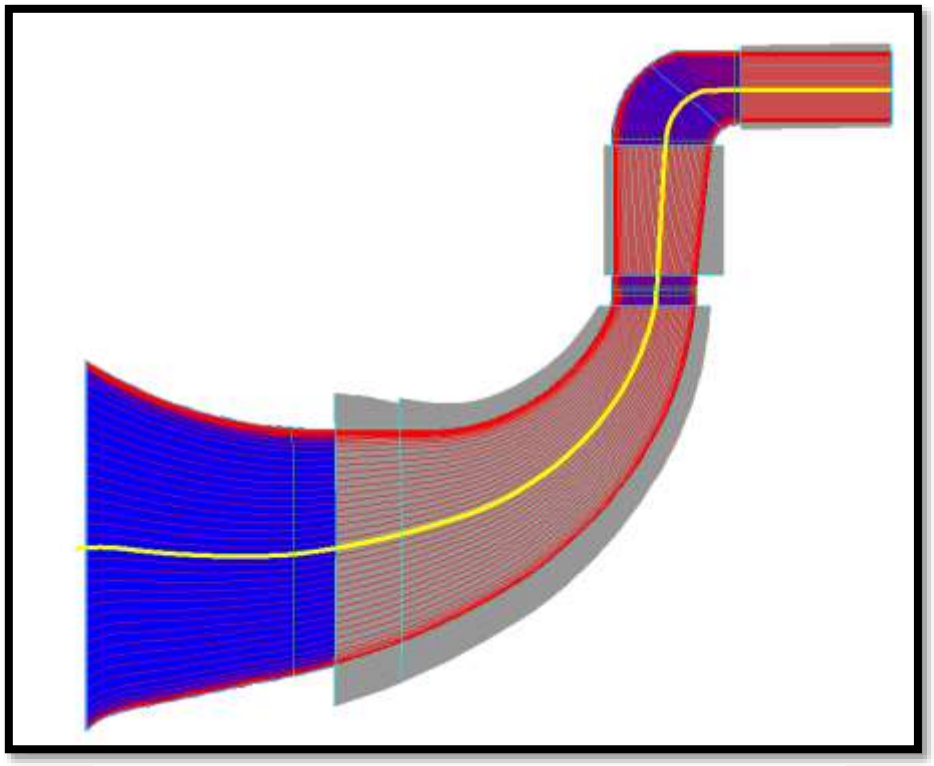

Figure 3-7: Compressor streamwise flow paths.

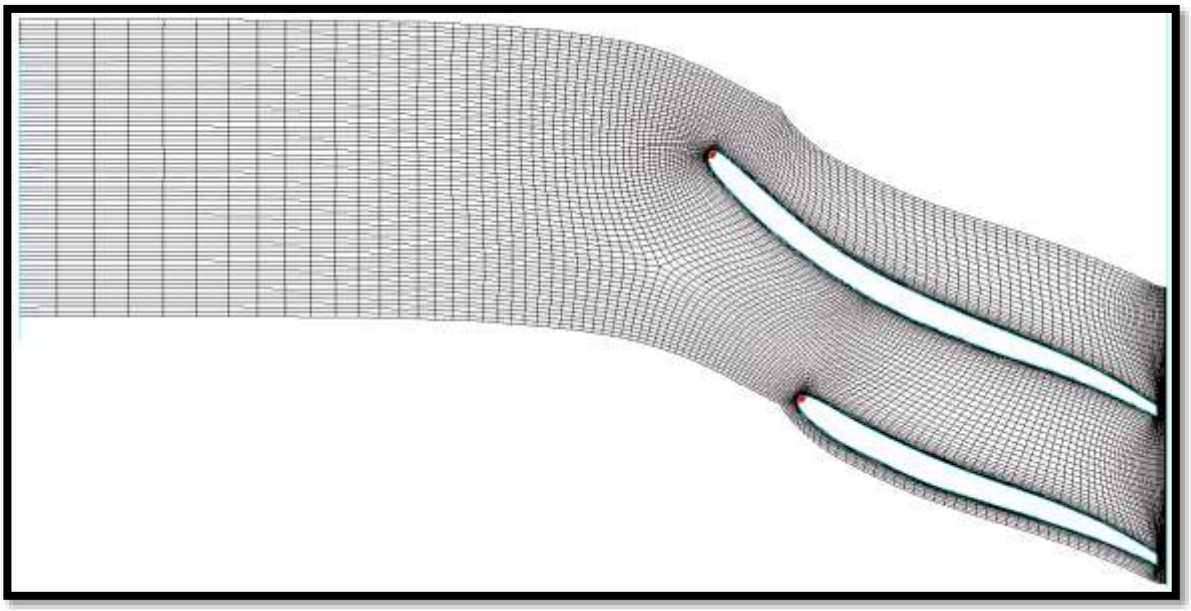

Figure 3-8: Impeller blade-to-blade view at 50% blade height.

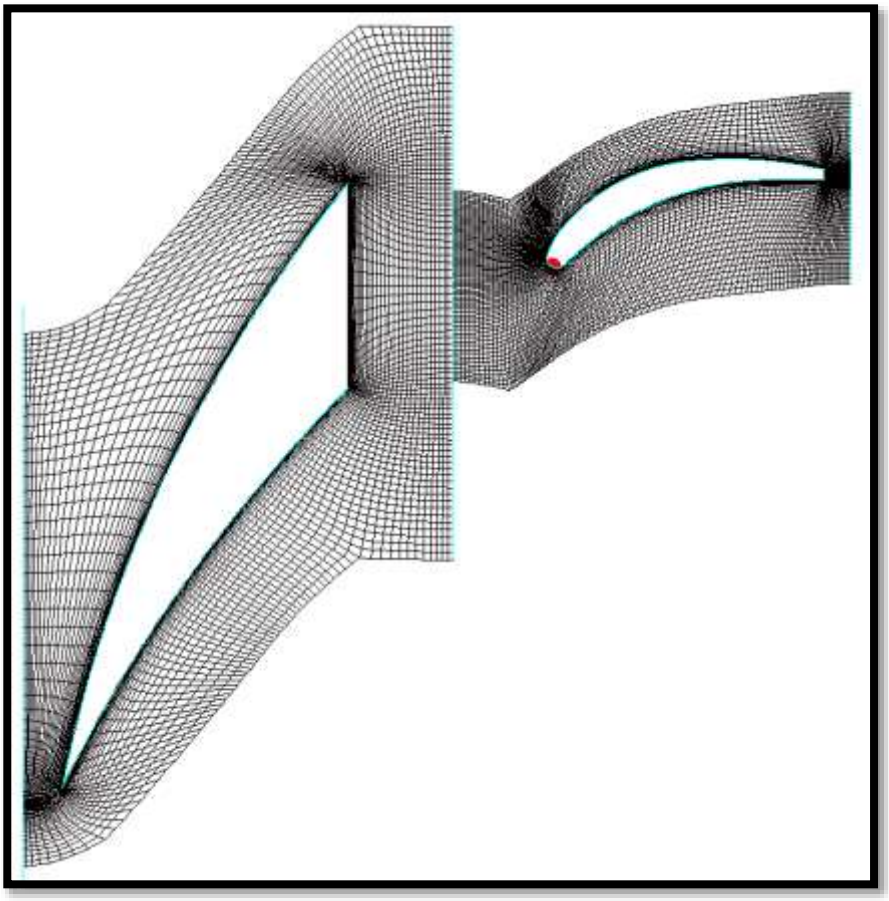

Figure 3-9: Wedge diffuser and deswirler blade-to-blade view at 50% blade height.

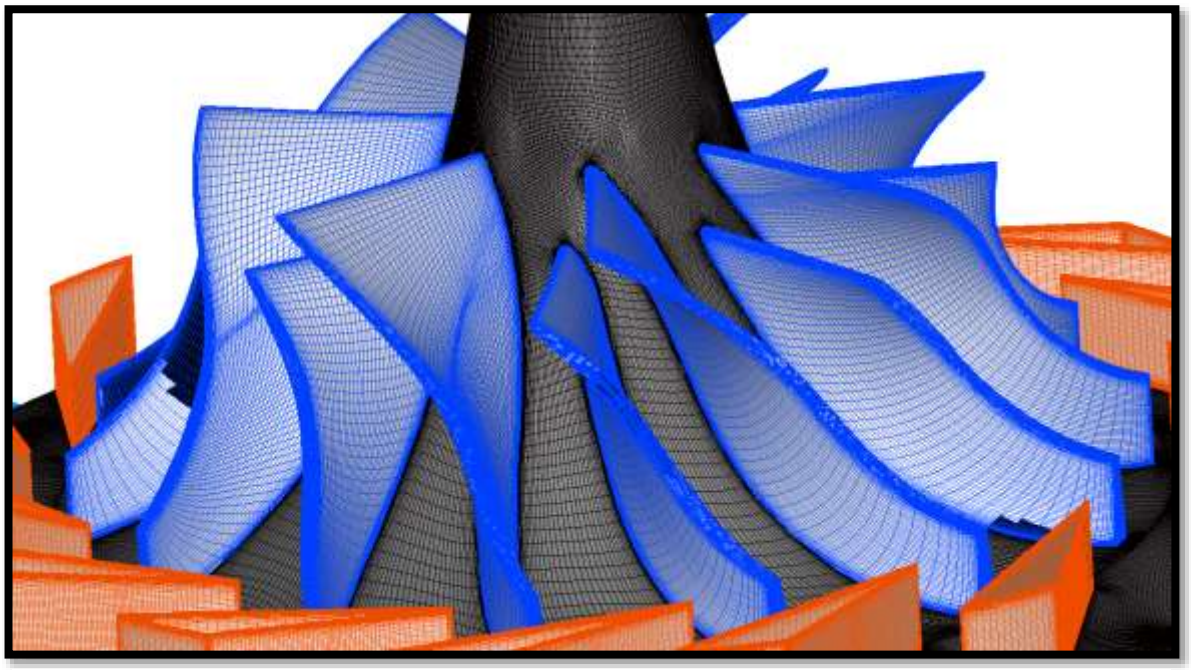

Figure 3-10: 3D impeller blade mesh.

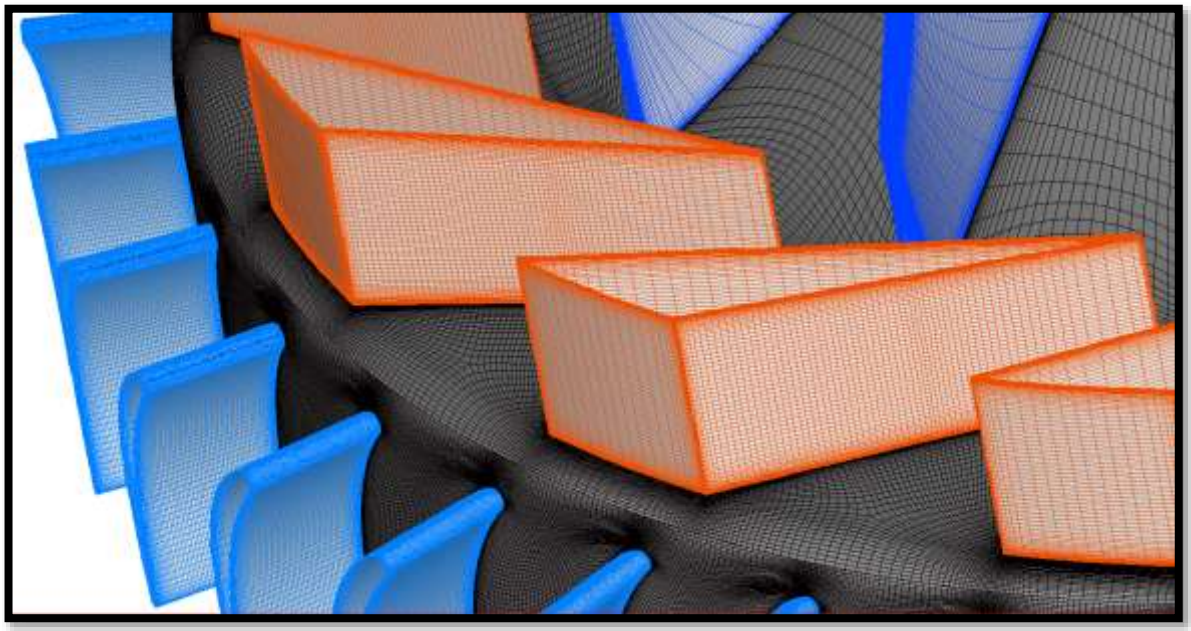

Figure 3-11: 3D wedge diffuser and deswirler blade mesh.

3.3.3 Combustor mesh

The combustor was meshed with Hexpress using a base mesh file from Hexpress Hybrid as a reference. This file was used to generate the mesh of a similar combustor that was simulated successfully and provided to the student. The base mesh file commands were interpreted and modified to meet the needs of this study by refining the mesh in the required regions to fully capture the geometry while leaving the mesh elsewhere the same as it would have been in the base file. Figure 3-12 shows the mesh in the combustor from the upstream direction. Figure 3-13 shows a mesh element slice of the combustor with a zoomed in view of the detail at the combustor holes and the fuel tube. This, together with Figure 3-12, show the mesh refinement regions in the combustor. These locations correspond to the combustor holes, inlet and tubes. Without these refinements, the geometry and the flow entering the combustor was not captured accurately enough for the solution to converge. These refinements contributed the most towards the number of mesh elements in the combustor.

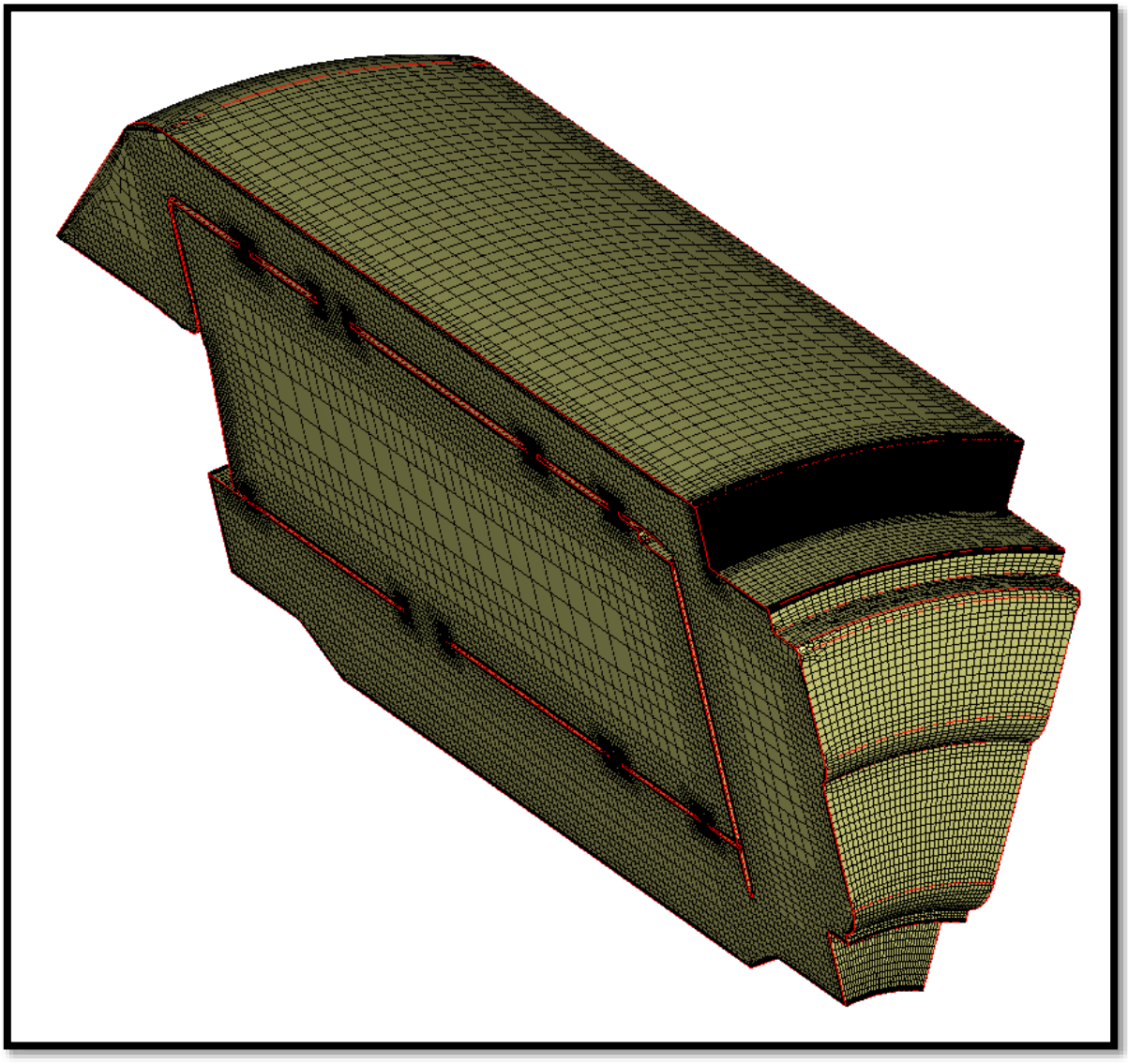

Figure 3-12: Combustor mesh along the axis.

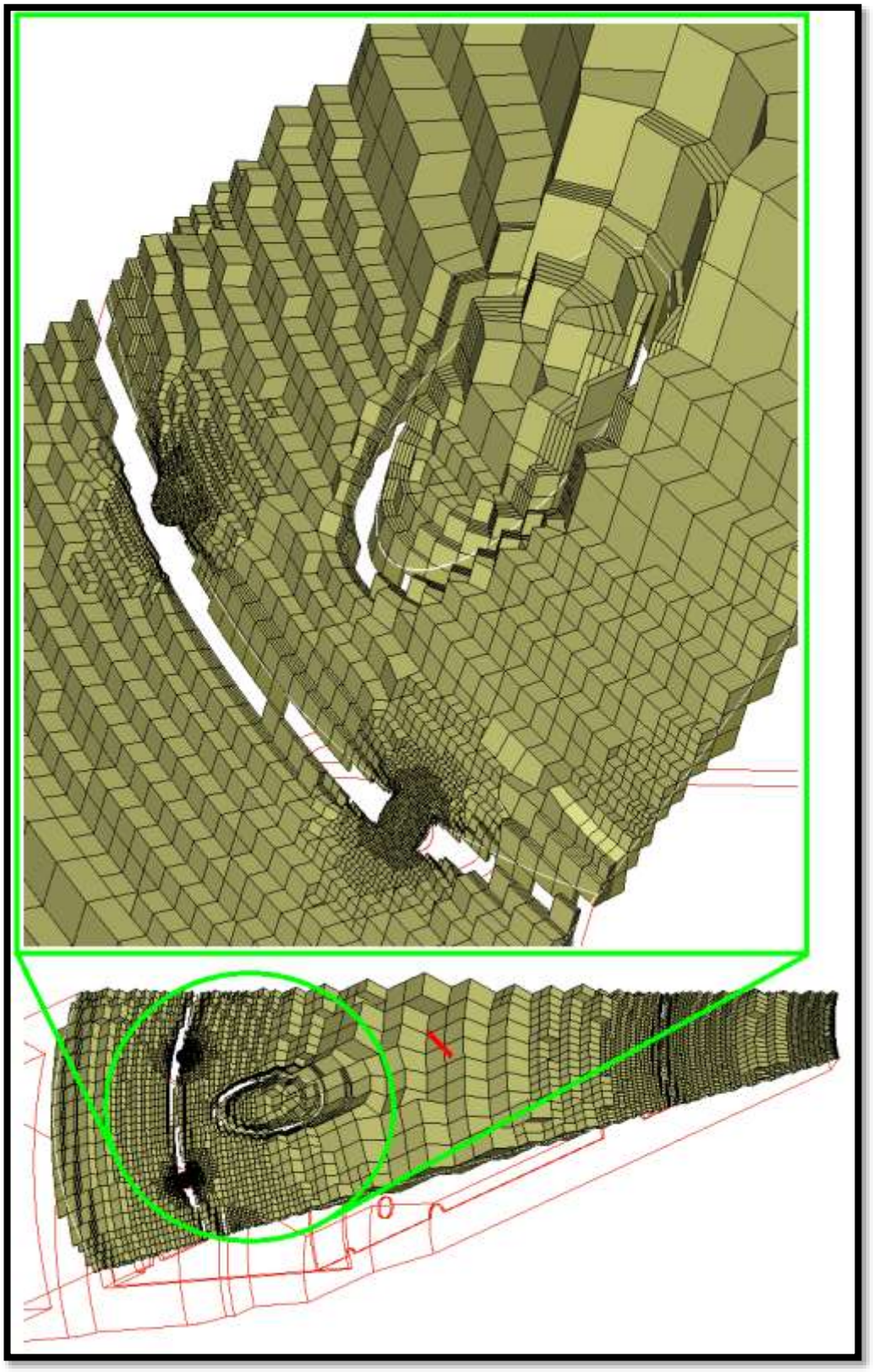

Figure 3-13: Combustor internal mesh element slice and zoomed in section.

.

3.3.4 Turbine mesh

The turbine mesh was generated in AutoGrid5 similarly to that of the compressor mesh using the meshing wizard. As with the compressor mesh, the turbine mesh was generated in line with best practices except for the number of elements in the NGV and rotor which was on the lower limit of 500'000 mesh elements per row (Sideroff, n.d.; Visavale, n.d.; Dunham & Meauze, 1998; "Best practice guidelines for turbomachinery CFD", 2015; "USERGUIDE FINE™/Open with OpenLabs™ 6.2", 2018). This was done to reduce the simulation time and RAM requirements. This will, as mentioned previously, be suitable to capture the secondary flow to determine the blockage in the flow passages of the micro gas turbine (Snedden, 2011).

Figure 3-14 to Figure 3-16 show the mesh used for the turbine so that the locations where the mesh was refined, the mesh at the mesh block interfaces and the 3D mesh can be seen.

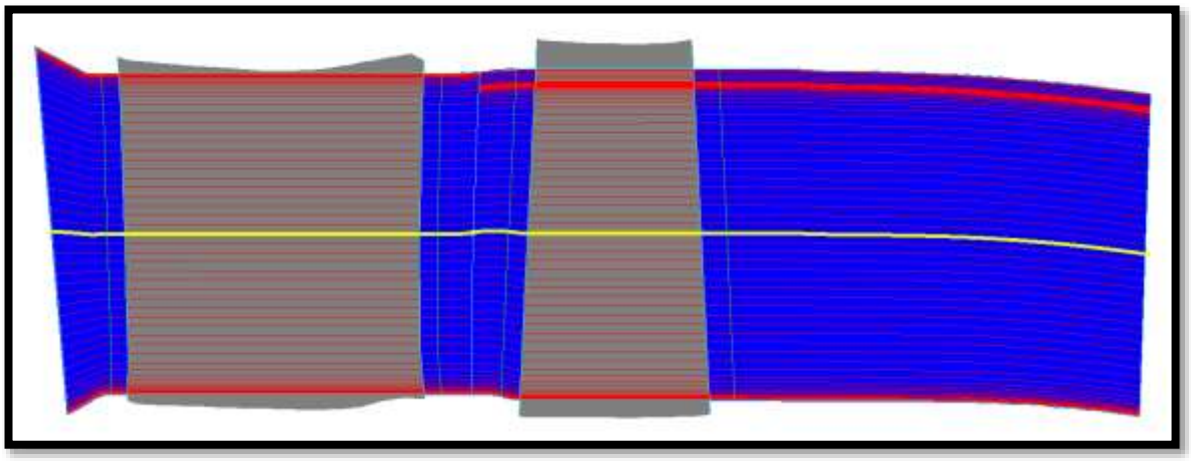

Figure 3-14: Turbine streamwise flow paths.

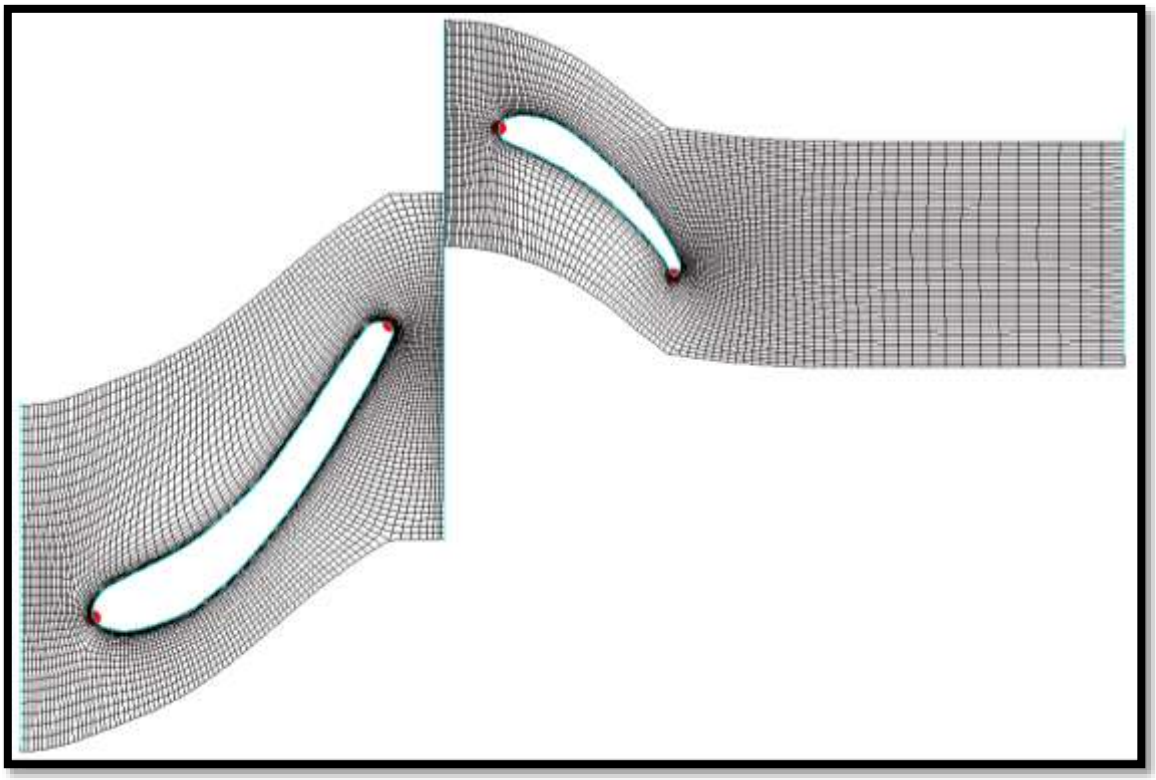

Figure 3-15: Turbine blade-to-blade view at 50% blade height.

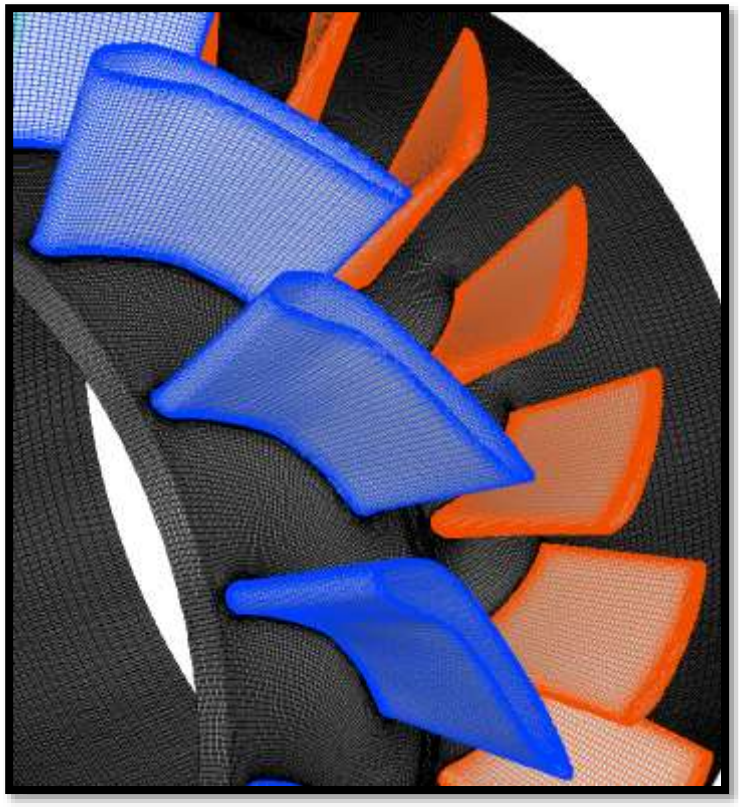

Figure 3-16: 3D turbine blade mesh.

3.3.5 Outlet domain mesh

The outlet region, containing the nozzle, was meshed in Hexpress Hybrid. The region surrounding the nozzle was refined to be able to capture a shock in this region. A shock can be expected here because the nozzle is used to choke the flow to limit the velocity and thus also the mass flow through the engine. This will generally happen at rotational speeds higher than the design speed to prevent engine damage due to over-speeding. The mesh for the outlet and nozzle is shown in Figure 3-17 and will henceforth be referred to as the outlet.

The mesh of the outlet domain was fine enough to capture the shock outside of the nozzle as shown by the boundary condition study done in Section 3.4.4.

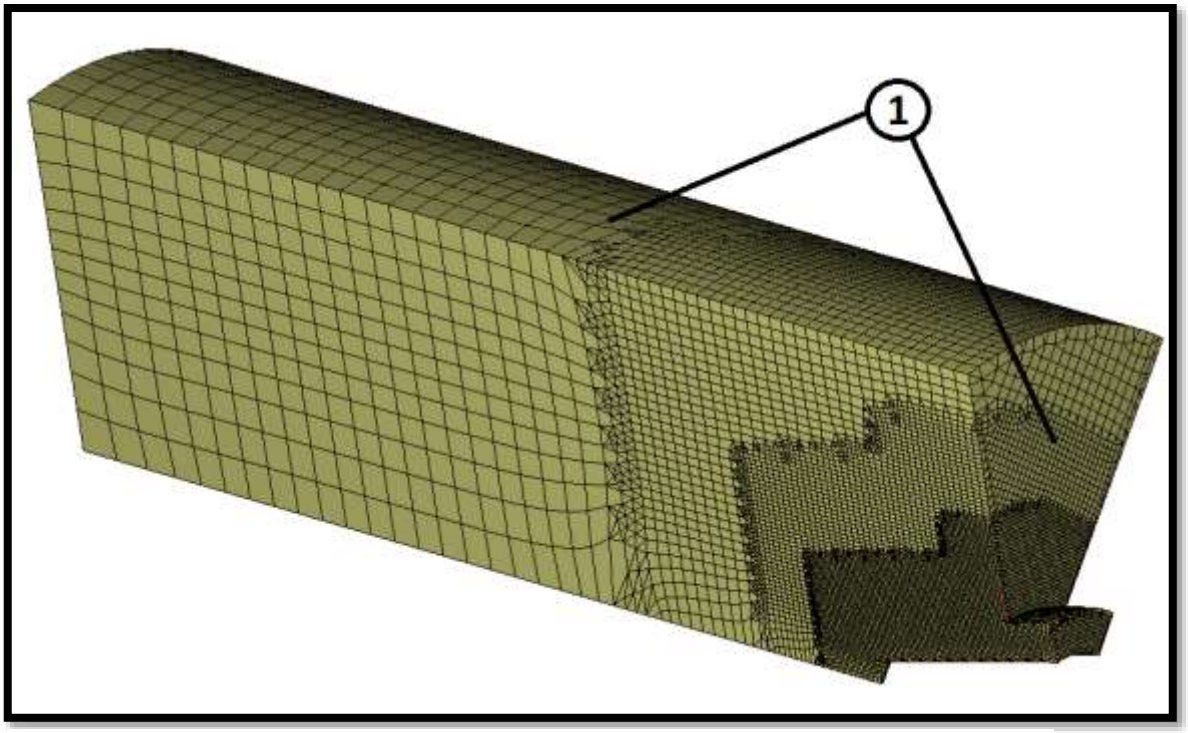

Figure 3-17: Outlet domain mesh.

3.3.6 Combustor mesh interfaces

The compressor and turbine mesh at their internal mesh block connections were automatically made so that the mesh is of comparable size. Having a significant increase in the mesh size when going from one domain to the next will induce similar errors as those induced when having a too large expansion ratio. It was thus a trade-off between adding cells and allowing a reasonable size difference between the connected block cells expansion ratio to minimize the simulation time and RAM requirements caused by adding cells.

Figure 3-18 shows the deswirler and combustor mesh at the mesh block interface.

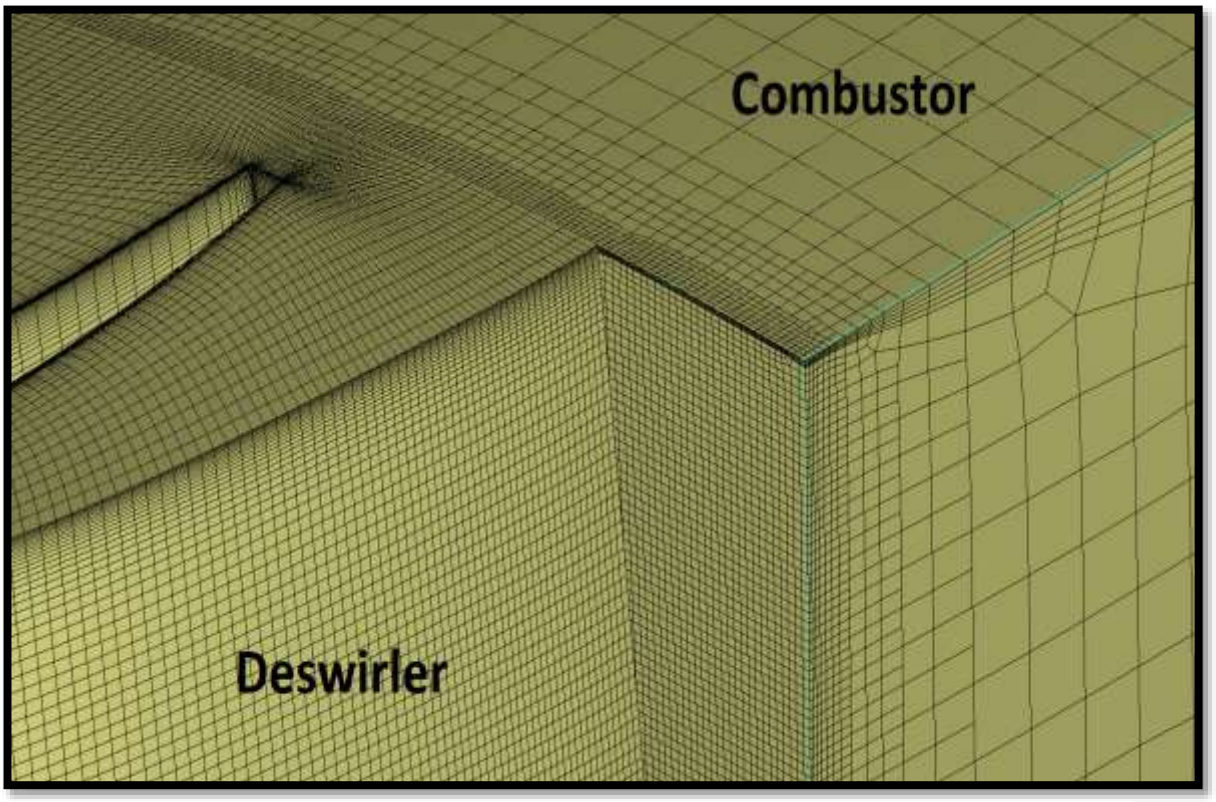

Figure 3-18: Compressor-combustor mesh interface.

It was found that if the mesh at the combustor inlet did not have a similar size as that of the deswirler outlet mesh, the solver would crash due to having too little resolution in the solution on the combustor inlet. As a result, the mesh at the combustor inlet was fine.

Figure 3-18 shows that the meshes on both blocks were of comparable size except at the hub and shroud walls where the deswirler has finer boundary layers than that of the combustor. Fine boundary layers were not required in the combustor because it would drastically increase the number of mesh cells without having a significant contribution to the accuracy of the simulation. This is, firstly, because the significant flow characteristics in the combustor are the swirling and separated flow required for mixing the fuel with air and the hot and cold air and, secondly, because the flow in the combustor was slow compared to the flow speed in the compressor the combustor did not require fine boundary layers. The boundary layer mesh is still important and cannot be neglected because it creates blockage in the annulus which affects how much flow passes through each row of holes in the combustor liner. Because of the above arguments and both mesh domains having an acceptable Y+ of below 10 as shown in Section 3.4.2, this interface was found to be acceptable.

Figure 3-19 shows the NGV and combustor mesh at the mesh block interface. It is clear that the NGV and the combustor have comparable mesh sizes at their interface. The combustor does not have a boundary layer mesh as fine as that of the NGV mesh at the interface because of the same reasons presented at the deswirler-combustor interface.

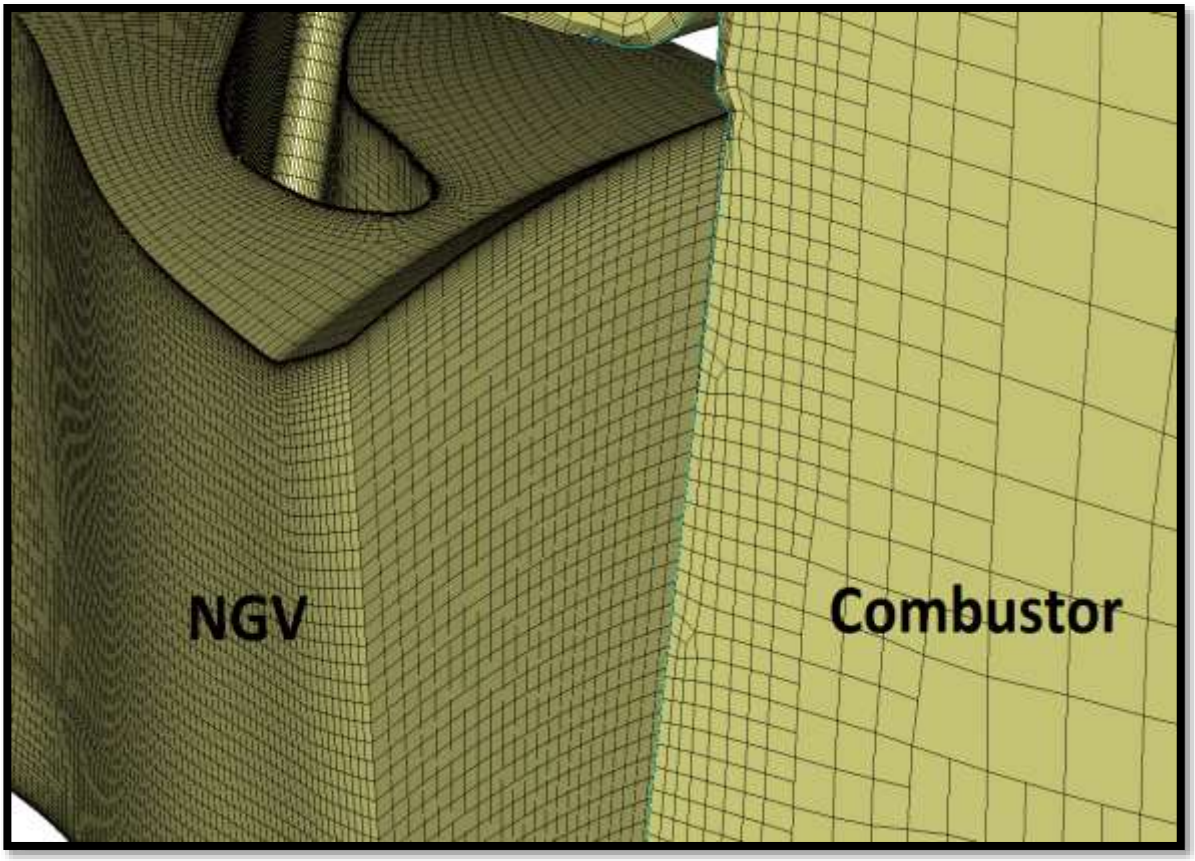

Figure 3-20: Turbine-combustor mesh interface.

Figure 3-20 shows the turbine rotor and outlet mesh at the mesh block interface. It is clear that the mesh on the rotor is finer than that of the outlet. Comparing the cell heights in the centre of the interface showed that the mesh elements on the outlet are four times larger than the mesh elements on the rotor. This is less than 20, which is acceptable according to the software user guide ("USERGUIDE FINE™/Open with OpenLabs™ 6.2", 2018).

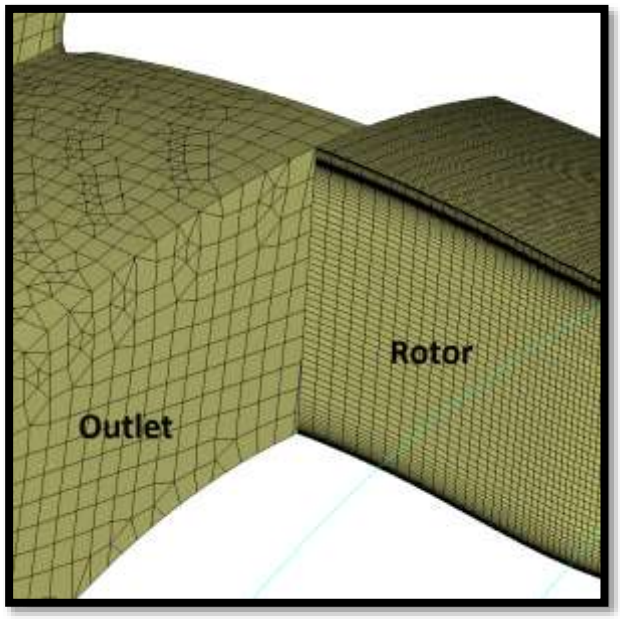

Figure 3-19: Turbine rotor-outlet mesh interface.

3.3.7 Mesh summary

Table 3-1 lists the number of cells in each mesh block as well as the periodicity of each mesh block.

Table 3-1: Cells per mesh block.

Component	Number of cells	Periodicity applied	
Compressor	2 281 599	Impeller	7
		Diffuser	15
		Deswirler	42
Combustor	2 047 135		12
Turbine	946 080	NGV	15
		Rotor	23
Outlet domain	124 954		8
Complete mesh	5 399 768		

From Table 3-1 it is clear that the mesh was large and most of the mesh elements were in the compressor and combustor. Simulating the components using periodic boundary conditions greatly reduced the mesh elements required for the simulation. Note that periodic boundary conditions were used and not mirror or any other similar boundary condition.

The mesh quality met the mesh requirements of the Numeca FineOpen solver which was as follows ("USERGUIDE FINE™/Open with OpenLabs™ 6.2", 2018):

- Minimum skewness > 15^0
- Average skewness > 75^0
- Maximum aspect ratio < 2000
- Maximum expansion ratio < 5

No mesh independence study was done because the mesh is currently as fine as possible, considering the RAM constraints on the project as discussed in Section 3.3.1. Rather than a mesh independence study, the following was used to ensure that the mesh is of high quality:

1. The mesh was generated in line with the best practices for simulating turbomachinery and from meshed components that were found to be sufficiently refined (Sideroff, n.d.; Visavale, n.d.; Dunham & Meauze, 1998; Dunn et al., 2009; "Best practice guidelines for turbomachinery CFD", 2015; "USERGUIDE FINE™/Open with OpenLabs™ 6.2", 2018).
2. For a similar sized micro gas turbine, it was found that a mesh of 600'000, 3'500'000 and 9'000'000 cells calculated almost the exact same values for the thrust, mass flow and torques at 120 kRPM which resulted in Trebunskikh, Ivanov & Dumnov using the 600'000 cell mesh (Trebunskikh et al., n.d.). The study by Trebunskikh et al. resolved the boundary layers with wall functions but the simulations run in this study solve the boundary layer which meant that the mesh would be larger than 600'000 cells. The base mesh of both studies was of comparable size.

A domain extent study was not done because of the following:

1. The distance of the inlet upstream of the compressor was according to best practices because it was two times the height of the impeller blade.
2. The outlet domain proved that it could capture a shock as shown in Section 3.4.4. This is sufficient because the main reason why the outlet domain was included in the simulation was to capture the shock at the nozzle outlet.

3.4 SIMULATION SETUP

The Numeca FineOpen simulation platform was used for the simulations of this study. This section covers how the steady simulation was set up to deliver the results by following the step-by-step process as set out by FineOpen. The process commences with specifying the fluid properties and models, followed by the boundary conditions and initial conditions of the simulation with the final step being to set the numerical parameters and computation control variables.

3.4.1 Fluid properties used in the simulation

The micro gas turbine was modelled using a steady state simulation and real gas properties. Real gas properties were used because they most accurately model the fluid as it allows the properties to be functions of temperature. The air properties downstream of the combustor was modelled as burnt air (Walsh & Fletcher, 2004) in order to take the change in fluid properties into account which is caused by burning fuel in the presence of air in the combustor. Figure 3-21 and Figure 3-22 show the fluid properties used in the simulation.

The properties of air used in the simulation were the default air properties provided by Numeca. All air properties, apart from the gas constant which was a constant, were specified as a piecewise-linear profile as a function of temperature and can be found in APPENDIX A This was the most realistic and accurate fluid model for air within FineOpen.

The gas properties used for burnt air were those used in industry by gas turbine design teams (Walsh & Fletcher, 2004). Not a lot of information on the material properties of burnt air is available because these properties depend on the composition of the burnt air which is determined by several factors such as the type of fuel used, amount of fuel used as well as how complete the combustion process was. Due to the lack of gas properties for burnt air, only the specific heat was defined using a piecewise-linear profile. The heat conduction was defined using a constant Prandtl number while the viscosity was defined using the Sutherland Law as defined in Figure 3-22. As with air, the gas constant was a constant.

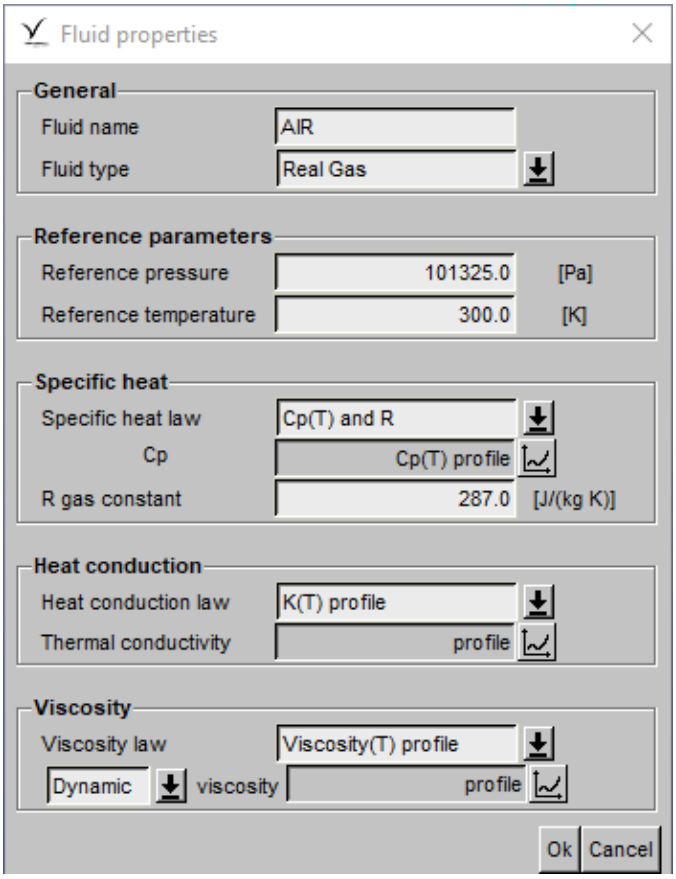

Figure 3-21: Fluid properties of air.

It should be noted that the gas constant is dependent on temperature, but this could not be incorporated into the FineOpen fluid model because it only accepts a constant value. This meant that the simulation would not be able to predict the Mach number accurately, the reason being that the gas constant is used to determine the speed of sound in the fluid as per Eq. 3-1 which is then used in Eq. 3-2 to calculate the Mach number. Because the Mach number dictates where the flow chokes (at Mach 1), this flow phenomenon would also not be predicted accurately. This was a limitation of the flow solver being used and will be taken into consideration when interpreting the results (Korpela, 2011).

$$c = \sqrt{\gamma R T} \qquad \textit{Eq. 3-1}$$

$$M = \frac{V}{c} \qquad \textit{Eq. 3-2}$$

With:

- M: Mach number
- V: Flow velocity magnitude [m/s]
- c: Speed of sound in fluid [m/s]
- γ: Specific heat ratio
- R: Gas constant [J/kg.K]
- T: Temperature, static [K]

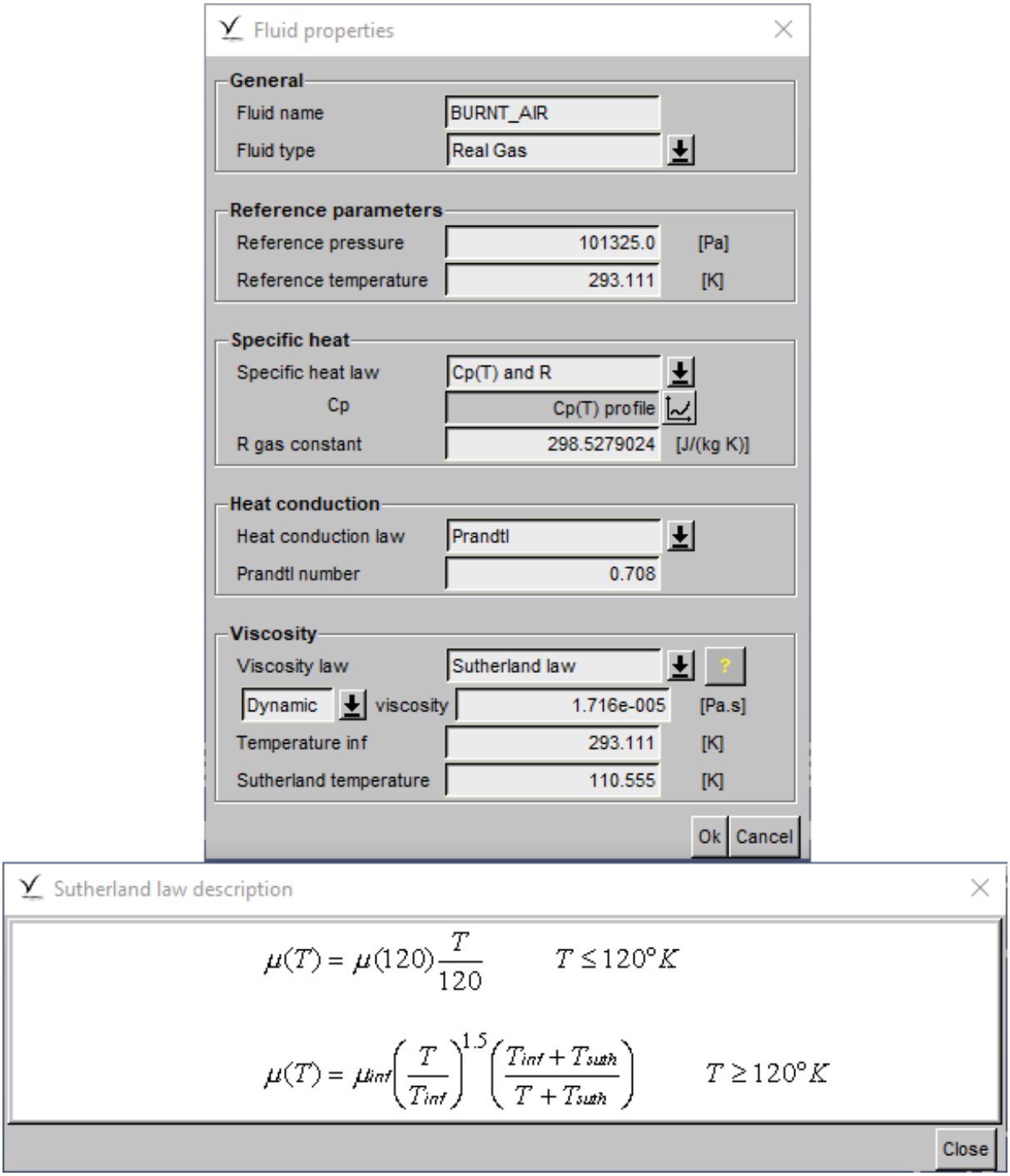

Figure 3-22: Fluid properties of burnt air.

To minimise the loss in accuracy in the simulations, the gas constants for air and burnt air was selected as follows.

Air: The default gas constant was used for air since the temperature change in the compressor was not expected to be high while it was also unlikely that the flow will choke in the diffuser or deswirler of the compressor. This was because the flow is slowed down in the diffuser flow passages rather than accelerated as it would be the case in the turbine.
Additionally, because the flow in the compressor tends to separate as a result of adverse pressure gradients, it is unlikely that the compressor was designed to choke amidst these flow features.

Burnt air: Because it is expected that the flow will choke in either the NGV or in the nozzle, the gas constant at the average temperatures in this region was used. The average temperature was determined from the turbine component simulation to be 1015K.

The Prandtl number is a dimensionless number comparing momentum diffusivity with thermal diffusivity and describes the relative thickness of the velocity and thermal boundary layers. The Prandtl number was specified for the simulation to be a constant for burnt air while in reality, the Prandtl number is dependent on both temperature and pressure. The Prandtl number is, however, almost constant in the temperature and pressure range encountered in the micro gas turbine. Figure 3-23 shows a plot of the Prandtl number for air at various absolute pressures plotted against temperature (ÇENGEL & GHAJAR, 2015; "Engineering Toolbox. Air - Prandtl Number", 2018). Note that the atmospheric temperature and the turbine inlet temperature is indicated in Figure 3-23 and the total-to-static pressure ratio of the compressor was designed to be between 2.62 and 3.65, depending on the version of the BMT 120 KS engine considered (Oppong, 2016). It can then be concluded that no

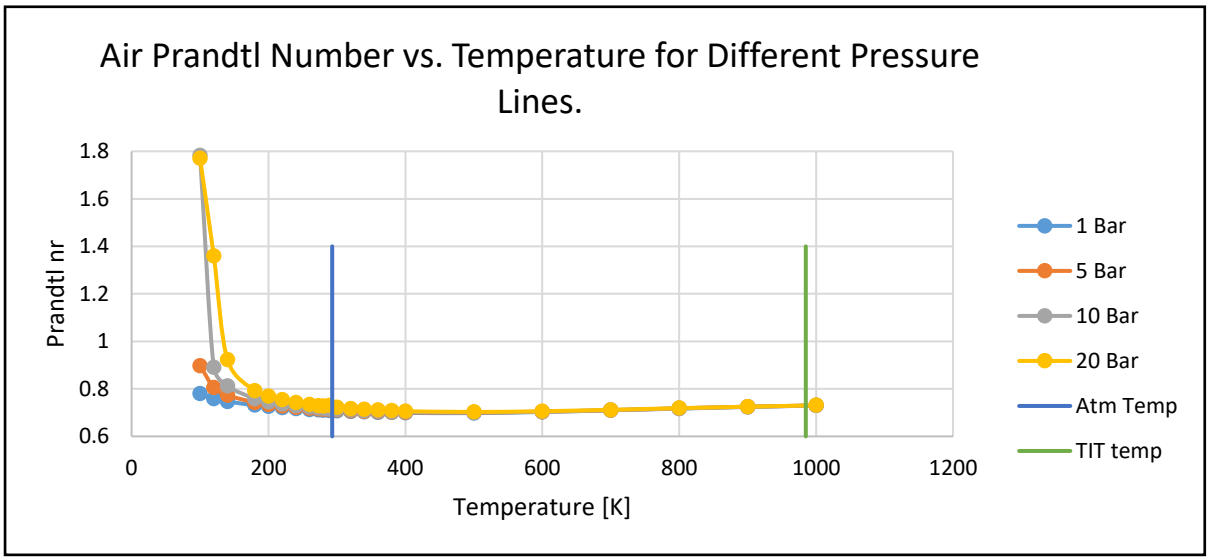

Figure 3-23: Pressure and temperature effects on Prandtl number (ÇENGEL & GHAJAR, 2015; "Engineering Toolbox. Air - Prandtl Number", 2018).

significant change in the Prandtl number will occur in the simulation because the 1 bar and 5 bar pressure lines are identical and remain almost constant above atmospheric temperatures.

The Prandtl number and the viscosity inputs used for burnt air (Figure 3-22) was close to that of air. This is because the fuel mass flow rate of 0.005 kg/s is small compared to the 0.288 kg/s of air flowing through the engine.

The Sutherland law for viscosity with 3 coefficients was used as indicated in Figure 3-22. This law calculates the viscosity of the fluid based on the fluid temperature. This method will be more accurate than a constant viscosity but less accurate than a piecewise-linear curve using experimental data because the viscosity is dependent on the temperature. The Sutherland law was chosen because of lacking experimental data. This law is based on the kinematic theory of ideal gasses and an idealised intermolecular-force potential. It most often gives fairly accurate results with errors less than a few percent over a wide range of temperatures (Sutherland, 1893; "Sutherland's law", 2008).

The material properties that were used for the simulation were thus as accurate as possible, keeping in mind the complexities of combustion and the properties of burnt air. The material properties matched those that were used to design compressors and turbines in industry (Walsh & Fletcher, 2004).

3.4.2 Turbulence model

The turbulent Navier-Stokes equations were solved for the simulation. The reason for this being that the Reynolds numbers in the simulation are of the order of 10^5 and the flow encounters several blades, steps and recirculation zones along its flow path with jets of air flowing through the combustor liner which would result in turbulent flow throughout the micro gas turbine.

The study by Dunn et al. (2009) concluded that none of the current turbulence models was able to accurately capture the velocities in a turbine. The Baldwin-Lomax and the two equation SST k-ω model were slightly more accurate than the other models, but still not close enough to the experimental results. It was also found that using a two-equation turbulence model did not improve the accuracy by a comparable margin when looking at the increase in the computational time from a one equation to a two-equation model.

Because of simulation time and RAM limitations as discussed earlier, a one equation RANS model was preferred to other multi-equation RANS models because it reduced the simulation time and RAM requirements of the computer.

Taking the above into account, it is clear that using a two-equation model would not increase the accuracy sufficiently to justify the increase in simulation time and RAM requirements. FineOpen does not have the Baldwin-Lomax model, therefore the Spalart-Allmaras model was used to model turbulence in the flow. The extended wall function was not activated because this destabilised the simulation and caused the flow solver to crash. Unless required by the

Y+ criterion, no other modelling features were considered to be added to the Spalart-Allmaras model because this would increase the computational time and RAM requirements. Table 3-2 gives the Y+ values for each subcomponent in the simulation.

Table 3-2: Y+ considerations for the turbulence model.

Component		**Average Y+ (100'000 RPM)**
Compressor	Impeller	3.4
	Diffuser	4.8
	Deswirler	3.4
Combustor		8.5
Turbine	NGV	2.2
	Rotor	1.9
Outlet domain		30.9

It should be noted that the Spalart-Allmaras model requires a Y+ smaller than 10 while the Spalart-Allmaras model with an extended wall function for design-cycle analysis, requires a Y+ of between 20 and 50 ("USERGUIDE FINE™/Open with OpenLabs™ 6.2", 2018). The Y+ values given in Table 3-2 dictated that the extended wall function Spalart-Allmaras turbulence model had to be used for simulation of the outlet domain. The Y+ would change as the rotational velocity changes because it causes the flow to speed up, but it is not expected to have a noticeable impact on the results.

3.4.3 Modelling combustion

The BMT 120 KS engine was controlled by its control unit. This unit would, among other tasks, control the amount of fuel delivered to the fuel supply port on the engine. By doing this, the control unit controls the engine speed, as discussed in Section 5.1. The fuel entering the engine through its fuel supply port is delivered to the vaporiser tubes by the fuel delivery tubes shown in Figure 3-24. The fuel flowing through the fuel delivery tubes is heated by the combustion process taking place in the combustion chamber but only evaporates as the fluid travels down the vaporiser tubes. The evaporated fuel and air mixture then leaves the vaporiser tubes and enter the primary combustion zone where it is ignited by the glow plug when starting the engine up. Once the engine is started, the fuel rich flow leaving the vaporiser tubes is ignited by the flames in the primary combustion zone.

As mentioned in Section 3.4.1, combustion is a complex process to model, therefore combustion was modelled by defining a heat source in the combustor domain. Two methods were used; the first being to apply a global heat source to the entire combustor domain. The second method was to apply the heat source in the primary combustion zone where fuel burns between the inner and outer combustor liners. The region where heat was added in the primary zone is indicated by the grey cylinder in Figure 3-25. The cylinder was chosen

because the 2 options were either a cylinder or a sphere and the former enclosed a bigger section of the primary combustion zone. A semi-cylinder with a hollow core would be the best fit because the entire region where combustion takes place would then be enclosed by the semi-cylinder. This would then heat up a larger area in the combustor resulting in a lower maximum temperature in the combustor which is caused by adding heat very concentrated.

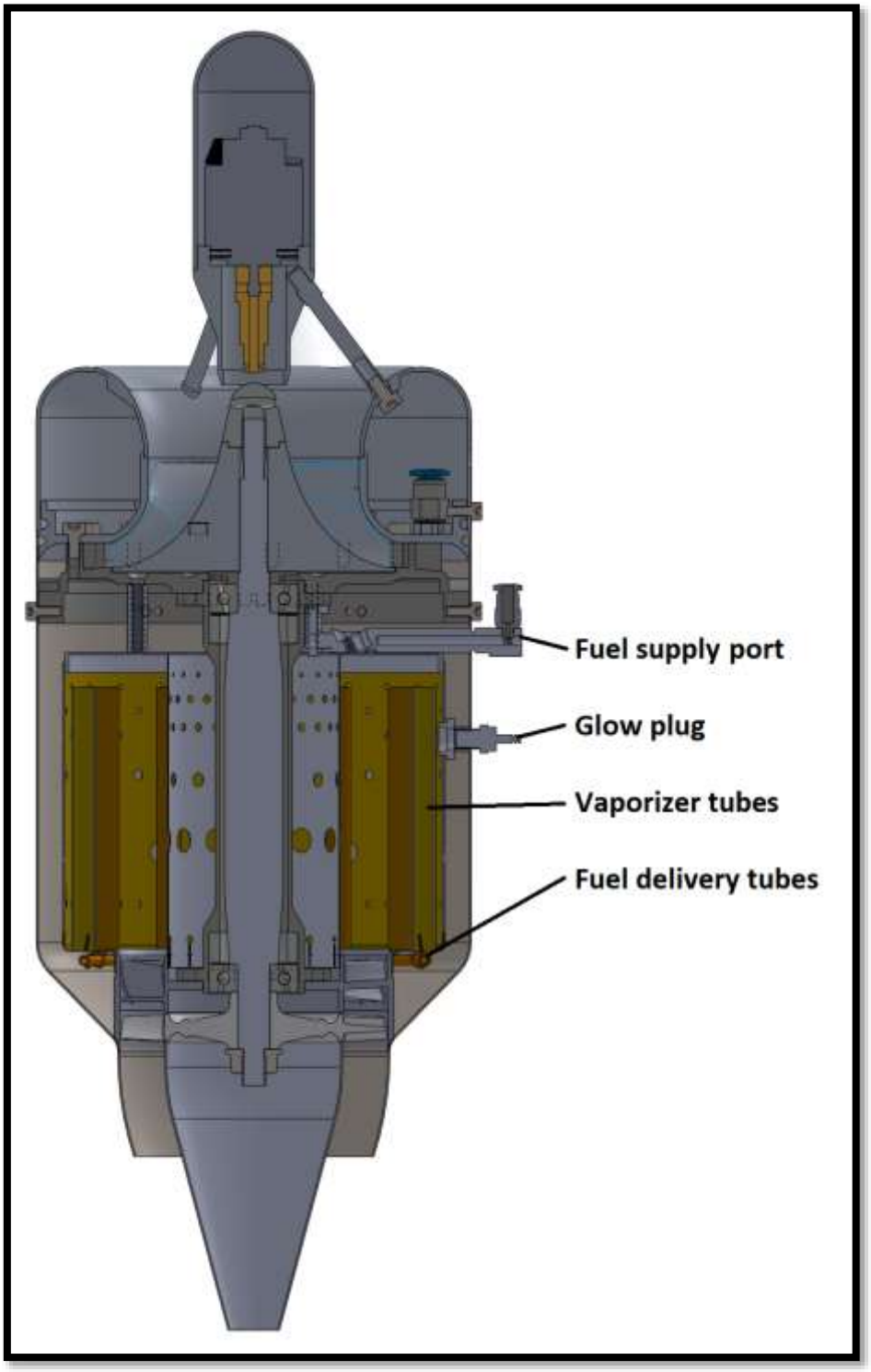

Figure 3-24: Combustion chamber's fuel delivery components.

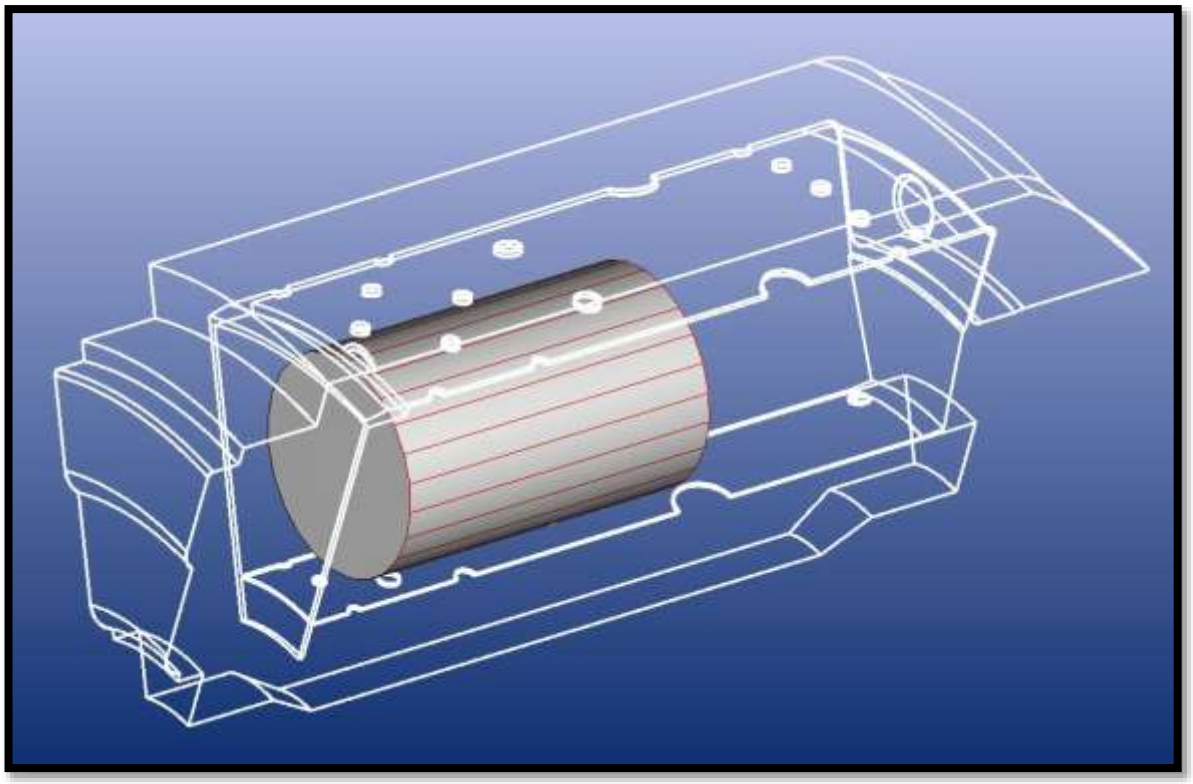

Figure 3-25: Primary zone heat addition zone.

The magnitude of the heat source was adjusted so that the exhaust gas temperature (EGT) of the simulations matched the EGT listed in the experimental results of Krige (2013). The EGT was used rather than the turbine inlet temperature (TIT) because the EGT was the only temperature measurement made by Krige (2013) downstream of the combustor. This is not ideal because the EGT is affected by the turbine pressure ratio and mass flow rate. The EGT was measured in the experiments downstream of the turbine rotor and was measured in a similar location in the simulation.

The fuel mass flow rate can also be used to determine how much heat to add to the combustor. To do this, the fuel type and its heating value are required to determine the magnitude of the heat source for a specific fuel mass flow rate. This will not be as accurate as using temperatures (EGT) because using the mass flow assumes that ideal complete combustion takes place which is seldom the case in reality.

Using the measured EGT from the experiments was not ideal since the accuracy of this measurement is unknown. This is because the temperature profile downstream of the combustor varied in both the radial and circumferential directions while the thermocouple measured the temperature at only one unknown location. This meant that the EGT of the simulations and experiments could not be matched exactly but would, however, give a good indication that the simulated and experimental engines had comparable EGTs. Other factors that reduced the accuracy of the temperature measurements include not using radiation shields on not measuring the temperature using a stagnation tube.

3.4.4 Boundary conditions

The mesh domains were connected using rotor/stator interfaces and utilised the full non-matching mixing plane approach to transfer data from one domain to the next. This approach was selected because it was the only way in which domains with non-matching periodicities could be connected. It is also the most complex and complete model available for connecting periodic domains because it does not neglect rotor movement in the connection and precisely conserves mass, momentum and energy through the interface. ("USERGUIDE FINE^{TM}/Open with OpenLabs^{TM} 6.2", 2018).

The total temperature at the inlet to the compressor domain was 10^0C (283 K) and the total pressure 100 kPa. These values are the environmental static temperature and pressure measured in the test facility (Krige, 2013). Applying this boundary condition resulted in modelling the inlet to the engine as realistically as possible when compared to how the environment would act during the experiments. The simulation would adjust the static and dynamic values at the boundary to meet the mass flow and pressure ratio demands of the engine.

The outlet boundary condition of the simulation domain had a static outlet pressure of 100 kPa which represents atmospheric pressure in the test facility (Krige, 2013).

The kerosene fuel added to the combustor was modelled by adding a total fuel mass flow of 0.005 kg/s through the tips of the fuel tubes. This is the fuel mass flow specified by GasTurb for the micro gas turbine at design speed with a heat release efficiency of 98% as no additional information was available regarding the fuel mass flow rate. The fuel flow rate was held constant for all simulations because it is a small value compared to the air mass flow rate and changing it would not affect the results to justify the effort. The fuel mass flow rate used was based on a prediction by GasTurb using a 120 N micro gas turbine at design speed with the GasTurb model having the same performance requirements as that of the BMT 120 KS.

On completion of the simulations, the minimum fuel mass flow rate was calculated based on heat release efficiency, the heat added in the combustor and the heating value for kerosene of 43.12 MJ/kg as specified by GasTurb which was similar to that specified by Farokhi (2014). This showed that the fuel mass flow rate for 80 kRPM should be 0.0032 kg/s and for 120 kRPM should be 0.0058 kg/s. This differed by 1.01% and 0.27%, respectively, from the constant value used in the simulations. Because these differences were small, the constant fuel mass flow rate was deemed suitable for the simulations.

All the walls in the simulation were treated as adiabatic, no-slip walls and it was assumed that a minimal amount of heat escapes from the fluid into the environment through the engine components during steady state operation, as per convention.

A rotational velocity was specified for the impeller and rotor hub, blade and mesh block to model the rotating components. The rotational velocity of the mesh block was required by the solver because the flow in the rotating mesh blocks are solved in a relative frame of reference.

When specifying the boundary conditions on the two faces indicated by ① on the outlet domain in Figure 3-17, three types of boundary conditions were considered:

1. External boundary condition.
2. Inlet boundary condition at atmospheric conditions.
3. Slip wall boundary condition.

The first boundary condition would be the most accurate but it required a large domain that extends far enough from the nozzle so that the flow from the nozzle dissipates before reaching the boundary. The large domain that this boundary condition requires was not used due to the increased mesh elements related to a larger domain and the RAM limitations of the project.

The inlet boundary condition was considered because the flow leaving the nozzle would drag the surrounding fluid along with it causing these surfaces to act like inlets. The disadvantage of having these surfaces as inlets was that the flow leaving the nozzle had residual swirl from the turbine as seen in Table 6-12, Section 6.4, and caused the mass flow rate residual plots to oscillate sporadically. These oscillations were large and made the mass flow residual plots meaningless since it could not indicate when the mass flow rate has converged.

The slip wall boundary conditions were considered because it would prevent the mass flow from oscillating, but it does introduce recirculation zones above the nozzle outlet. To determine the effect of using slip wall boundary conditions, it was compared to the inlet boundary condition.

Straight and swirling flow through the nozzle was investigated for the two boundary conditions with the swirl angles selected to be 0^0, 10^0 and 20^0 and so that the fluid velocity was 0^0, 10^0 and 20^0 from the axial direction. This was selected because the swirl angle at the pitch line (half-way between the hub and shroud) should be less than 20^0 according to best design practices to limit the downstream losses (Walsh & Fletcher, 2004). The simulation was pressure driven so that a shock would form to choke the flow as this would be the most complex flow to solve for the micro gas turbine. The results are shown graphically in Figure 3-26 and Figure 3-27 and are tabulated in Table 3-3.

Table 3-3: Comparing simulation results for outlet domain.

Nozzle simulated	Mass flow [kg/s]			Percentage difference		
	0^0 Swirl	10^0 Swirl	20^0 Swirl	0^0 Swirl	10^0 Swirl	20^0 Swirl
Inlet boundary conditions	0.0466	0.0462	0.0446	-	-	-
Wall boundary conditions	0.0465	0.0467	0.0452	0.21%	1.08%	1.35%

From Table 3-3 it is clear that the mass flow difference was negligible when simulating the outlet domain as having either inlets or walls. It was also found that the outlet domain was a requirement when capturing a shock because the shock forms outside the nozzle as shown in Figure 3-27.

The shock generated by the flow for the wall and inlet boundary condition simulations were compared using the no swirl simulation. The results are shown in Figure 3-26 and Figure 3-27.

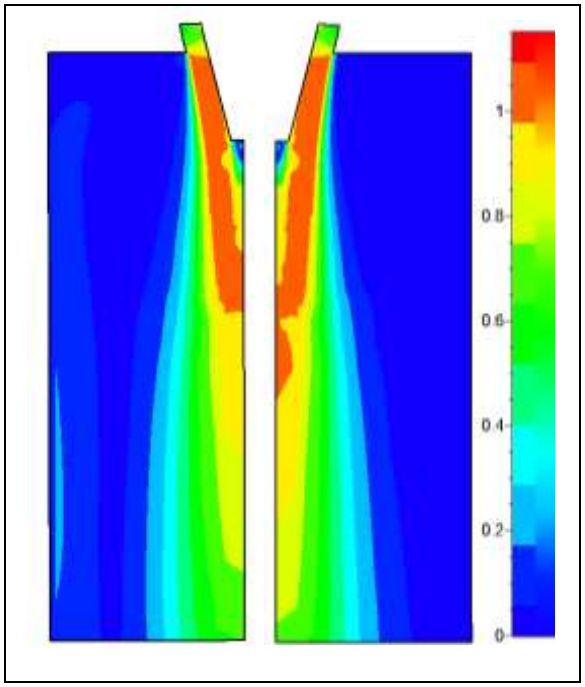

Figure 3-26: Full Mach number plot for different boundary conditions on the outlet domain.

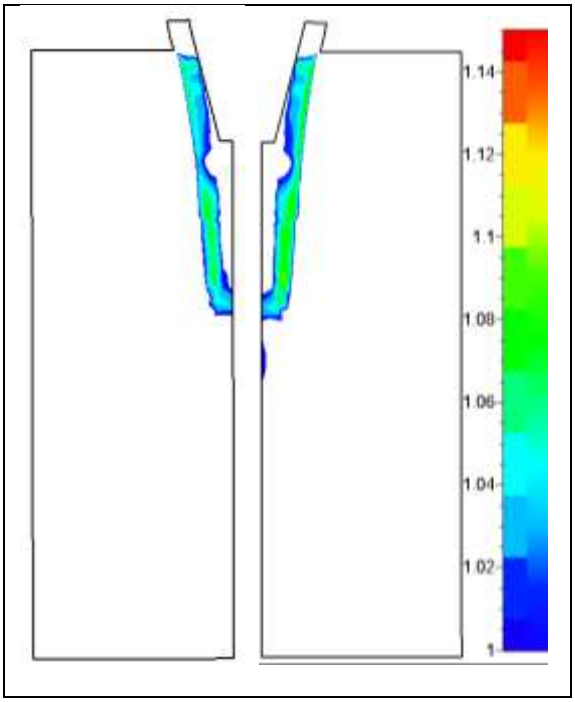

Figure 3-27: Limited Mach number plot for different boundary conditions on the outlet domain.

It is clear that both simulations captured almost the exact same shock up to approximately halfway into the domain. This means that simulating with wall or inlet boundary conditions would have a minimal effect on the flow solution through the micro gas turbine but will resolve the sporadic oscillating residual and mass flow plots.

3.4.5 Initialising the solution

The initial solution was set to be zero because this resulted in the flow solver giving the least amount of problems. It was attempted to initialise the flow from a file, turbomachine initialisation and best guessed constant values, but these methods caused the flow solver to crash. This happened because when initialising from a file, the mesh blocks were not identical to each other as required and the complexity of the flow could not be captured with constant best-guessed values.

The zero initial solution was developed into a better initial solution by running the simulation using coarse grid initialisation. This involved using a coarser version of the fine mesh to spread the boundary information faster through the domain while running the solver. This solution was then used to initialise the fine grid simulation and the simulation time was sped up.

Once a converged solution was available, it was used to initialise the subsequent simulations which in turn also expedited the simulation time.

3.4.6 Numerical discretisation schemes

The 2nd order central difference discretisation scheme was used to discretise the turbulent Navier-Stokes equations. The highest accuracy that could be selected was 2nd order and was consequently the preferred choice. This discretisation scheme allowed the use of the CPU booster that speeds up the simulation by scaling the Courant-Friedrichs-Lewy (CFL) number in the domains based on the reference CFL number selected for the domain. When the reference CFL number was too high, the flow solver crashed and consequently required a lower reference CFL number. The reason for the crash was that transonic flow developed at the leading edge of the impeller and in the wedge diffuser as the rotational velocity and mass flow rate increased (Swanson & Turkel, 1990). The reference CFL number was hence significantly reduced as the flow started to choke in these components.

The CFL number dictates the convergence speed as well as the stability of the flow solver that is used to march in time to reach the steady-state, converged solution (Tu et al., 2013; "USERGUIDE FINE^{TM}/Open with OpenLabs^{TM} 6.2", 2018). The CFL number is desired to be as large as possible because the larger the CFL number, the faster the solution converges but it is limited by the stability of the flow solver. When the stability limit is reached, the flow solver crashes which is an indication that the CFL number should be reduced. For the 140 kRPM

operating point, the reference CFL number in the impeller was required to be as low as 0.7 while it is 1000 in the combustor, turbine and nozzle.

The central difference scheme was preferred to the central matrix scheme because the former was more dissipative ("USERGUIDE FINE™/Open with OpenLabs™ 6.2", 2018). This was desirable because the solution was dispersive and required damping to add dissipation to the solution which assists the flow solver with stability.

The Roe upwind scheme was considered as the discretisation scheme for the 120 kRPM and 140 kRPM rotational velocities. The reason being that upwind schemes can capture shock waves without causing oscillations in the solution as a result of their artificial damping (Swanson & Turkel, 1990). This made the flow solver more robust and less prone to crashing because of instabilities attributed to transonic flow when trying to solve a shock wave (Müller, 1990).

The Roe upwind scheme required the CFL number to be the recommended value of 1 in all domains for the stability of the flow solver, greatly increasing the simulation time ("USERGUIDE FINE™/Open with OpenLabs™ 6.2", 2018). The accuracy of this discretisation scheme was forced to be 1st order because of "not a number" residuals in the 1st iteration when using 2nd order discretisation schemes. This may be because of several possibilities including incompatibility with the fully non-matching rotor stator interfaces present in the model or the complex geometry of the micro gas turbine. The use of the 1st order Roe upwind scheme was halted due to its inferior accuracy compared to that of the 2nd order central difference scheme.

1st order schemes yield less accurate results owing to the numerical discretisation error of diffusion, especially when simulating complex flow that is not aligned with the mesh blocks. 2nd order schemes do find it more difficult to converge ("FLUENT 6.3 User's Guide - 25.8.1 First-Order Accuracy vs. Second-Order Accuracy", 2006).

3.4.7 Convergence criterion

Several criteria have to be met for the simulation to be considered as converged. These criteria are:

1. The residual plot is constant or oscillating around a constant value.
2. The pressure ratio over the micro gas turbine remains constant.
3. The inlet and outlet mass flow plots are constant.
4. The difference between the inlet and outlet mass flow rates are approximately 0.1%.

The residual in FineOpen is calculated as flux balance on all the faces of each cell. It should be noted that the residual plot generated by Numeca was normalised by the first residual calculated for the global residual plot. This means that the residual was not referenced to zero, but to how much the variables are changing compared to the first iteration, therefore having a constant residual indicating that the solution has converged as much as possible for

the current mesh. If the residual is required to be lower, a finer mesh had to be used, but this would adversely affect the simulation time and RAM and was therefore not an option.

If the pressure ratio and mass flows are constant over several iterations, the solution has stabilised in the micro gas turbine. To determine if the solution throughout the micro gas turbine is also converged, the difference between the inlet and outlet mass flow rates should be approximately 0.1% for several iterations. The reason why the inlet and outlet mass flow rates should the same is that it is a steady-state simulation with no mass being stored in the micro gas turbine.

The mass flows were matched to 0.1% because the expected range was 0.102 – 0.296 kg/s, according to the experimental rotational velocities. 0.1% of these mass flow rates were between 0.0001 – 0.0003 kg/s which was an order of magnitude less than the least significant digit reported in the experiments. Solving mass flow differences below 0.1% would not add any value to the results.

CHAPTER 4 CFD VALIDATION

This chapter is dedicated to validating the CFD results against the experimental results from Krige (2013). The first sections compare the simulated and experimental results with each other and comment on the differences with the second section comparing the primary heating results with the global heating results. Following this, there is an investigation into whether the matched EGT enabled the simulated micro gas turbine to validly operate at the set rotational velocity. This will be done by examining the power extracted by the turbine and consumed by the compressor. The fourth section of this chapter scrutinises the accuracy of the constant gas constant "R", while the final section contains the summary of this chapter.

The validation of CFD results is necessary because when the simulated and experimental results are similar, the simulations would be able to calculate the performance prediction of the actual engine. These performance predictions can be done at various operating conditions and/or with different component designs and it reduces the time and cost of developing an engine (Slagter, 2011; Ando, 2014; Paquin, 2015). The cost of developing an engine can also be reduced by numerically identifying component mismatches and resolving them by designing new components without the need to manufacture and test each new engine design from scratch.

The experimental results that were used as the baseline to validate the simulations were not perfect, as can be expected. Table 4-1 lists the uncertainty of the measurement equipment used to collect the experimental results (Krige, 2013). The uncertainty in the rotational speed was expected to be within a couple of percentages due to the BMT's Ground Support Unit controlling the speed through the fuel mass flow rate, but this was not quantified. The calibration of all measurement equipment was done by Krige (2013) except for the bell mouth that was used to measure the mass flow rate.

Table 4-1: Uncertainty in the experimental results (Krige, 2013).

Quantity	Uncertainty
Mass flow rate	± 1.20%
Pressure	± 0.30%
Temperature	± 2.2 K (approximately a 0.2% error on 900K)
Thrust	± 0.25%

4.1 SIMULATED RESULTS VS EXPERIMENTAL RESULTS

This section investigates how well the CFD simulations predicted the variables measured in the experiments. The EGT values were made to match and are included to illustrate how close these temperatures were matched. In Figure 4-1 to Figure 4-4, the percentages to the right of the data point are those of the primary zone heating results and the percentages to the left are those of the global heating result.

Note that the simulations were performed at 80 kRPM, 120 kRPM and 140 kRPM while the experimental results only reached speeds up to 125 kRPM. The reason why simulations were run at 140 kRPM was that the future goal of this CFD method is to identify component mismatches in a micro gas turbine. To be able to do this, the simulations would have to solve rotational speeds above the safe operating speed of the engine in order to confirm that the component designed to choke, was choked. If the wrong component chokes, the engine has a component mismatch.

Figure 4-1 shows how closely the EGT of the experiments and simulations are matched by adjusting the magnitude of the heat source.

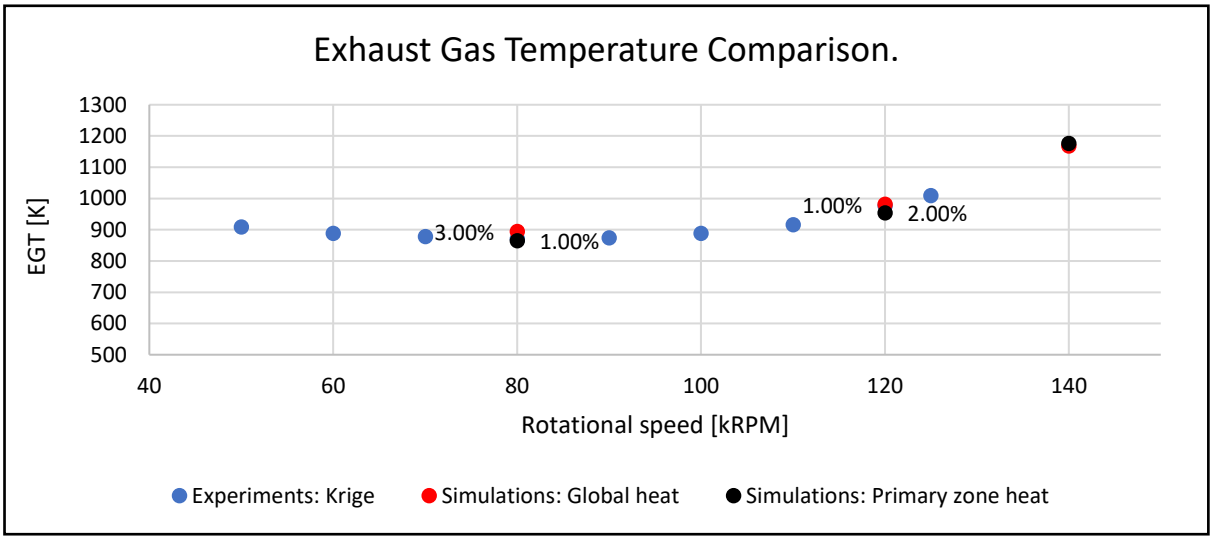

Figure 4-1: EGT comparison between simulated and experimental results.

From Figure 4-1 it is clear that the experimental and simulated results differ by less than 3%. The difference in the EGT values was an order of magnitude larger than the uncertainty in the EGT values. Ideally, the EGT should be matched such that the percentage difference between the experimental and simulated results are approximately the same or less than the uncertainty. This was not done because of the long simulation time:

- Global heating: 12 hours, starting the solution from scratch.
- Primary zone heating: 74 hours, starting from a converged solution at a different heat source magnitude.

Figure 4-2 shows the graphical comparison between the simulated and experimental air mass flow rate results for different rotational speeds.

From Figure 4-2 it is clear that all of the simulations under predicted the mass flow through the engine by a considerable margin and this is discussed in Subsections 4.1.1 and 4.1.2. This margin was an order of magnitude more than the uncertainty in the mass flow rate. The results produced by the primary zone heating method were approximately 9.3% higher than the global heat results.

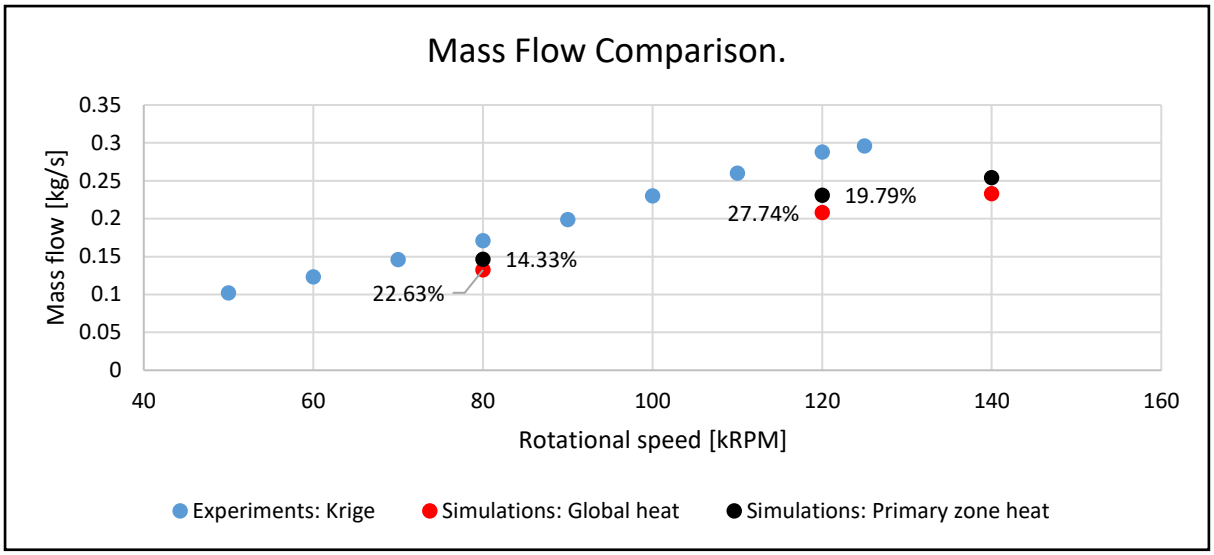

Figure 4-2: Air mass flow rate comparison between simulated and experimental results.

At 80 kRPM, the mass flow results are closer to the experimental results than at 120 kRPM and were most likely caused by neglecting solid mechanics effects and geometrical features in the simulations. The reason for this phenomenon will be discussed together with the pressure ratio results.

Figure 4-3 illustrates the total-to-static pressure ratio which refers to the total atmospheric pressure of 100 kPa as in the experiments (Krige, 2013) and the simulations. The static pressure was measured at the compressor outlet downstream of the deswirler.

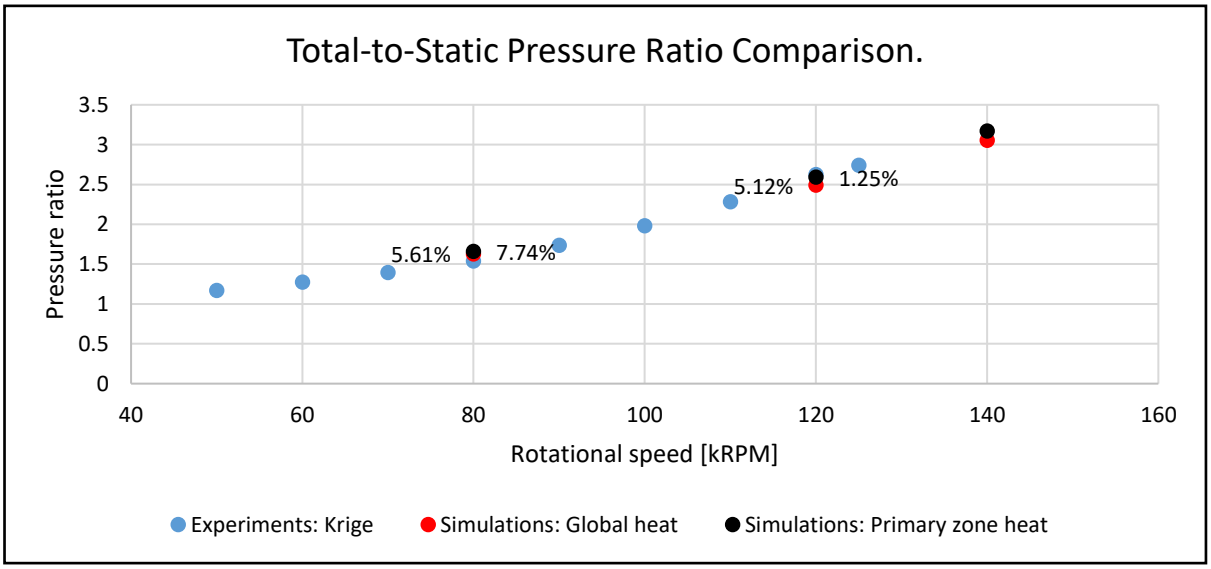

Figure 4-3: Total-to-static pressure ratio comparison between simulated and experimental results.

The primary zone heating predicted higher pressure ratios than the pressure ratio predicted by global heating. It can also be observed that the simulation overpredicted the pressure ratios at low speeds and under predicted them at high speeds. The reason for this can be explained when taking the next three aspects related to the performance of the engine into consideration:

1. The geometrical simplification, mentioned in Section 3.2, included neglecting hub and shroud fillets which induce endwall secondary flow contributing to losses in gas turbines. Therefore, the simulated engine would have fewer losses and perform better than the experimental engine.
2. Blade flapping caused by the high rotational velocities reduces the performance of the actual engine. This means that the experimental results would have more losses than the simulated engine resulting in the simulated engine to perform better.
3. The blades of the rotating components elongate as a result of the centrifugal forces acting on them, in turn, causing the tip gaps to reduce during the experiments. Reducing the tip gap reduces tip leakage and increases the compressor and turbine efficiency exponentially. This is coupled to an increase in mass flow and pressure ratio due to fewer losses (Brasz, 1988). The simulations did not take this phenomenon into account resulting in the underestimation of the mass flow rate and pressure ratio of the engine as the rotational velocity increased. Consequently, the experimental engine will outperform the simulated engine exponentially.

Considering these points, the following trends in Figure 4-2 and Figure 4-3 could be explained:

- At 80 kRPM the pressure ratios were overpredicted because of 1. and 2. causing the simulated engine to outperform the experimental engine. The effect of 3. was too small for the experimental engine to make up the performance difference.
- At 120 kRPM the effect of 3. was significant and caused the experimental engine to outperform the simulated engine even though the experimental engine had more losses than the simulated engine.
- The simulation mass flow results diverge from the experimental results because, as discussed above, the losses and solid mechanic effects of the rotating components were not simulated.

It is also possible that these trends are related to the simulation model or a combination of this and the explanation above.

Figure 4-4 shows the comparison between the experimental and simulated thrust results. The simulated thrust plotted in Figure 4-4 was calculated by Eq. 4-1 (Farokhi, 2014).

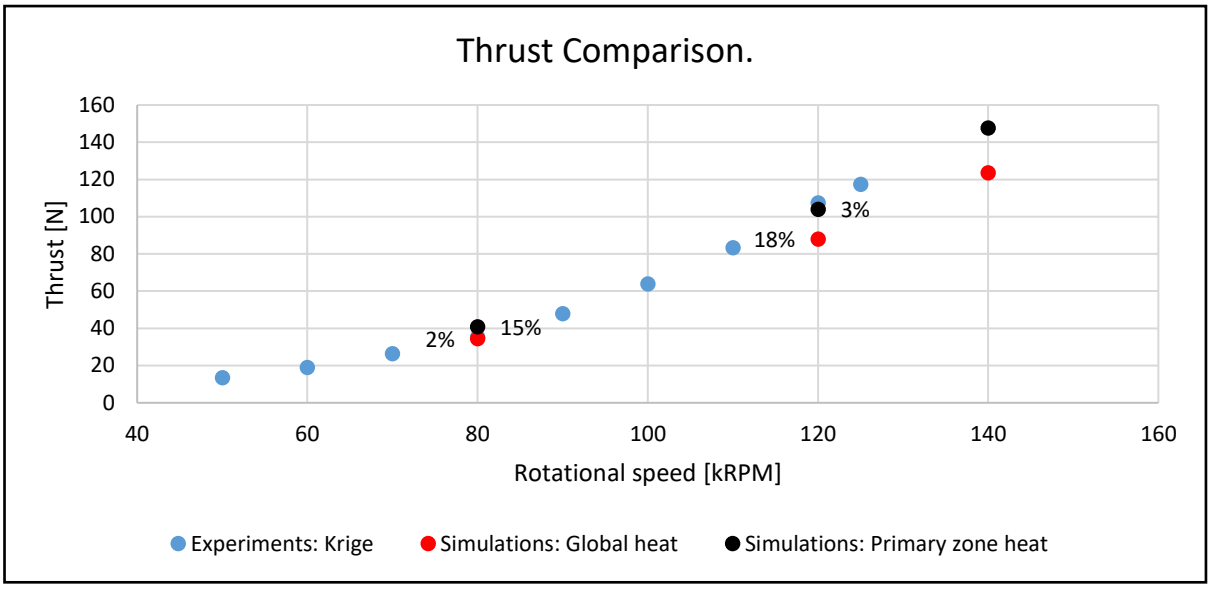

Figure 4-4: Thrust comparison between simulated and experimental results.

$$Thrust = \dot{m}_{nozzle}V_{nozzle} - \dot{m}_{inlet}V_{inlet} + (P_{nozzle} - P_{inlet})A_{Nozzle} \quad Eq.\ 4\text{-}1$$

With:

- $\dot{m}$: Mass flow rate [kg/s].
- V: Velocity [m/s].
- P: Pressure [Pa].
- A: Area [m^2].

From Figure 4-4 it is clear that the experimental and simulated thrust was similar with the exception of the global heat simulation at 120 kRPM. The primary zone heating results were out by 15% at 80 kRPM but was a good indicator of the thrust performance of the engine because the simulated and experimental results only differed by 5 N. The large difference of 15% is a result of the small thrust value at 80 kRPM.

The simulations overpredicted the thrust at low speeds and under predicted them at high speeds as can be seen in Figure 4-4. This was expected because the pressure ratio and thrust are linked by the fraction of the compressor pressure ratio the turbine used and what was left to accelerate the flow through the nozzle. Overpredicting the engine pressure ratio would lead to over predicting the pressure ratio over the nozzle and the simulated engine producing more thrust than the experimental engine did. The same argument can be made when explaining why under predicting the pressure ratio resulted in the thrust being underpredicted as well.

Taking the argument presented above into consideration, the difference between the results produced by the two simulation methods can also be explained since the primary zone heating model predicted a higher pressure ratio and thrust.

4.1.1 Mass flow deficit: Experimental causes

The reason for the mass flow deficit can usually be explained as a combination of experimental and numerical inaccuracies. The experimental inaccuracy is discussed in this subsection and the suggested way forward is also mentioned.

Seeking to find the origin of possible experimental inaccuracies, the results in Section 4.1 were scrutinised. The deficit in the mass flow rate, as seen in Figure 4-2, is in strong contrast with the good thrust results shown in Figure 4-4. If the mass flow rate was underpredicted by between 14.33% and 19.79% for primary zone heating it was expected that the corresponding thrust results would also be significantly underpredicted. However, in Figure 4-4 it can clearly be seen that this was not the case.

This observation is supported by studying the thrust equation in Eq. 4-1 (Farokhi, 2014). Assuming that the pressure difference between the inlet and outlet of the engine are approximately the same since the engine is stationary with an unchoked nozzle, the mass flow rate is directly proportional to the thrust. Consequently, the thrust values calculated from the simulation results should then be approximately 14% and 20% lower than the experimental results, which is not the case. In fact, the thrust values at 80 kRPM were overpredicted.

According to the compressor map in Figure 4-12Figure 4-12, the compressor was operated in the surge region of the map. The results in Section 6.2, however, contradicts this as it indicates that the compressor was not surging. This means that the experimental mass flow rate was probably overestimated.

Taking these arguments into account as well as the fact that the bell mouth inlet was not calibrated for the experiments, it is likely that the experimental mass flow rates were incorrect. Also comparing the results of the study by Trebunskikh et al. (refer to Section 2.6) with this study, it was found that both of the studies predicted accurate results for the pressure ratio and thrust. Where the two studies differed was with the mass flow results. The mass flow results documented in this study was significantly different from the experimental results, while that of Trebunskikh et al. was accurate. Because of this, an investigation into the accuracy of the experimental mass flow measurements should be conducted. This would consist of calibrating the bell mouth inlet and recalculating the experimental mass flow rate using the pressure measurements taken during the experiments.

4.1.2 Mass flow deficit: Numerical causes

Following the discussion on the possible experimental causes of the mass flow deficit, the numerical causes are discussed in this subsection.

Studying numerical causes for the mass flow deficit, it was found that the temperatures in the combustor reached unrealistically high values. The particular zones in question are indicated

in Figure 4-5 using an iso-surface of 2500 K. A temperature of 2500 K was chosen because the flame temperature in the simulations modelling the combustion process was 2400 K, as discussed in Subsection 5.2.1 (Trebunskikh et al., n.d.; Gonzalez et al., 2007).

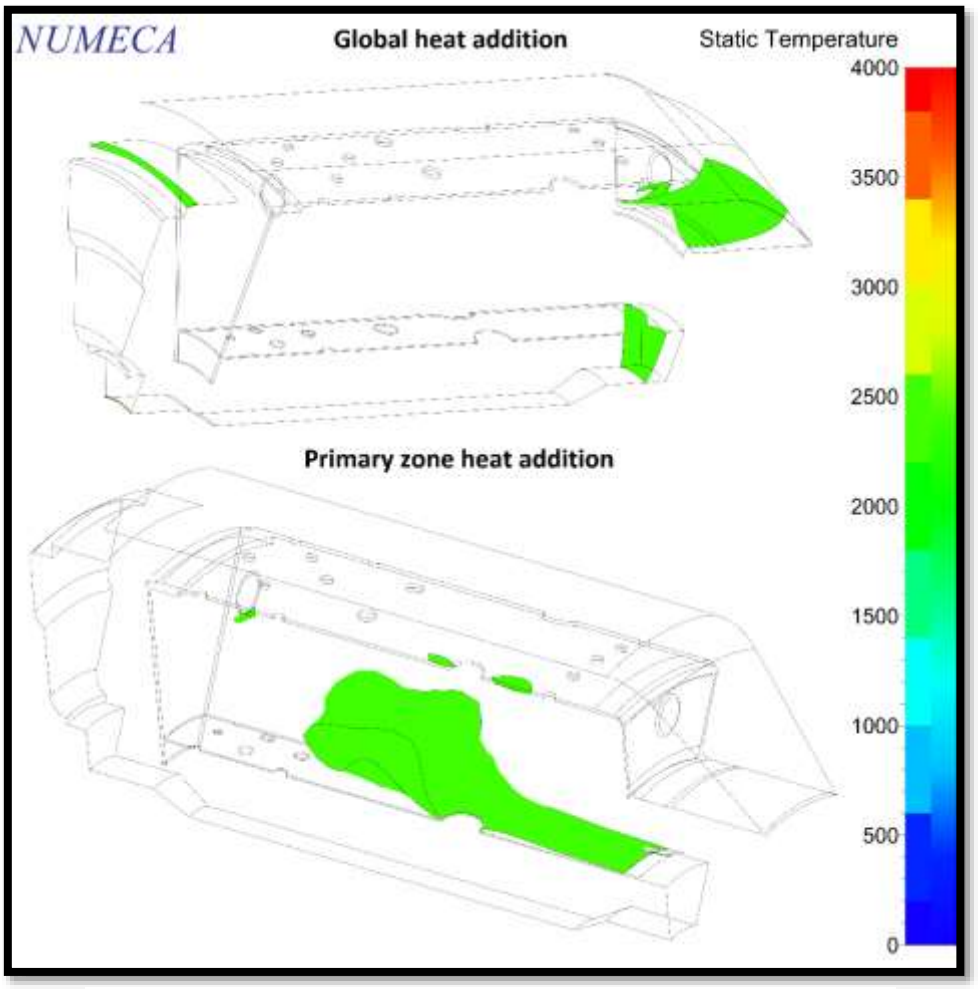

Figure 4-5: Combustor 2500 K iso-surface comparison.

It will be clear from Section 5.2 that these regions have temperature results close to almost double the maximum temperature when simulating combustion of 2400 K and it was caused by the burnt air material properties used for the simulations. To better understand the shortfalls of the burnt air material model, the fluid properties used in the simulation was studied. Figure 4-6 shows the asymptotic burnt air fluid model that was used in the simulation, the exponential burnt air fluid model from Walsh & Fletcher and experimentally recorded C_P values of air (Capitelli et al., 2000).

It should be noted that the asymptotic burnt air model was based on the exponential burnt air model from Walsh & Fletcher but was altered to have an asymptotic characteristic at temperatures above 1800 K. This was required for stability in the simulation since the solver crashed when the exponential material property curve was applied.

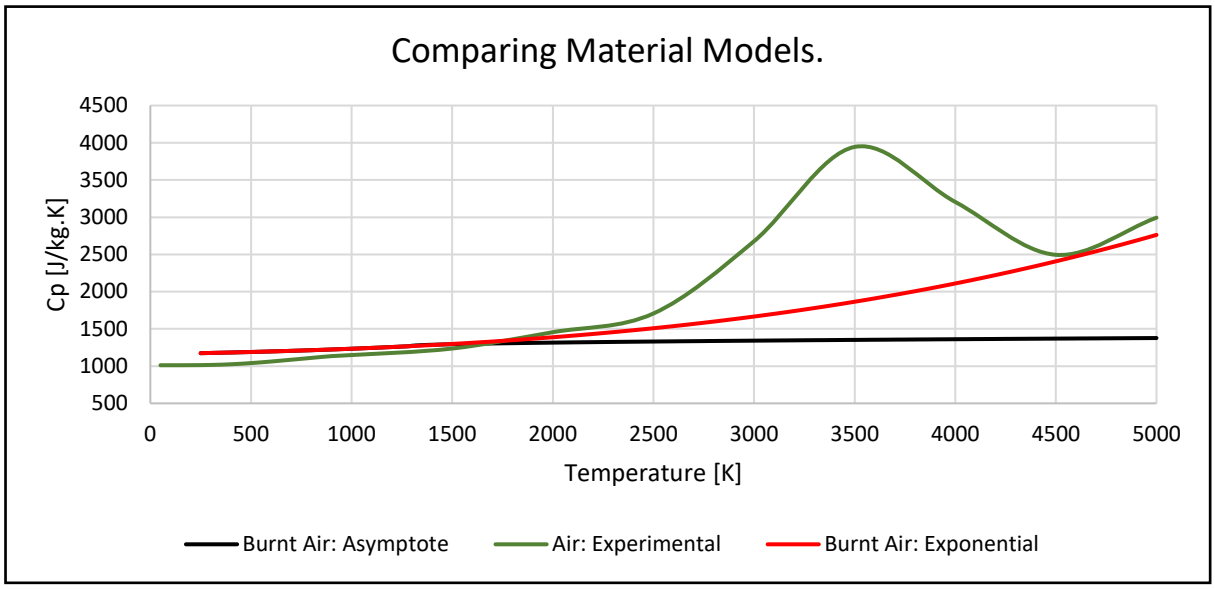

Figure 4-6: Comparison between the burnt air material model and experimentally recorded air properties.

Interpreting Figure 4-6, the following is important with regards to the exponential burnt air model and the experimental air model:

1. The air and burnt air properties cannot be expected to be the same because they have different compositions since kerosene is introduced into the combustor and burnt in the air when running the engine.
2. For the simulated engine at design speed, the fuel to air mass flow rate ratio was 1:47.2. Because of the small amount of fuel that was added in comparison to the mass flow rate of air, it can be expected that the two material models would be relatively similar.
   2.1. This is true for temperatures below 2500 K.
   2.2. The peak in the C_P value of the air between 2500 K and 4500 K was not captured by the burnt air model but should have been at least partially captured in accordance with no 1.

The discrepancy described in no 2.2 means that, for a selected heat transfer rate and mass flow rate, the burnt air model predicts a much higher fluid temperature increase than the air model as indicated in Eq. 4-2 (Farokhi, 2014). This explains the unrealistic temperature zones in Figure 4-5.

$$\dot{Q} = \dot{m} C_P (T_{out} - T_{in}) \qquad \textit{Eq. 4-2}$$

With:

- $\dot{Q}$: Heat transfer rate (source or sink) [W].
- $\dot{m}$: Mass flow rate [kg/s].
- C_P: Specific heat at constant pressure [J/kg.K].
- T_{in}: Temperature before the combustor [K].
- T_{out}: Temperature after the combustor [K].

The consequence of heating the fluid to unrealistically high temperatures is that the pressure ratio across the compressor was overpredicted:

- Heating the fluid in the gas turbine combustor is an isobaric process. This means that the heat addition reduced the density while the pressure stayed approximately constant.
- The heated fluid consequently took up a larger volume and attempted to exit the combustor through both the inlet and outlet.
- The fluid attempting to exit the combustor through the inlet would resist the mass flow rate of the compressor. To overcome this resistance, the compressor had to increase its outlet pressure and thus also its pressure ratio in order to operate at the specified rotational velocity.

To determine if the slightly overpredicted pressure ratio could have such a large effect on the mass flow rate, a compressor map was studied. The reason being that the compressor sets the engine mass flow rate and pressure ratio for every rotational velocity. The engine compressor map was available, but a generic map was preferred for this discussion because it would be clearer compared to the compressor map from Krige (2013), shown in Figure 4-12. The compressor map from Krige (2013) compares well with the shape of the compressor map shown in Figure 4-7 and can be applied to discuss the performance of the BMT 120 KS compressor (Korpela, 2011).

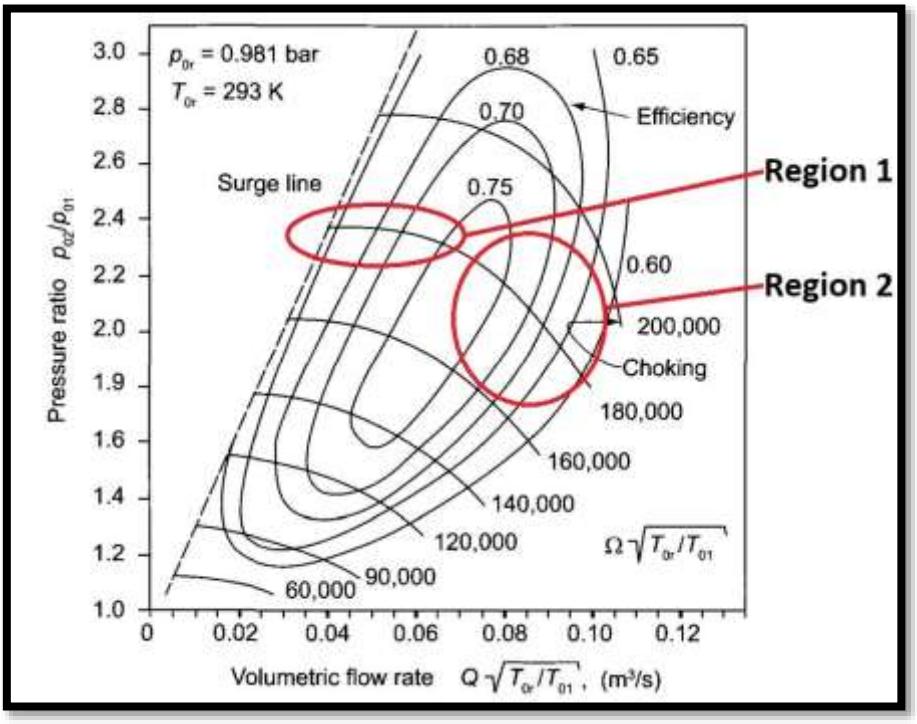

Figure 4-7: Centrifugal compressor map (Korpela, 2011).

The compressor map in Figure 4-7 indicates two regions where the slope of the speed line is noticeably different. From these two regions and the fact that the simulation and experimental results had slightly different pressure ratios and a large difference in mass flow rate, the compressor operated in region 1. This is similar to the indicated engine working line

on the compressor map from Krige, 2013 as indicated in Figure 4-12. This means that the small increase in pressure ratio, caused by having unrealistically high temperatures, can be the reason for the significant difference in the mass flow rate.

The traits in Figure 4-2 can, therefore, be explained based on the size of the unrealistic temperature region and thus the amount of heat added to the combustor. When studying the results of the mass flow simulation as recorded in Figure 4-2, it is clear that the percentage difference between the simulation and experimental results increased from 80 kRPM to 120 kRPM. This difference can be explained by studying the difference in size of the 2500 K iso-surface for primary zone heating, as shown in Figure 4-5 and Figure 4-8. Primary zone heating was chosen because it has a concentrated iso-surface and simplifies the process of comparing the two zones. The same comparison can be made using global heating with the same conclusion as that for primary zone heating, the reason being the increase in both the EGT and heat addition when increasing the operating speed from 80 kRPM to 120 kRPM.

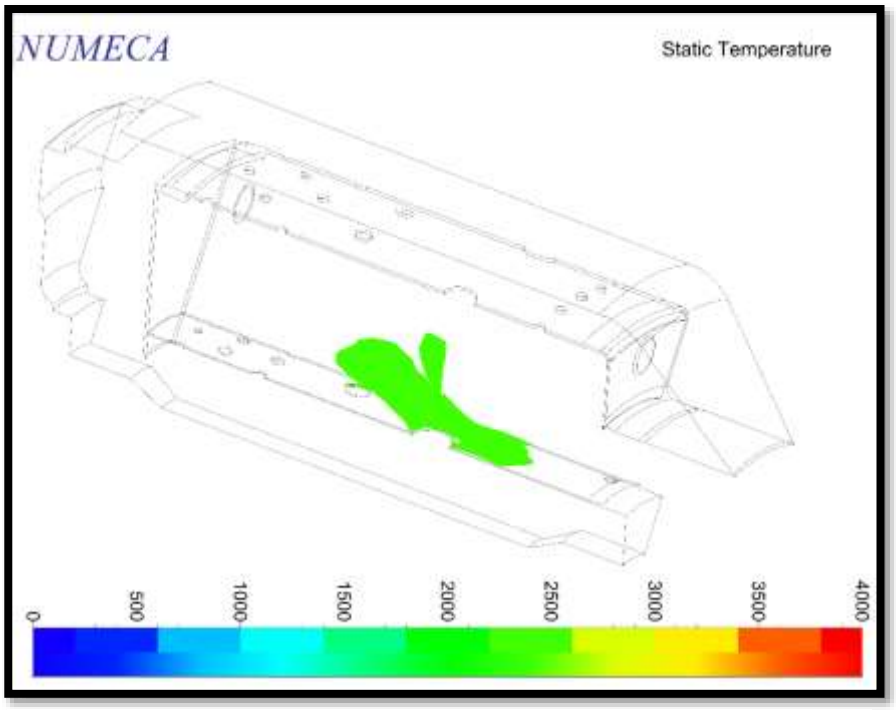

Figure 4-8: 2500 K iso-surface for primary zone heating at 80 kRPM.

It is clear from the comparison between the sizes of the 2500 K iso-surface (Figure 4-5 and Figure 4-8) for primary zone heating, that the 80 kRPM simulations had a smaller unrealistic temperature zone. The unrealistic backpressure would, therefore, be higher for the 120 kRPM simulations and will, in turn, drive the simulation mass flow rate further from the experimental results as the rotational velocity increases. This adds to the effect of the geometrical simplifications and neglecting the solid mechanics of the rotating components as explained in Section 4.1 and caused the experimental and simulated mass flow rates to diverge.

The full non-matching mixing plane approach used to connect the micro gas turbine domains might not be a suitable option when it is located too close to an important flow feature. This was expected to be the case for the interface between the deswirler and the combustor since it was located close to the trailing edge of the deswirler. This concern was investigated because the simulations that were done by Krige (2013) correlated well with the experimental results including the mass flow rate. This lead to the decision to run a compressor only simulation with the following being important:

- Using approximately the same mesh density and structure that were used for the engine simulation with the domain extended to increase the distance between the trailing edge of the deswirler and the outlet.
- Rotational velocity of 80 kRPM.
- The outlet pressure boundary condition was specified as an average static pressure with a magnitude equal to the value calculated in the primary zone heating simulation of 165.8 kPa.

This simulation calculated the mass flow rate as 0.166 kg/s, 2.9% lower than the experimental mass flow rate of 0.171 kg/s. Studying the outlet pressure contour of the compressor and the inlet pressure contour of the combustor for the two heat addition methods and the compressor only simulation, clear differences were noted. These differences are shown in Figure 4-9 where the contours were taken at the same distance behind the trailing edge of the deswirler so that they could be compared without taking their locations into account. Also, note that the top contours were that of the compressor outlet and the bottom contours that of the combustor inlet profile.

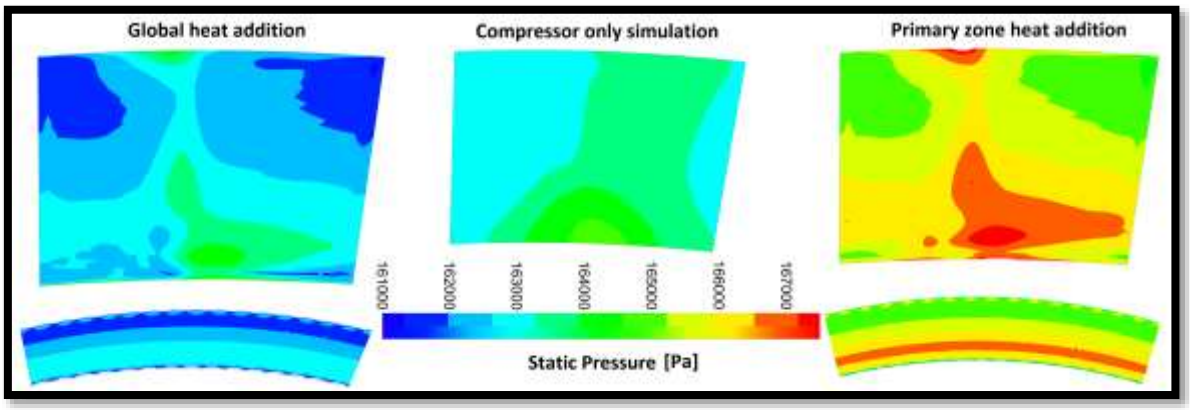

Figure 4-9: Static pressure on compressor outlet and combustor inlet comparison.

The compressor only simulation has a high-pressure column in the centre of the contours from hub to shroud. The full engine simulations had a similar high-pressure column as well as a high-pressure band, horizontally across the outlet, in the tangential direction. Studying the combustor inlet pressure contours it was clear that the pressure was constant in the tangential direction and only varied with the radius. This combustor inlet contours are a result of the full non-matching mixing plane approach averaging the pressure at a given radius (pitchwise) on the compressor outlet contour and applying the averaged value to the combustor inlet at the same radius ("USERGUIDE FINE™/Open with OpenLabs™ 6.2", 2018).

It was expected that all three of the compressor outlet pressure contours would be approximately similar, but this was not the case. Examining the pressure contours in the combustor shown in Figure 4-10 indicates that the flow in the combustor did not cause the horizontal high-pressure band, because the pressure contours in the combustor increased as the radius increased and it did not have a parabolic pressure profile.

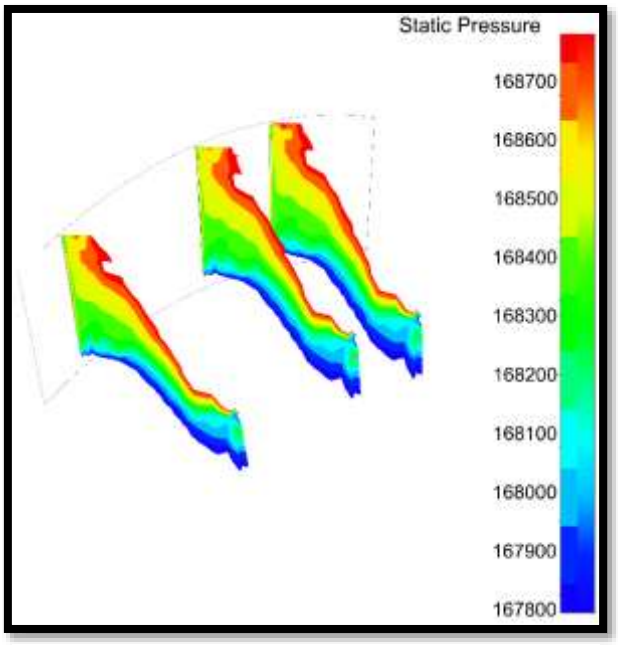

Figure 4-10: Static pressure in combustor at its inlet.

This means that the horizontal high-pressure band was caused by the interface seeing that the compressor flow solution without the interface did not have this band and it was not caused by the combustor. The interface causes the high pressure band because of the following two reasons:

1. The interface passes pitchwise averaged values from one domain to the next in the direction of the fluid velocity which causes the inlet profile of the combustor shown in Figure 4-9 ("USERGUIDE FINE™/Open with OpenLabs™ 6.2", 2018).
2. The flow leaving the deswirler is complex and requires, as a rule of thumb, a distance equivalent to approximately 3 chord lengths to develop, but a longer distance is preferred. However, flow cannot develop through the interface and led to the realisation that a few millimetres behind the deswirler, the detail of the flow leaving the deswirler was destroyed. This prevented the simulation from solving the flow through the compressor accurately since the flow leaving the deswirler could not develop.

It could thus be expected that by increasing the distance between the trailing edge of the deswirler and the interface, the flow through the compressor would solve more accurately. This is expected to eliminate the high-pressure horizontal band and may resolve the mass flow rate deficit.

The geometry of the components is important when comparing the simulation and experimental results because having compressor or turbine blades that do not resemble those in the actual engine will likely result in them having lower efficiencies. The latter would require the magnitude of the heat source to be higher than it would have to be when using the correct blade geometries. Figure 4-11 shows the relation of the heat source magnitude to the mass flow rate together with the experimental mass flow rate using partially converged results for both heat addition methods at 80 kRPM.

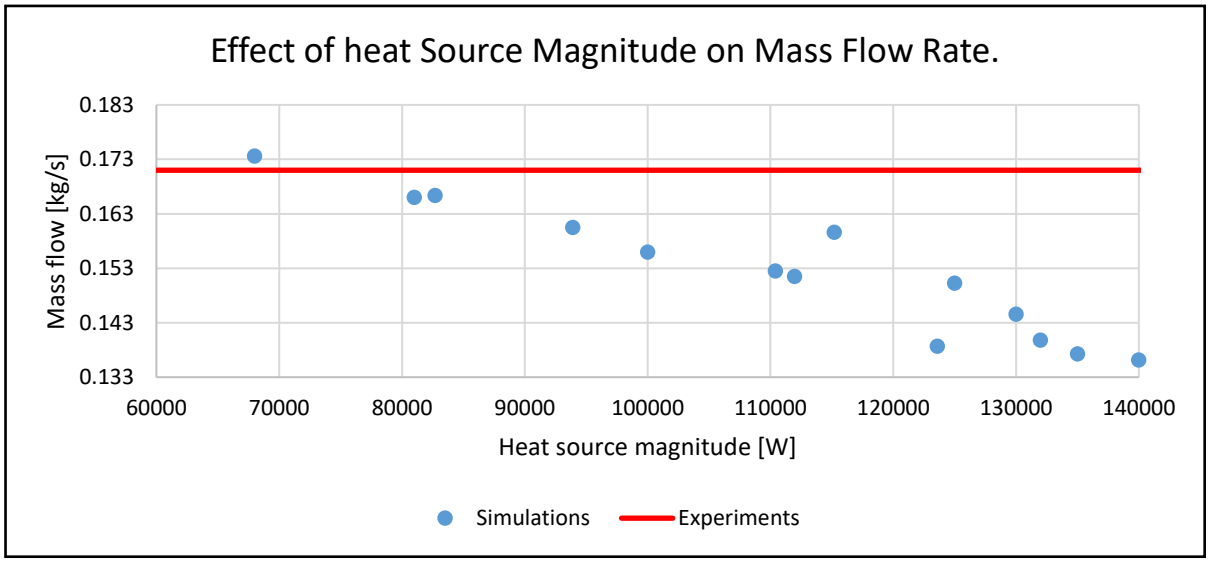

Figure 4-11: The effect of the heat source magnitude on the mass flow rate.

Following the discussion above it is clear that when the heat source magnitude was too big due to inaccurate geometries, the mass flow was predicted too low. Reducing the magnitude of the heat source will cause the simulation mass flow to converge to the experimental mass flow producing an invalid simulation because the power in the compressor and turbine would not be matched.

4.2 GLOBAL HEAT VS PRIMARY ZONE HEAT

This section discusses the difference between the two methods used to model combustion, based on Figure 4-2 to Figure 4-4. This will give the reader a better understanding of how the two models differed and what caused these differences.

When studying the differences between the two heat addition methods in Figure 4-2 and Figure 4-3, a clear trend is apparent. The primary zone heating method calculated a higher mass flow rate and pressure ratio than the global heating method. This trend was plotted on the compressor map for the BMT 120 KS in Figure 4-12 indicating the simulation and experimental results (Krige, 2013). Note that the compressor map in Figure 4-12 contains a combination of 1D, CFD and experimental and was edited for this study to only show the 80 kRPM and 120 kRPM speed lines as well as the engine operating curve.

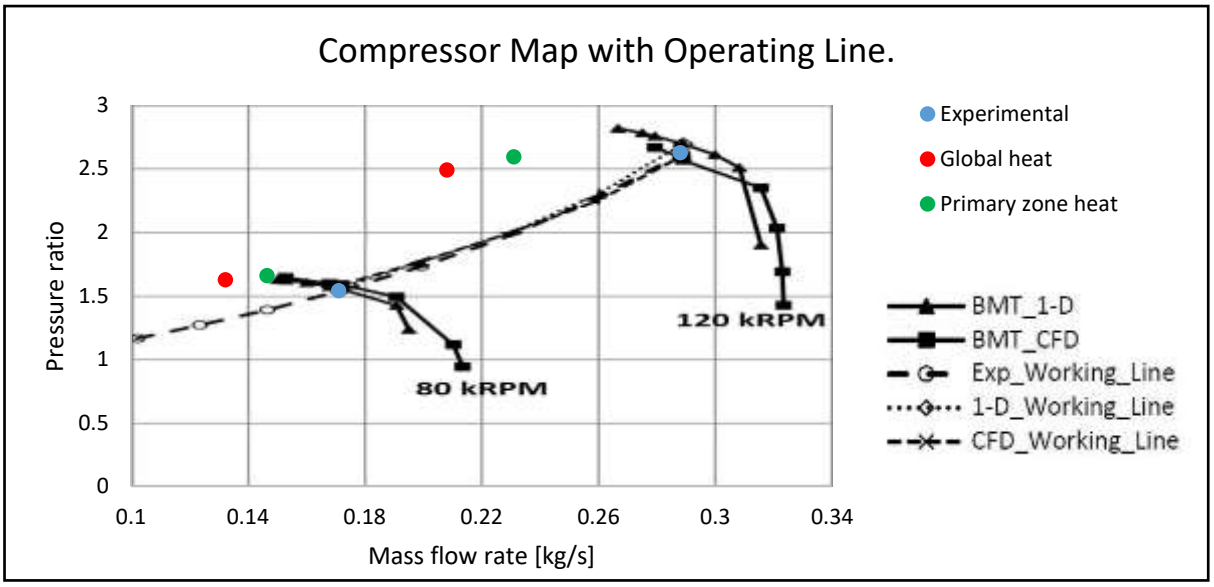

Figure 4-12: BMT 120 KS compressor map with simulation and experimental results plotted (Krige, 2013).

The compressor map in Figure 4-12 clearly indicates that the mass flow would decrease as the pressure ratio increased when operating on a speed line, as discussed in Subsection 4.1.2. This implies that the decrease in both the pressure ratio and mass flow of the engine when switching from primary zone heating to global heating at the same rotational velocity cannot be explained using the compressor map since this behaviour does not follow the speed lines. This means that because the only difference between the two simulation methods was the heat addition method, this had to be the cause of the trend.

This phenomenon could be caused by the numeric model and support functions used to introduce local heat into the combustor as opposed to global heat. Global heating adds heat to all the elements in a defined domain while local heating has to search within a domain for the mesh elements that need to be heated. Depending on how this was implemented, the characteristics of the simulated model would be affected, including damping. This can then affect the solution, in a similar manner as using different numerical scheme or turbulence models would (Haque et al., 2007; Dunn et al., 2009; Snedden, 2011; Villalpando et al., 2011).

4.3 COMPARING THE COMPRESSOR AND TURBINE POWER

The accuracy of the EGT matched simulations were evaluated by determining if the power produced and consumed by the rotating components were matched. The reason being that the energy added in the combustion chamber in the form of heat had to be enough to allow the turbine to extract the required energy from the flow to power the compressor. If this was the case, the micro gas turbine was able to operate at the set rotational velocity boundary condition from a practical point of view.

To determine if the magnitudes of the heat sources were correct, the power (P) produced by the rotor and consumed by the impeller had to be compared for each rotational velocity. Because both components rotate at the same speed (ω), only the torques (τ) had to be compared, as shown by Eq. 4-3.

$$P = \omega \times \tau \qquad \textit{Eq. 4-3}$$

The new criteria to have a valid working micro gas turbine was that the torque produced by the turbine had to be equal or slightly higher than the torque required by the compressor. This would ensure that the turbine power the compressor and overcome the losses in the bearings, allowing the micro gas turbine to run. If this was not the case, the turbine would not be able to turn the compressor and the gas turbine would not be able to operate at the simulated rotational velocity with the specified magnitude of the heat source. To resolve this, the magnitude of the heat source had to be increased until this condition was met, regardless of whether the EGT of the simulation matched that of the experiments. Table 4-2 compares the torque on the impeller and rotor at 80 kRPM, 120 kRPM and 140 kRPM for both heat addition methods.

Table 4-2: Impeller and turbine torque comparison.

		Torque [N.m]		
Rotational velocity		Impeller	Rotor	Difference
Global heat	80 kRPM	0.9539	1.0208	6.6%
	120 kRPM	2.1672	2.2642	4.3%
	140 kRPM	2.8910	2.9675	2.6%
Primary zone heat	80 kRPM	1.0656	1.2047	11.5%
	120 kRPM	2.3988	2.5829	7.1%
	140 kRPM	3.4196	3.1382	8.2%

The torque difference was acceptable because the rotor torque was slightly more than the torque on the impeller allowing for bearing losses. The numbers in Table 4-2 thus proves that the simulated engine was valid and would operate under the simulated conditions.

4.4 CONSTANT GAS CONSTANT "R"

In Section 3.4.1 it was stated that the gas constant "R" can only be specified as a constant value. Because of this and selecting the value of R based on temperature values from component simulations, the accuracy of the gas constant was evaluated for the design speed, 120 kRPM. This ensured that the chosen gas constant would not have a large influence on the simulated results so that a meaningful conclusion could be drawn from the simulations.

The gas constant was used to calculate the Mach number which is important to identify component mismatches due to choking which is important for future work. It was thus desirable that the gas constant was accurate in the regions prone to choking. During the

course of the simulations, it was found that the flow could potentially choke at the leading edge of the main blade of the impeller but should ideally choke in the NGV or nozzle. These locations were therefore investigated. The average temperature in each of the 2 regions was determined as follows using the results of the simulation at design speed:

Impeller: The average temperature at the location of the shock was calculated by creating a plane through the centre of the sonic region at the leading edge of the main blade of the impeller while averaging the temperature on that plane.

Turbine and nozzle: The average temperature in the turbine and nozzle was calculated by averaging the TIT and the nozzle exit temperature. This was determined by taking the average temperature on the NGV inlet plane and on the nozzle outlet plane, respectively.

The results are tabulated in Table 4-3 as well as the values selected in the setup of the simulation, as discussed in Section 3.4.1.

Table 4-3: Gas constant comparison values.

Region	Average simulation temperature [K]	Gas constant from [J/kg.K]		Difference in gas constants
		Simulation requirement	Selected in setup	
Impeller	282	287	287	0.0%
Turbine and nozzle	1028	298.8	298.5	0.1%

It is clear that the gas constant values used in the setup of the simulation were very close to the values required by the simulation. It should also be noted that the gas constant is not sensitive to a change in temperature, the reason being that a 100 K change in temperature would change the gas constant by only 0.8 J/kg.K. From Eq. 3-1 and Eq. 3-2, it is clear that a 0.8 J/kg.K change in gas constant would be negligible compared to the 100 K change in temperature when multiplying the gas constant with the temperature to calculate the Mach number. It was therefore acceptable to use 120 kRPM to validate the gas constant for simulations up to 140 kPRM and down to 80 kRPM.

4.5 SUMMARY

The simulation methodology can be used for performance indications of the BMT 120 KS engine, both inside and outside the designed operating range of the engine. It is useful when determining if changing an engine component improves the engine performance. This methodology is able to solve the 140 kRPM rotational velocity and can also be used to identify component mismatches when the mass flow deficit is resolved.

The predictions made by the primary zone heating method were closer to the experimental results than the results from the global heating method but this came at a high time cost. Improving the results by a couple of percentages by using primary zone heating took more than 6 times longer than global heating, even when starting from a converged previous solution. This time requirement has to be taken into account when deciding whether global heating or primary zone heating are used to model combustion.

An attempt to reduce the difference between the experimental and simulated results by refining the mesh was not attempted because of the RAM limitations. Additionally, it was expected that the simulations results would not improve significantly because, as noted in Section 3.3.7 and shown in Section 3.4.2, the global mesh density is sufficient and the Y+ also met the requirements of the turbulence model.

The pressure ratio and thrust results compared well with the experimental results. The small differences were likely due to the solid mechanics of the rotating components and geometrical simplifications made. The CFD simulation only solved the fluid mechanics aspect of the problem, therefore solid mechanics was per definition not part of the simulation scope of this study.

The experimental results used an uncalibrated bell mouth inlet to determine the mass flow rate using pressure measurements and may be partly responsible for the mass flow anomaly. The uncertainty in the experimental mass flow rate (Table 4-1) was the uncertainty in the pressure measurements and did not include the uncertainty of whether the pressure measurements were converted accurately into a mass flow rate.

Possible numerical causes for the mass flow deficit were found to be one of the following: the unrealistic temperatures in the combustors and the interface between the compressor and combustor being too close to each other. If it was found that fixing these two aspects and the experimental results are accurate, it has to be considered to model combustion to get further insight into the reason why the mass flow differed.

It is expected that the mass flow rate deficit was caused by a combination of experimental and simulation inaccuracies. If none of the suggested methods identified the cause of the mass flow deficit, the inaccurate geometries would have to be replaced or another engine should be used. The steps regarding modelling combustion were not simulated because the student did not have access to the tools required to solve combustion.

Finally, studying the power balance between the turbine and compressor, it was determined that the simulated micro gas turbine would be able to operate at the set rotational velocities. It was also determined that the constant gas constant “R” would have a minimal effect on the results and was accurately set in the setup of the simulations.

CHAPTER 5 COMBUSTION HEAT SOURCE

This chapter is dedicated to determining if the heat source accurately modelled the burning of fuel in the combustor. The first section in this chapter discusses what effect the use of a heat source to model combustion had on the physics. The second section compares the temperature profiles for the 2 different heat addition methods with the expected temperature distribution of the actual combustion process. The final section summarises this chapter.

5.1 EFFECT ON PHYSICS

Before one can identify the effect of modelling combustion with a heat source on the physics of a micro jet engine, one has to understand the internal workings of the engine. A step change in the fuel mass flow rate was thus considered while the engine was operating at dynamic equilibrium. Step change has the following effect on an engine, assuming that it has a constant combustor inlet temperature:

1. Increasing the mass flow rate of fuel into the combustor also increases the amount of fuel burnt and the amount of heat transferred to the air.
2. The increase in the heat transferred to air elevates the TIT (Eq. 5-1). The reason is that, initially, the mass flow rate stays constant due to the inertia of the compressor which drives the mass flow, preventing a rapid increase in rotational velocity.
3. The increase in TIT allows the turbine to extract more power from the fluid that is delivered to the compressor and increases the engine speed (Eq. 5-2).
4. Increasing the rotational velocity of the compressor also increases the mass flow rate through the engine because the compressor drives flow through the engine.
5. The increased mass flow rate decreases the TIT because the fuel mass flow rate stays constant and thus also the heat source (Eq. 5-1).
6. The increased mass flow rate results in the turbine extracting more work from the fluid but this is countered to some extent by the reduction in the TIT, in turn reducing the work extracted by the turbine (Eq. 5-2).
7. The mass flow will continue to increase while the TIT decreases until the power consumed by the compressor matches the power generated by the turbine.
8. Once the energy in the engine is balanced, it can be said that it has reached dynamic equilibrium and then all the flow variables remain constant.
9. Comparing the final and initial flow conditions, the following will be noticed, assuming that the engine does not choke:
    a. Increased mass flow rate.
    b. Increased rotational velocity.
    c. Increased amount of heat added to the combustor.

d. The final TIT and EGT may either be higher or lower than their initial values due to the relation between temperature and mass flow (Eq. 5-1).

$$\dot{Q} = \dot{m}C_P(T_{out} - T_{in}) \quad \text{(Farokhi, 2014)} \quad \textit{Eq. 5-1}$$

$$\dot{W} = \dot{m}C_P(T_{in} - T_{out}) \quad \text{(Farokhi, 2014)} \quad \textit{Eq. 5-2}$$

With:

- $\dot{Q}$: Heat transfer rate (source or sink) [W].
- $\dot{W}$: Work [W].
- $\dot{m}$: Mass flow rate [kg/s].
- C_P: Specific heat at constant pressure [J/kg.K].
- T_{in} for $\dot{Q}$: Temperature before the combustor [K].
- T_{out} for $\dot{Q}$: Temperature after the combustor [K].
- T_{in} for $\dot{W}$: Temperature before turbine [K].
- T_{out} for $\dot{W}$: Temperature after turbine [K].

Modelling combustion using a heat source will clearly affect 1. above because the heat source replaces the burning of fuel. Because this study uses an alternative method to model combustion, all the physics related to burning fuel is sacrificed in order to reduce simulation time:

- Igniting and re-ignition of the flame in the combustor.
- Flameout in the combustor.
- The exact location where fuel burns.
- Running rich or lean.

Another difference between an engine simulation and a real engine is the fact that the rotational velocity is a boundary condition and not a variable that is solved as noted in Section 3.4.4. This will, however, also be the case if combustion was modelled which meant that having a constant rotational velocity does not make the method described in this report inferior to other methods where combustion was modelled.

It can thus be concluded that the use of a heat source was a viable option as an alternative to modelling combustion because the only difference between the two methods was that the heat source could not identify fuel related problems.

5.2 METHOD OF HEAT ADDITION

This section analyses the difference between adding global heat and primary zone heat to the fluid in the combustor. It involves studying the temperature contours and iso-surfaces in the combustor as well as the streamlines through the combustor. The two heat addition methods were compared with CFD simulation results where combustion was modelled on a similar combustor and micro gas turbine. The temperature profiles are also analysed based on what

the expected temperature profile would be, according to the design of the combustor as documented by Lefebvre & Ballal (2010).

5.2.1 CFD results when modelling combustion

This section is devoted to showing the results of simulations in which the combustion process was modelled. These results were from the KJ 66 micro gas turbine simulation with an impeller diameter of 66 mm by Gonzalez et al. (2007) and from an annular combustor only simulation by Trebunskikh et al..

Figure 5-1 indicates the temperature distribution when modelling the combustion process in the combustor (Trebunskikh et al., n.d.; Gonzalez et al., 2007). It should be noted that the temperature in the combustion chamber reaches temperatures of 2400 K.

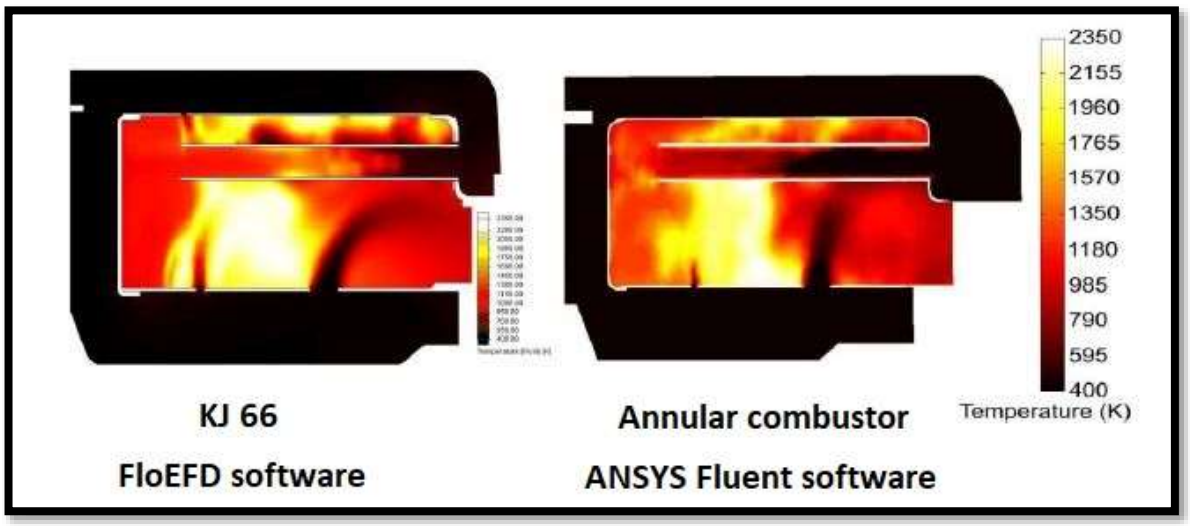

Figure 5-1: Temperature distribution obtained by modelling combustion (Trebunskikh et al., n.d.; Gonzalez et al., 2007).

A uniform combustor outlet temperature profile was ideal but not practical due to the cooling requirements at the rotor blade tip and hub (Lefebvre & Ballal, 2010). This is also a result of cooling the combustor liner to prevent it from melting as a result of the high flame temperature. The combustor outlet temperature profile thus has a parabolic shape with higher temperatures in the core of the outlet than at the hub and shroud, as could be expected from a good design (Lefebvre & Ballal, 2010). The combustor exit temperature contours, when modelling the combustion process in the combustor, are shown in Figure 5-2 (Gonzalez et al., 2007).

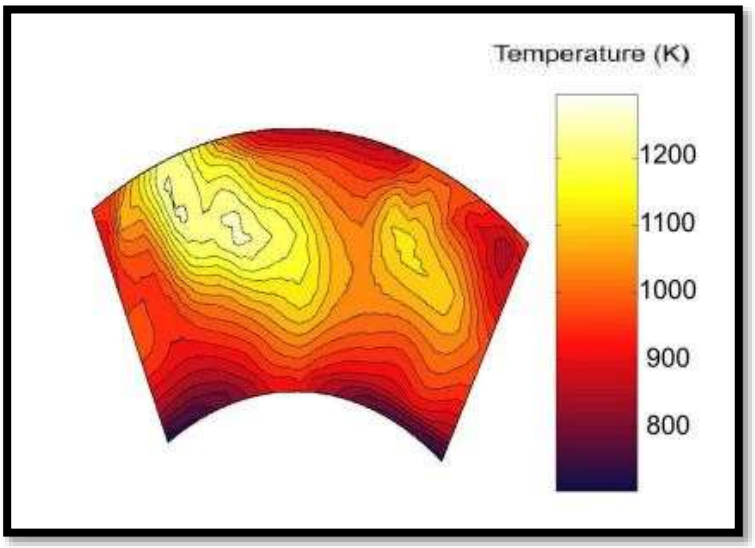

Figure 5-2: Combustor outlet temperature profile when modelling the combustion process (Gonzalez et al., 2007).

5.2.2 Global heat addition

Figure 5-3 shows the temperature contours in the centre of the combustor when using global heat addition. This method was the easiest to apply and required less simulation time which made this method very attractive (Refer to Section 4.5).

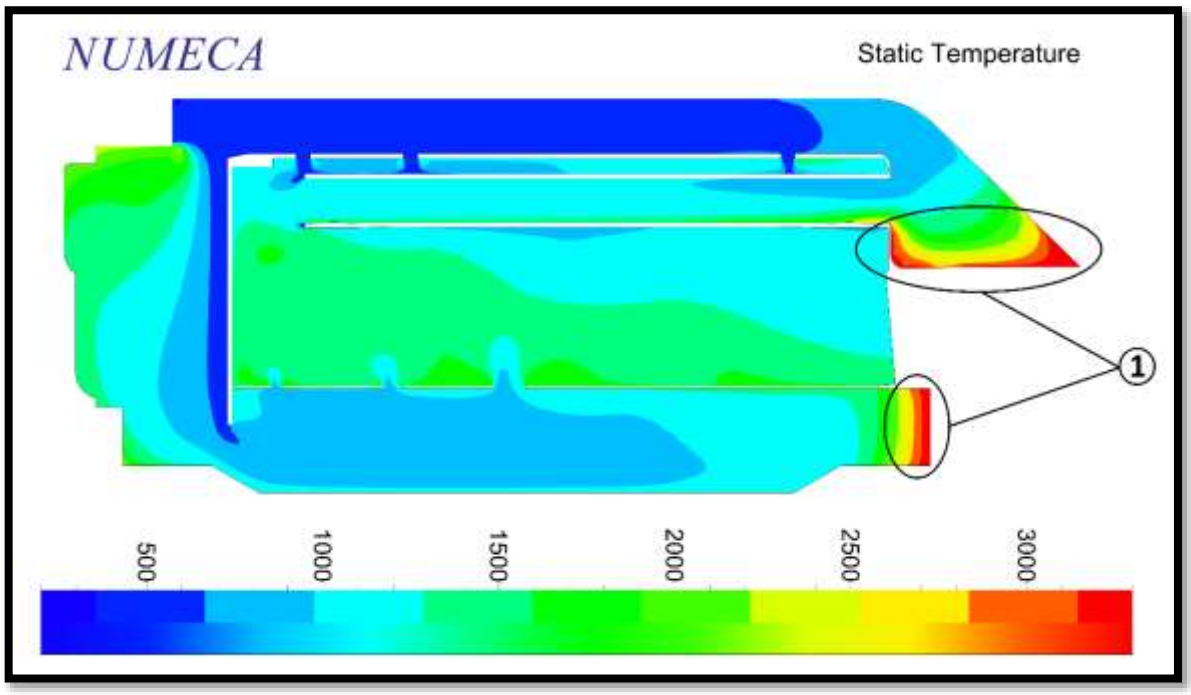

Figure 5-3: Global heat: Combustor temperature distribution contours at 120 kRPM.

Studying Figure 5-3, it is clear that the addition of global heat was inaccurate because, in reality, only the primary zone in the combustor was heated and not the entire combustor. This resulted in the low temperature zones (400 K), black regions in Figure 5-1, being heated in the combustor. Also, the combustion zone in Figure 5-1 with the highest temperature was not captured by the global heat simulation shown in Figure 5-3. It should be made clear that global heat does not give any indication of where hot and cold regions would be in the actual combustor.

Another observation was that two zones had temperatures reaching values of over 3000 K, indicated by ① in Figure 5-3. This is a non-physical phenomenon and rather a result of the heat source and flow continuously flowing around the combustor annulus as illustrated by the streamlines in Figure 5-4.

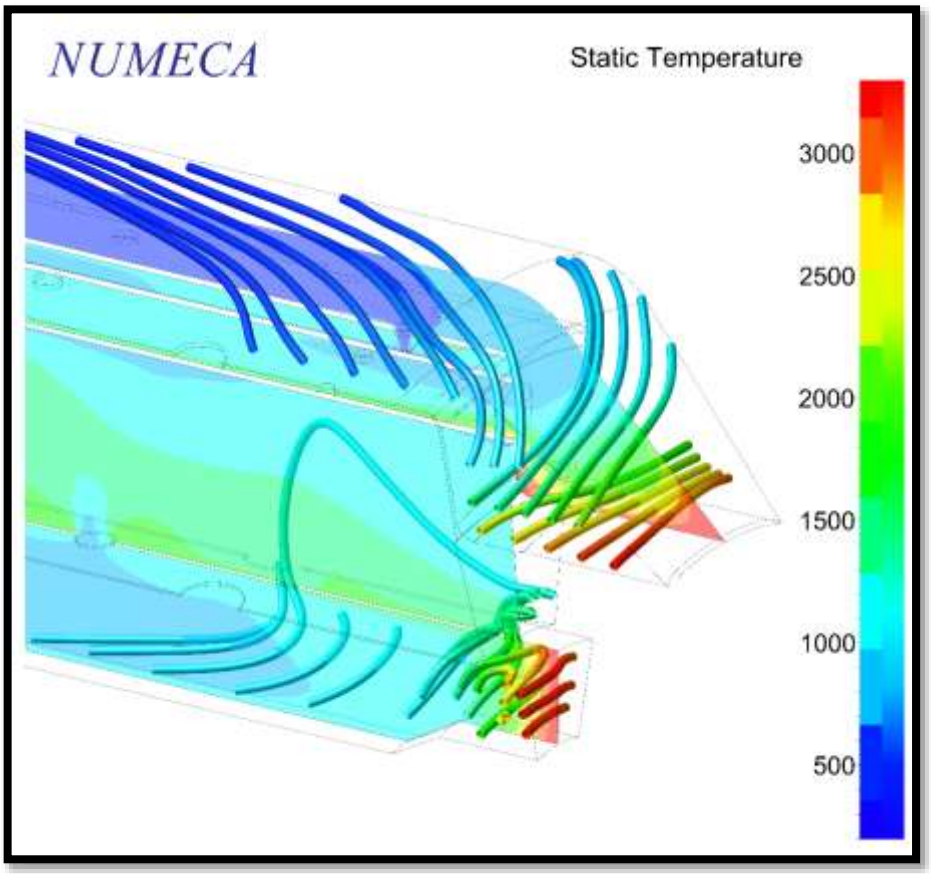

Figure 5-4: Global heat: Recirculating flow along the tangential direction in the combustor.

Circulating flow was introduced into the combustor by the compressor because the deswirler did not provide pure axial flow. When the fluid reached the front of the combustor, its axial flow velocity reduced to zero and only the tangential flow velocity remained. This caused the flow to continuously flow around the combustor annulus in the tangential direction in region ① in Figure 5-3. Because heat was added as joules per second (Watt), the fluid temperature in these regions was higher than the fluid in the adjacent regions as a result of the fluid particle remained longer in the domain. This phenomenon could be resolved by removing

these regions from the domain, expecting a minimal effect on the solution since the fluid in this region acted as a wall, not allowing fluid to pass.

An approximately uniform outlet temperature profile was expected rather than the parabolic profile since there were no significant temperature gradients in the combustor. This was because heat was added uniformly throughout the whole domain which prevented the traditionally hot primary zone fluid mixing with the cold cooling flow from the holes in the combustor liner (Figure 5-1). The primary zone did have hot fluid and the cooling flow was colder than the flow from the primary zone, but these temperatures were moderate compared to those in Figure 5-1. Figure 5-5 illustrates a more comprehensive temperature distribution in the combustor as well as the combustor outlet temperature profile. Note that

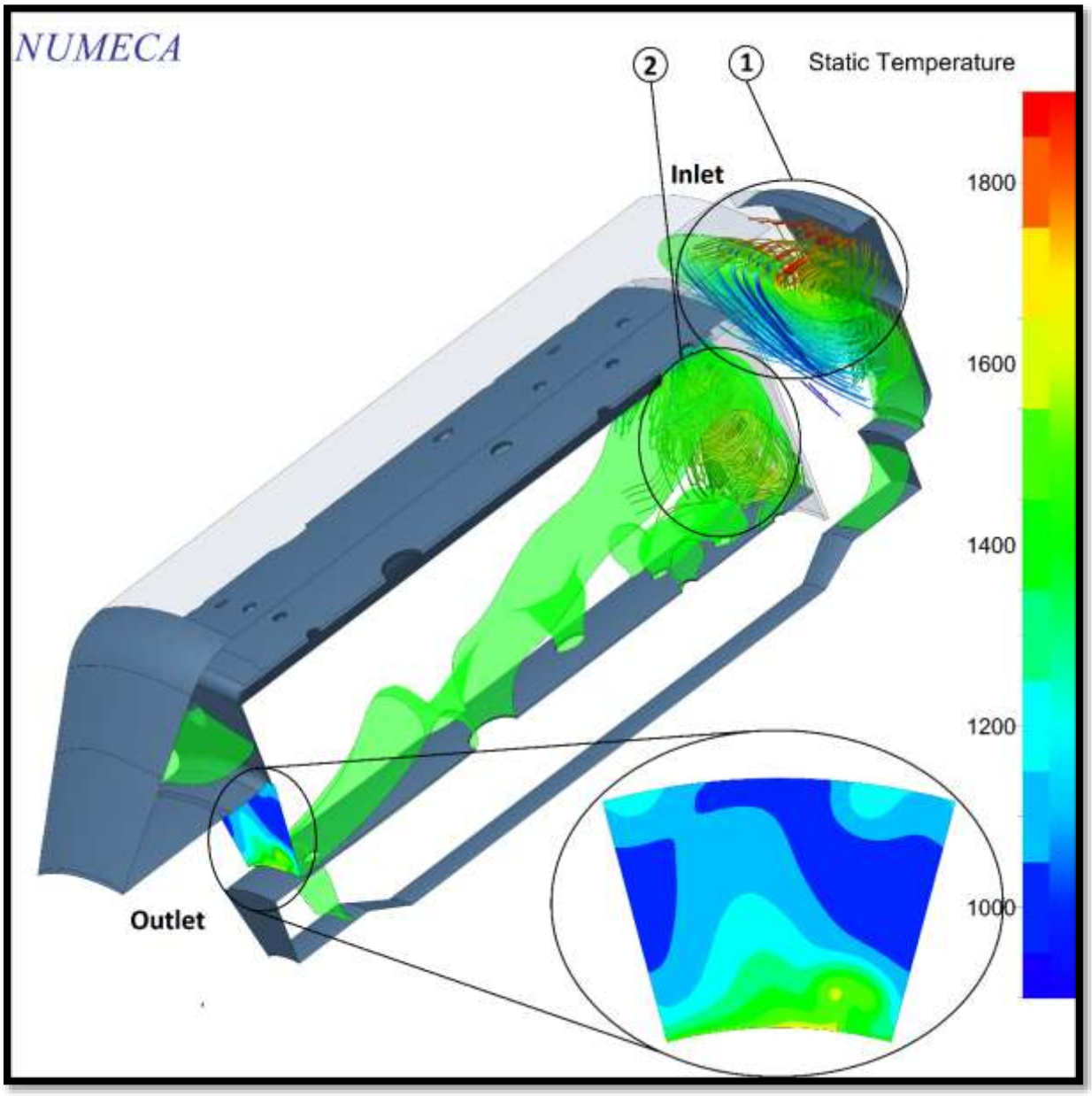

Figure 5-5: Global heat: Temperature distribution in the combustor with recirculation zones identified.

the green surfaces are iso-surfaces indicating where the temperature in the domain is equal to 1400 K.

Studying the outlet temperature profile it is clear that it is not uniform as was expected. The outlet temperature profile also did not match the profile in Figure 5-2 and the ideal temperature profile described in Section 5.2.1. The highest temperature region on the profile was at the hub and not in the centre of the profile. Also, the centre of the profile was mostly cold with a hot region extending from the hub upwards to the centre of the profile.

Because a fluid particle stays in a recirculation zone for a relatively long period of time compared to the time it takes the particle to move through the combustor, it was expected that these regions would cause hot zones. Studying Figure 5-5, it is clear that this was the case since the two high temperature zones labelled ① and ②, consisted of recirculating flow. These hot zones were bordered by the following:

Zone 1: The green iso-surface and the wall adjacent to the inlet.
Zone 2: The green iso-surface and the inner combustor liner.

The recirculating flow in ① was caused by fluid entering the combustor domain from the compressor with the hub suddenly dropping away acting like a step. This resulted in the fluid creating a recirculation zone and having a higher temperature than that of the adjacent fluid regions. As the fluid left the recirculation zone, it mixed with the cold flow entering the combustor which limited the size of this hot zone to the extent that it did not contribute directly to a specific feature on the combustor outlet temperature profile.

The recirculating flow in ② was caused by flow leaving the vaporiser tube and stopped by the combustor liner and is clearly indicated in Figure 5-9 in the following section. This hot zone extended downstream towards the combustor outlet and was the cause of the high temperatures at the hub. It is clear that the hot zone caused by the recirculating flow reduced as it moved closer to the outlet. The reduction was caused by the cooling flow entering the primary, intermediate and dilution zones of the combustor through the holes in the liner, mixing with the hot fluid. The cooling flow was, however, not effective in mixing with the hot fluid, pointing towards the combustor not having enough swirl to sufficiently mix the flow in order for the outlet temperature profile to be uniform.

Because the hot zone never lifted from the inner combustor liner surface, the hole areas on the inner and outer combustor liners were investigated. The hole areas on each liner give an indication of the mass flow entering the primary, intermediate and dilution zones from the outer combustor liner and the inner combustor liner. Table 5-1 contains the number of holes, their diameter and area in each row and are numbered so that row 1 is upstream from row 6. Because the vaporiser tubes are just below the outer combustor liner, it contributed towards flow from the outer liner.

Table 5-1: Areas of the inner and outer combustor liner.

Inner liner				Outer liner			
Row	Holes	Diameter [m]	Area [m^2]	Row	Holes	Diameter [m]	Area [m^2]
1	24	0.0012	2.71E-05	1	24	0.0016	4.83E-05
2	24	0.002	7.54E-05	2	24	0.0016	4.83E-05
3	24	0.002	7.54E-05	3	24	0.0016	4.83E-05
4	12	0.0035	0.000115	4	24	0.0025	0.000118
5	12	0.006	0.000339	5	12	0.005	0.000236
6	12	0.001	9.42E-06	6	48	0.0016	9.65E-05
		Total:	0.000642	Vaporiser tubes	12	0.005	0.000236
						Total:	0.000830

It was then calculated that the inner liner through-flow area was 30% less than that of the outer liner with the inner liner consisting of 44% of the total area. This may cause the hot zone to stick to the inner liner because the cooling flow through the inner liner is not sufficient to cool the flow above it.

Finding that the inner combustor liner was burnt after doing the experiments confirmedthe CFD finding that there was a hot fluid region above the inner liner. The temperature contour in Figure 5-6 from the primary zone heat addition simulation indicates the location where the inner liner was burnt, namely at the hottest region of 4000 K.

5.2.3 Primary zone heat addition

Figure 5-6 shows the temperature contours in the centre of the combustor when using primary zone heat addition. It is clear that the temperature contours from primary zone heating matched that of the combustion model shown in Figure 5-1 better than the temperature contours when using global heat addition as depicted in Figure 5-3. The reason for this is that cold air enters the primary combustion zone (Figure 5-6 and Figure 5-1) with the hottest regions in both being in the primary combustion zone.

The temperature reached values of 4000 K which was unrealistically high when compared to the maximum temperature of 2400 K when solving the combustion process. The extent of this hot zone and the temperatures that it reached was investigated further. An important observation to note at this point is that, although the magnitude of the temperature in the combustor reaches unrealistic temperatures, the location of the high temperatures are accurate. This is true because the hottest region depicted in Figure 5-6 is the location where the combustor inner liner was burnt.

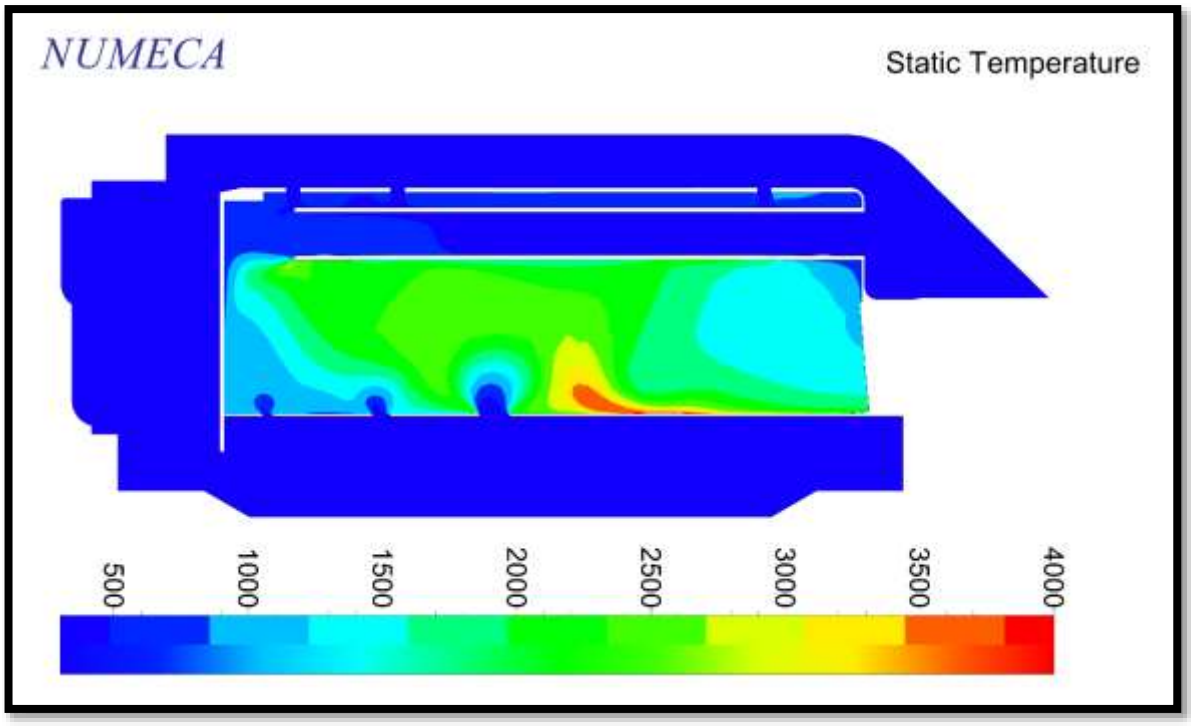

Figure 5-6: Primary zone heat: Combustor temperature distribution contours for 120 kRPM.

The green iso-surface with a temperature of 2500 K is shown in Figure 5-7. 2500 K was used for the iso-surface to show the region where the temperature was unrealistically high. Comparing the location of the iso-surface to that of the primary zone heating location, it is clear that the hot zone was caused by heating the fluid in the primary zone.

The secondary hole in the inner liner (①) had to cool the hot flow from the primary zone so that CO and any other unburnt hydrocarbons could combust while the dilution holes (② and ③) had to cool the fluid so that the TIT is acceptable (Lefebvre & Ballal, 2010). These holes did what was expected of them since the bulk fluid temperature was acceptable for the turbine. The dilution hole at ④ could not cool the hot film on the inner liner effectively because it was just upstream from the turbine inlet. Because this hole is situated close to the turbine inlet, it caused a cold spot (⑤) on the outlet temperature profile. This resulted in the combustor outlet temperature profile deviating even further from the ideal parabolic profile and the profile in Figure 5-2.

When comparing the iso-surfaces of the hot zones (Figure 5-5 and Figure 5-7), the following similarities were found with regards to their location:

- The hot zone size reduced as it moved downstream.
- The hot zone formed a layer on the inner liner after the dilution hole ② cooled the bulk fluid.

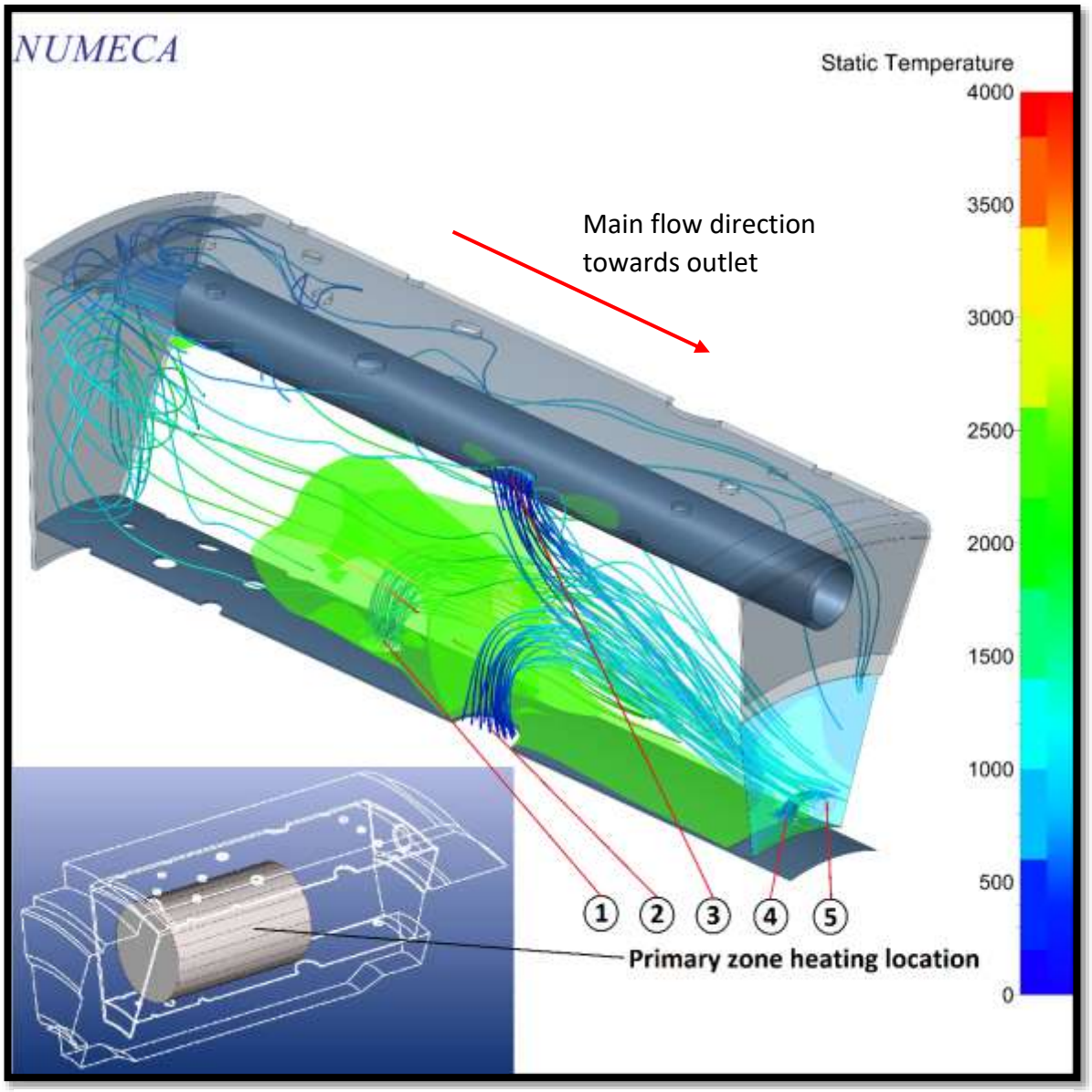

Figure 5-7: Primary zone heat: Extent of the hot zone and streamlines from the secondary and dilution holes.

Note that the iso-surfaces depicted in Figure 5-7 and Figure 5-5 were not drawn at similar temperatures but at a temperature that was considered hot for the temperature range in the combustor. Because of this, no direct correlation can be drawn with regard to temperature, but the flow can be analysed to determine the aerodynamic shortcomings of the combustor.

When taking the similarities in the above-mentioned bullets between the results shown in Figure 5-7 and Figure 5-5 into account, the same conclusion for global heating can be made for primary heating:

- The combustor does not have enough swirl in the combustor liner to mix the hot and cold fluid to achieve a better outlet temperature profile.
- The inner liner requires a higher through-flow area to prevent the hot zone from forming a layer on the inner liner.

- These findings were strengthened when studying Figure 5-8. It illustrates the temperature profiles through the hot zone and at the combustor outlet. The streamlines were drawn through the hot zone to determine the origin and destination of the hot fluid particles. This investigation clearly showed that the fluid flowing through the hot zone enters mostly from the vaporiser tubes and flows through a large recirculation zone, ② in Figure 5-5 and also shown in Figure 5-9. The fluid then passes through the hot zone and flows reasonably straight to the outlet, in turn, causing the hot region in the centre of the combustor outlet temperature profile. The dilution holes, (② and ③) in Figure 5-7 cool the sides of the combustor outlet temperature profile.

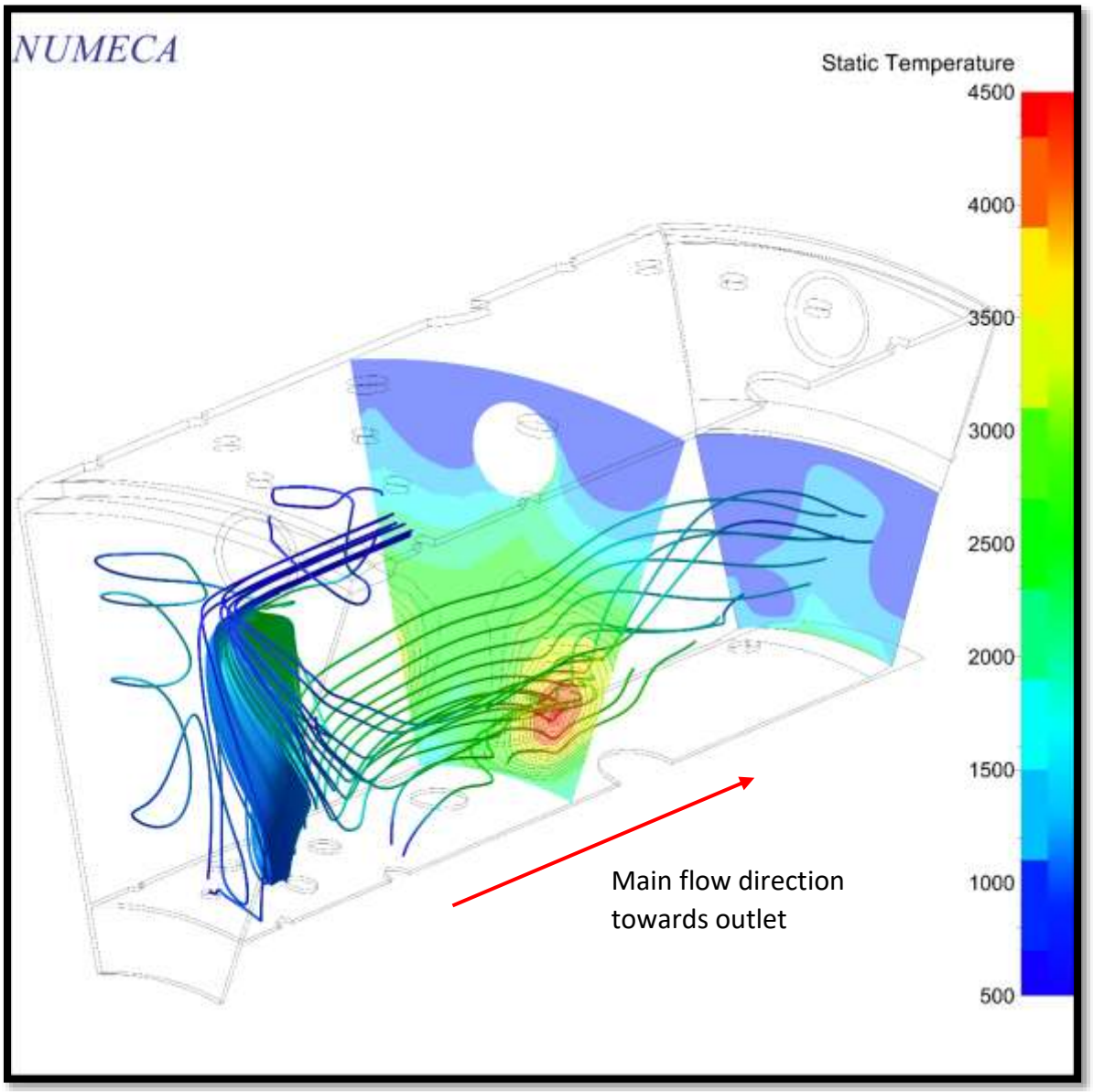

Figure 5-8: Primary zone heat: Hot zone influence on the combustor outlet temperature profile.

Studying the combustor outlet temperature profiles (Figure 5-8 and Figure 5-5), it should be noted that these profiles were similar, but the magnitudes of the profiles differed. The

primary zone heating profile had a larger temperature range than that of the global heating profile caused by the former adding heat in a more concentrated area and having colder cooling flow than the latter. Both profiles are not ideal and there is scope for improvement.

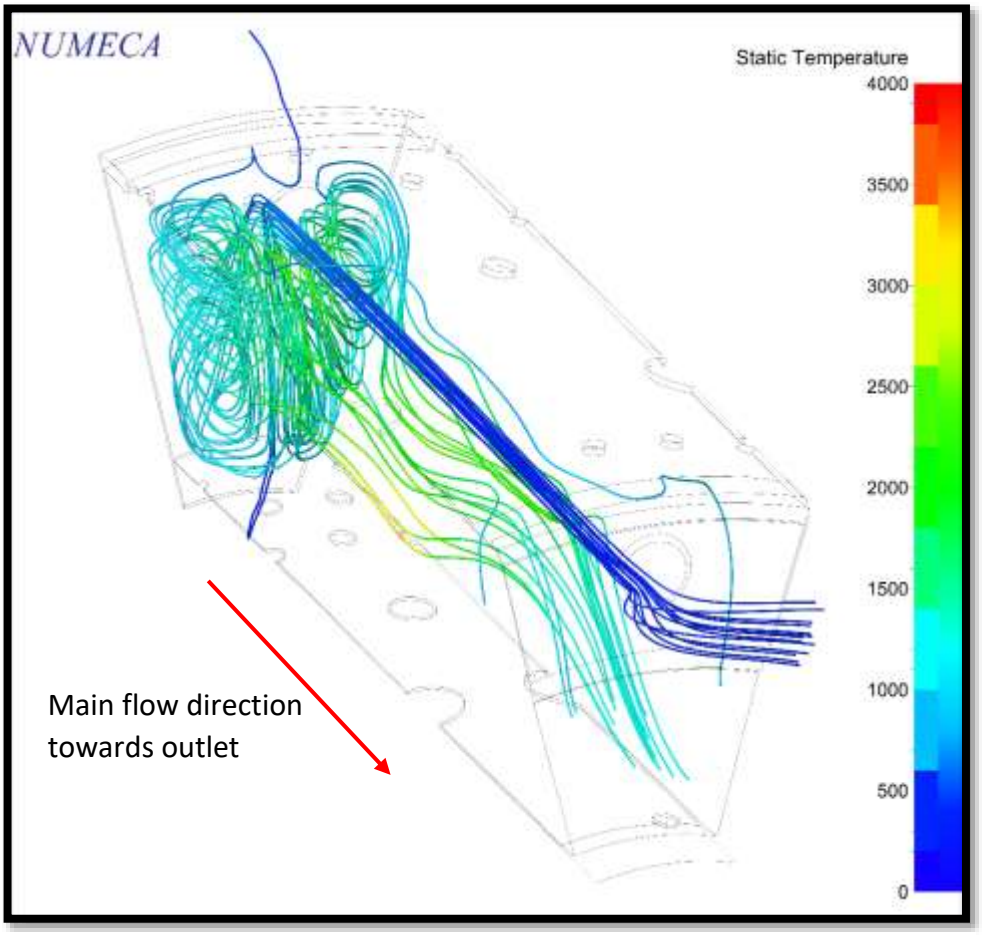

Figure 5-9: Recirculation zone caused by the flow leaving the vaporiser

The recirculation zone illustrated in Figure 5-8 shows only one side of the entire recirculation zone because of the location from where the streamlines were introduced. For both sides of the recirculation zones caused by the flow leaving the vaporiser tube, refer to Figure 5-9.

5.3 SUMMARY

When considering the changes in the physics of the simulation when replacing the combustion process with a heat source it was found that the heat source would model the combustion process adequately. Some physics could not be captured but these were specifically related to issues regarding fuel being burnt which cannot be predicted as it was not modelled.

With regards to the method of heat addition, it was found that adding heat in the primary zone modelled the combustion process better than the global heat addition simulations. The reason is that cold air entered the primary, intermediate and dilution zones through the

combustor liner to feed and cool the hot combustion fluid as it would in reality when using primary zone heat addition.

The results of both methods of adding heat indicate that the combustor design is not ideal: the combustor does not have enough swirl and the inner liner should have more and/or larger holes to improve the through-flow to cool the inner liner. Doing this will aid the flow to mix sufficiently so that the temperature distribution at the combustor outlet in the tangential direction is approximately constant and will ensure a parabolic temperature distribution in the radial direction.

The results for the two heating methods will not always lead to the same findings for every combustor that is simulated. The main reason why both heat addition methods produced the same conclusion is that a recirculation zone increased the fluid temperature of the global heat addition simulation in the primary zone. Therefore, the global heat results mimicked primary heat addition but if this recirculation zone was not present, the results would be different.

The temperature contours in the combustor have a high dependency on recirculation zones. As a result of this and because combustors contain several recirculation zones, the location where heat is added becomes an important aspect to consider when accurate temperature contours are desirable. This was confirmed by running component simulations of the combustor using primary zone heating. When the heating zone overlapped with the recirculation zone at the vaporiser tube outlet, the recirculation zone became extremely hot. It is thus important to keep this in mind when selecting the primary heating zone in order to achieve as accurate as possible temperature contours.

The primary zone heating produced a slightly more realistic combustor outlet temperature profile since the temperature at the shroud was cold. Both methods predicted that the highest temperatures would be at the hub which is a result of a poorly designed combustor. It was also determined that a hole placed in the inner liner just upstream of the NGV only degraded the combustor outlet temperature profile further.

Finally, one would like to think that the length of the combustor could be increased to improve the combustor outlet temperature profile. This is because the required combustor length from design calculations would indicate that a significantly longer combustor is needed due to the low-pressure ratio generated by the single stage compressor. This can, however, not be done because of the following reasons:

- Installation problems.
    - The purpose of a micro gas turbine is to be compact and with a 1 m combustor, the engine would not fit into the intended airframe.
- Rotordynamic issues (Corbo et al., n.d.).
    - Due to the high rotational velocities, the shaft connecting the compressor and turbine undergoes shaft whirl as the rotational velocity approaches the natural frequency of the shaft. As the length of the shaft increases, the whirl problem escalates, hence the need to keep the shaft as short as possible.

CHAPTER 6 DISCUSSION OF THE ENGINE PERFORMANCE AND FLUID FLOW

This chapter discusses the flow through the engine as well as the engine performance to determine if the method that was used to model combustion caused irregularities in the flow. A section on component mismatches is included to illustrate the necessary investigations needed if an engine does not perform to the design specifications. The flow in the compressor, turbine and nozzle are discussed for 80, 120 and 140 kRPM, respectively while studying both global heat addition and primary zone heat addition. The effect of the two different heat addition methods on the fluid flow through the engine is also contained here.

The following should be noted for the figures in this chapter:

- The relative velocity and Mach number were used for all the rotating components and the absolute velocity and Mach number for stationary components.
- All streamlines are coloured by velocity magnitude.
- The colour scale in the second row of the tables is the scale for that table with the heading of the table containing the plotted variable and its units.
- The relative Mach number was plotted in the impeller and rotor because the flow can only be considered as choked when it is choked relative to the movement of the flow passage.

6.1 IDENTIFYING COMPONENT MISMATCHES

This section contains possible component mismatches that can be expected in the micro gas turbine and how to identify these mismatches. This information can be used in projects aimed at identifying component mismatches as a last step before manufacturing an engine.

Flow can have one of the following features indicating a component mismatch:

1. Mach number > 1 which indicates that the flow choked with one of the following conditions being met:
    a. Any component choked at a rotational velocity below design speed.
    b. A rotating component or the combustor chokes at rotational velocities above design speed.
2. No component choked at the rotational velocities where the engine was designed to choke to prevent mechanical failure.
3. A TIT above 1150 K at speeds at or below design speed for a micro gas turbine to prevent the turbine from failing.
4. Separation of the flow over the suction side of the blades causing a sudden drop in the pressure ratio over the compressor which indicates stall.

5. The complete breakdown of the flow upstream of and in the compressor due to a vortex that has moved to a location in front of the leading edge of the impeller blade. When the vortex breaks the flow down, the pressure across the compressor forces the flow direction to change and flow will exit through the inlet of the engine. This phenomenon is called surge and the onset of surge is indicated by a large vortex just behind the leading edge of the impeller blade.

If one of these flow features are present in a micro gas turbine, the components in the micro gas turbine were not matched and the engine must be redesigned. This redesign would be driven by the specific component mismatch.

It is thus clear that the following must be investigated in the micro gas turbine:

1. For choked flow:
    a. Mach number iso-surfaces in the 3D flow domain with a magnitude of 1.
    b. Pitch average view of the Mach number contour for values below 1 in the turbomachinery.
2. Average TIT.
3. Streamlines in the rotating components to check for stalled blades.
4. The onset of surge using streamlines in both the 3D and pitch average view of the compressor.

Both checks, 1a and 1b, must be conducted for choked flow to determine if the entire flow path is choked and not just partially choked.

6.2 COMPRESSOR FLOW

The compressor is upstream from the combustor which meant that modelling the combustion process as a heat source would affect the mass flow and the pressure ratio of the compressor, the reason being the backpressure caused by heating fluid in the different regions. Keep in mind that primary zone heating predicted an 8.5% higher mass flow rate and a 3% higher pressure ratio than global heating.

The streamlines through the impeller and the velocity magnitude contours at the inlet and outlet are illustrated in Table 6-1. The figures are oriented so that the viewer look at the impeller wheel from the side with the inlet being on top and the outlet on the bottom left-hand side. From studying the figures, it is clear that there is no significant difference between the two heat addition methods. Every figure shows the secondary flow using red streamlines. The increasing flow in the tip gap of the impeller blades reduced the efficiency of the compressor. It is clear that the flow velocity increased as the rotational velocity increased, as expected, with the stagnation zone at the leading edge of the splitter blade being visible.

Table 6-1: Impeller streamlines coloured by velocity in $m.s^{-1}$.

Global heat addition	Primary zone heat addition
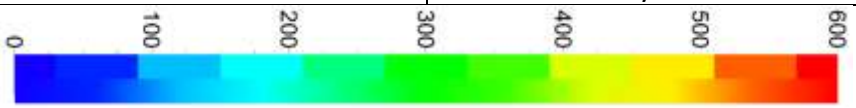	
80 kRPM	
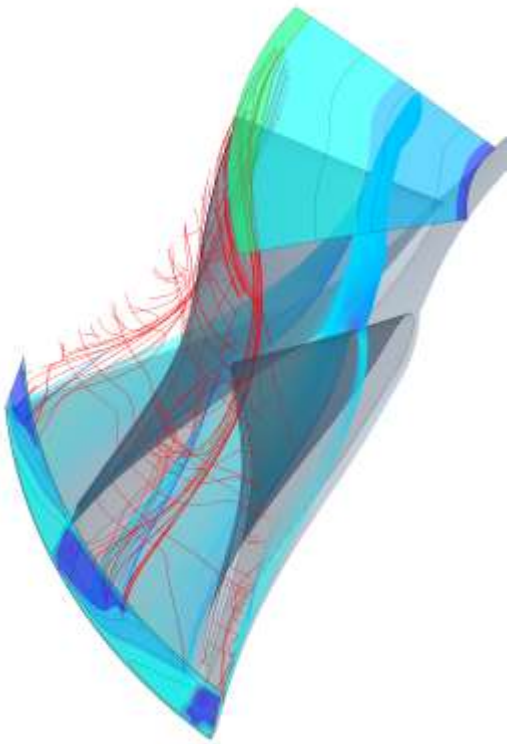	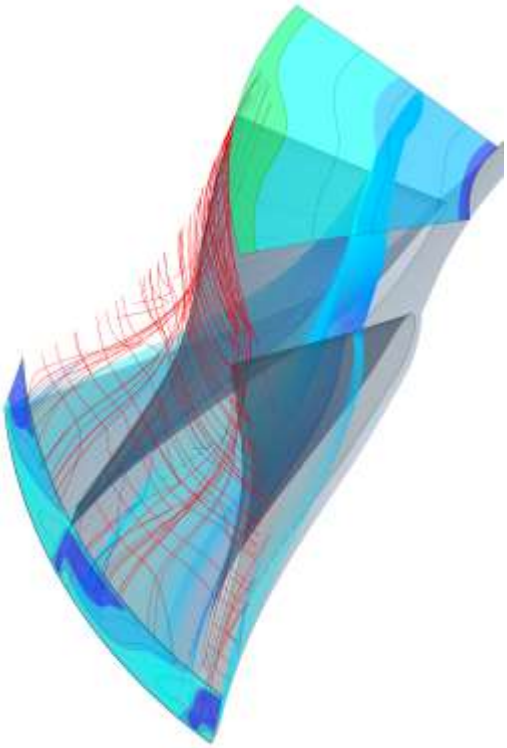
120 kRPM	
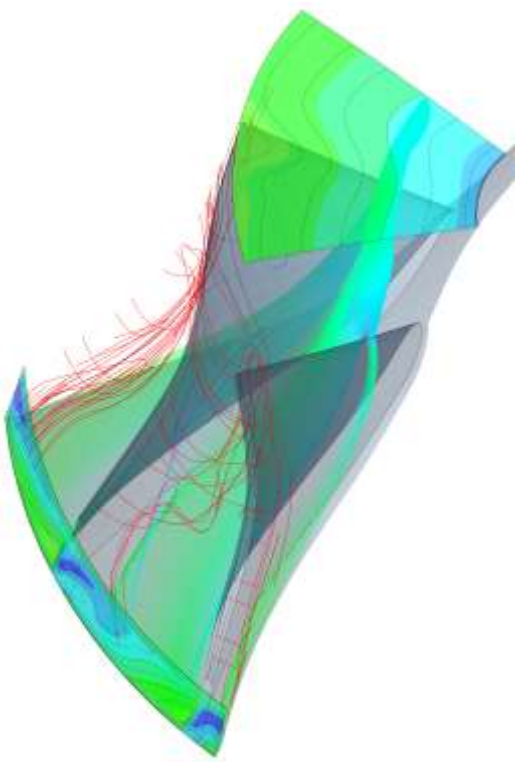	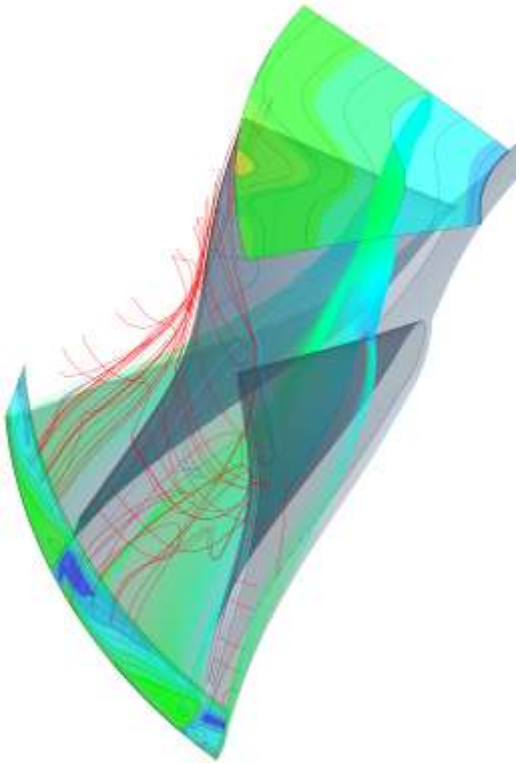

140 kRPM	
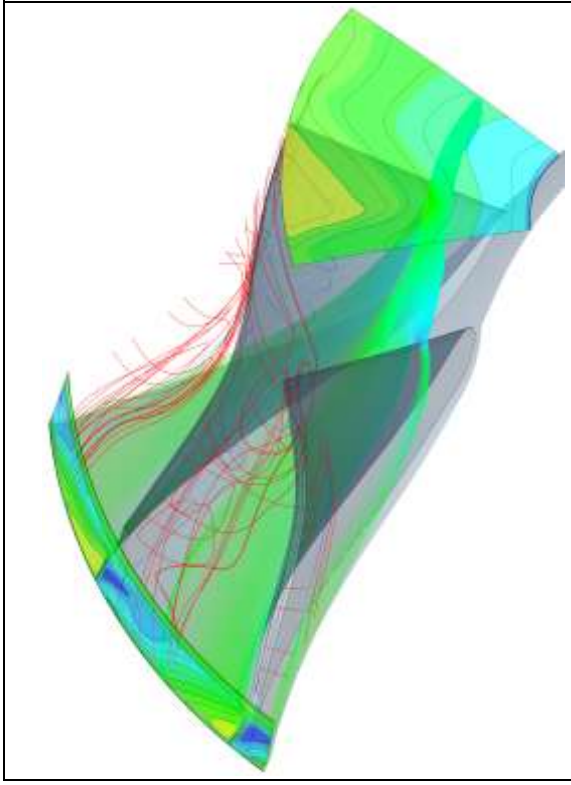	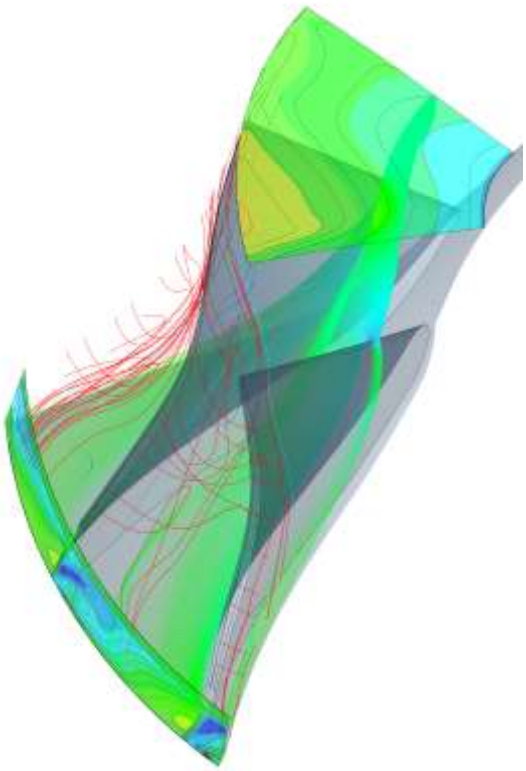

Table 6-2 illustrates the streamlines through the wedge diffuser when looking down at the diffuser from the suction side of the blade with the domain's inlet being at the bottom of the figures. As is the case with the streamlines through the impeller, it is noted that the flow velocities increase as the rotational velocity increases, as expected. A recirculation zone, circled in red, can be seen at the blunt trailing edge of the wedge diffuser and it reduces the efficiency of the compressor. For the primary zone heating simulation at 140 kRPM, only one streamline drawn picked this zone up because the results were captured using an automated process. This has several advantages including all the figures being captured from the exact same angle, they have the same scale and they only required a couple of minutes to run the macro. The disadvantages of this method are that the origin of the streamlines was fixed and if one or more of the streamlines did not pass through the recirculation zone, it was not shown on the graph. However, it does not mean that the recirculation zone did not exist seeing that a streamline showed this zone and it is similar to the recirculation zone depicted in the other figures.

It is clear that the fluid slowed down as it moved through the wedge diffuser and the flow area increased due to the radius increasing. This was expected since the purpose of a diffuser is to convert velocity, given to fluid by the impeller, to pressure.

Table 6-2: Wedge diffuser streamlines coloured by velocity in $m.s^{-1}$.

Global heat addition	Primary zone heat addition
	
80 kRPM	
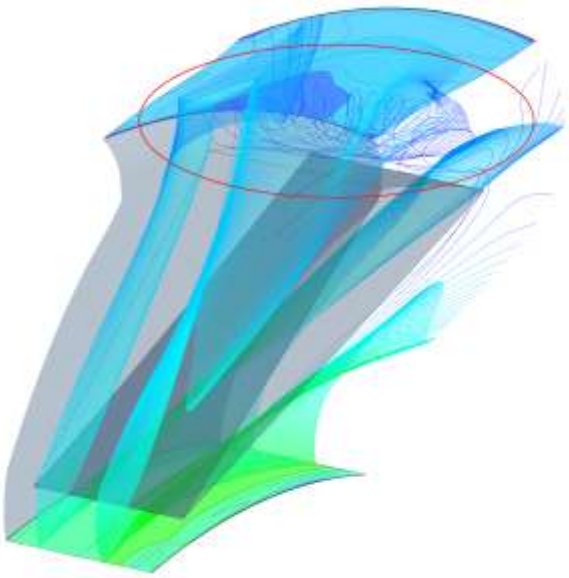	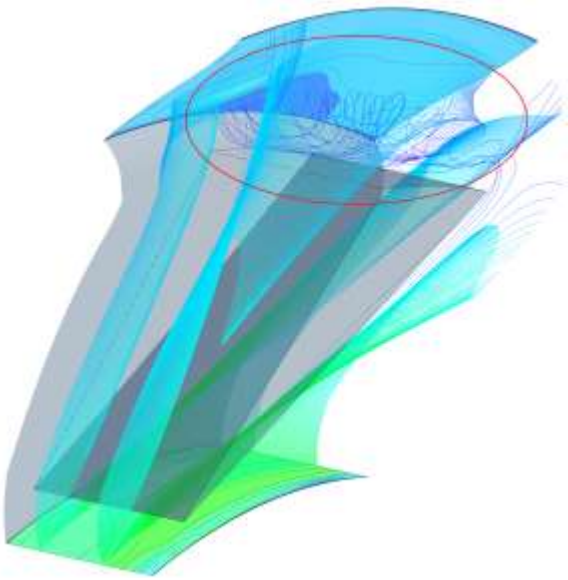
120 kRPM	
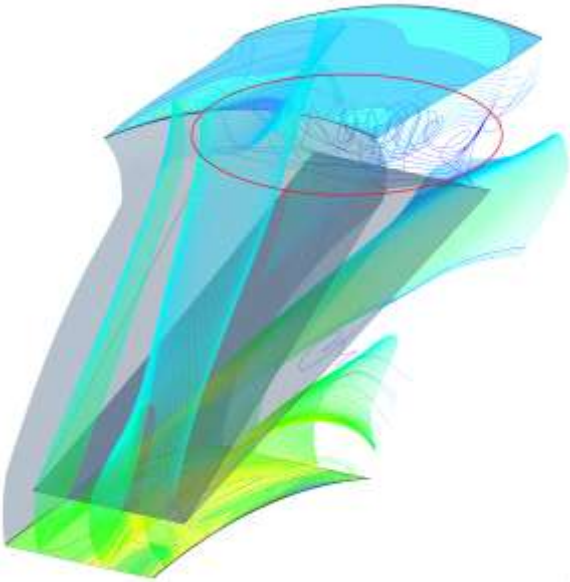	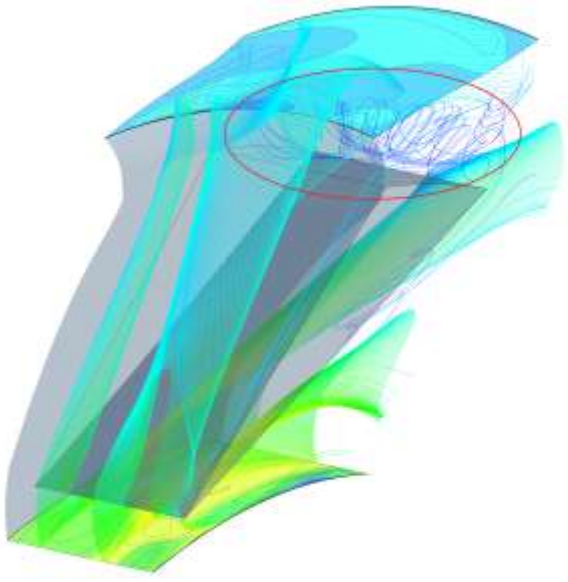
140 kRPM	

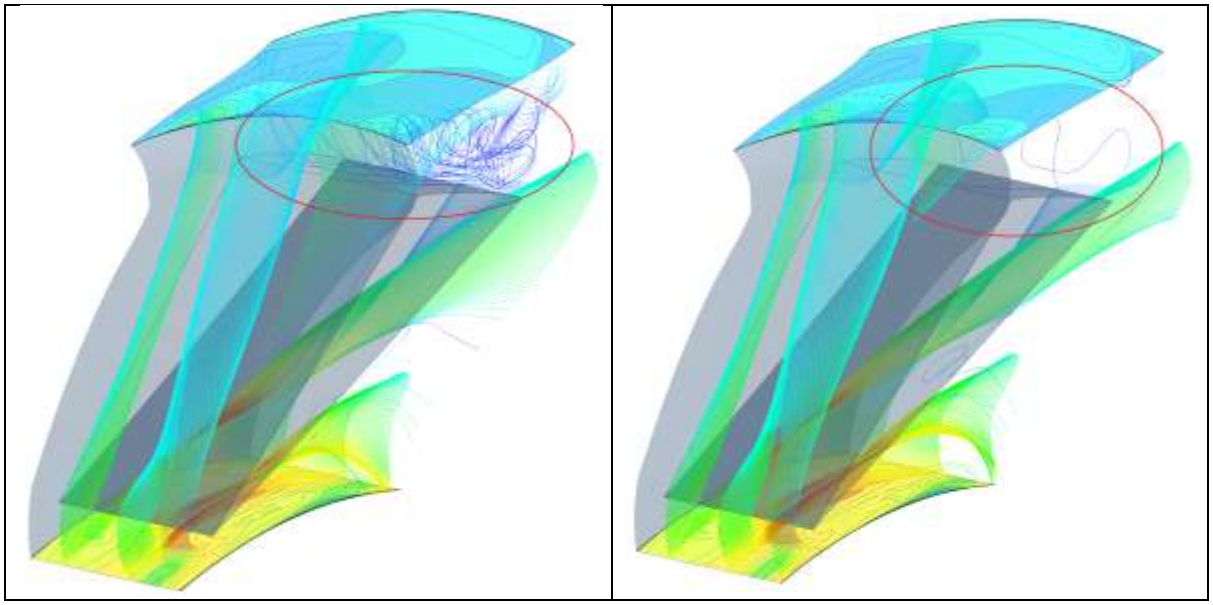

The streamlines through the deswirler are shown in Table 6-3 when looking at the deswirler from the suction side of the blade with the inlet being at the bottom of the figures. The deswirler provides axial flow to the combustor by removing residual swirl from the flow. It was clear, from the discussion in Subsection 5.2.2, that the flow had some residual swirl when entering the combustor. The velocity reduced further as the flow moved through the domain and was converted to pressure. It should be noted that the deswirler had a reversed flow zone on its suction side near the trailing edge and is circled in red. This phenomenon was caused by the adverse pressure gradient on the suction side of the blade which forces the fluid to flow in an upstream direction near the blade surface. The reversed flow zone induces losses in the deswirler, in turn, reducing the efficiency of the compressor, however, the advantage of having less swirl in the combustor outweighs these losses. This could not be considered a component mismatch because the zone was too small.

Table 6-3: Deswirler streamlines coloured by velocity in m.s^{-1}.

Global heat addition	Primary zone heat addition
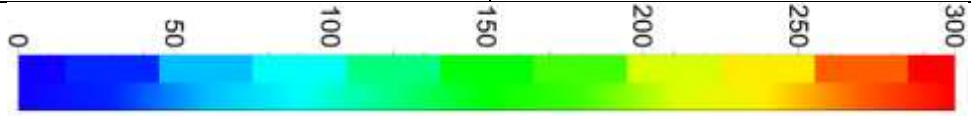	
80 kRPM	

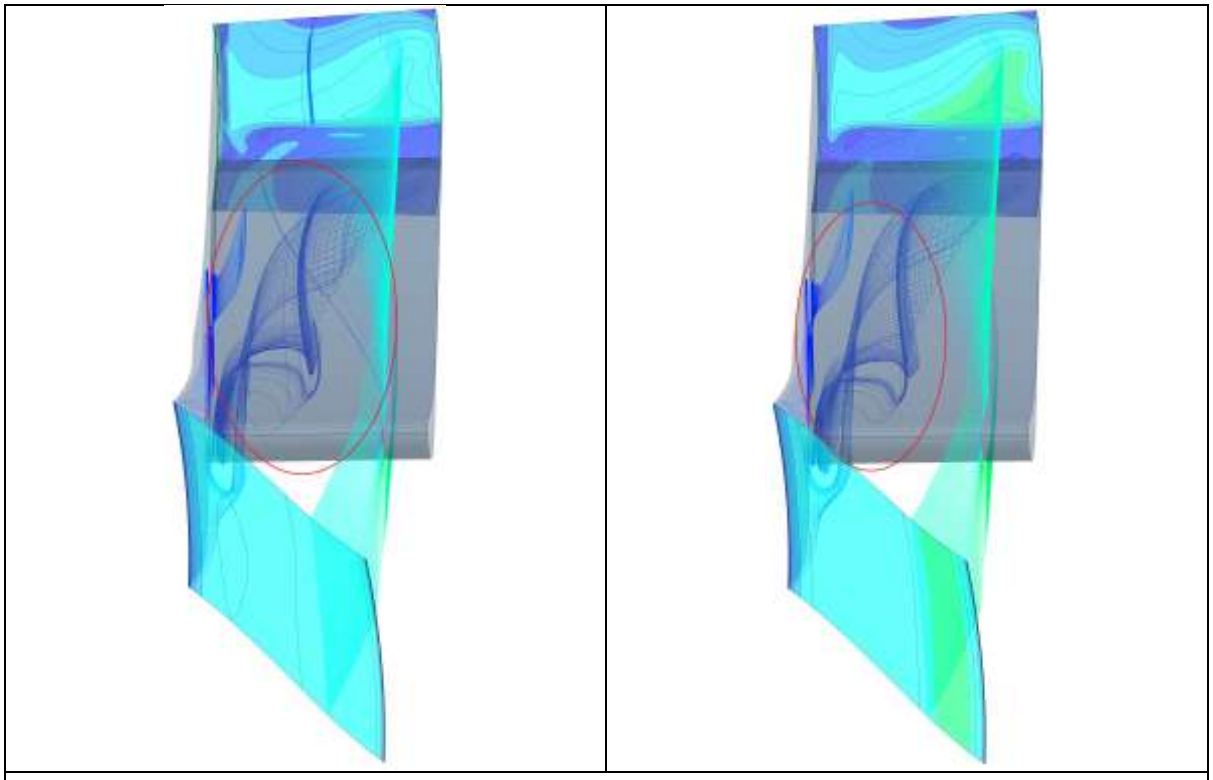

120 kRPM

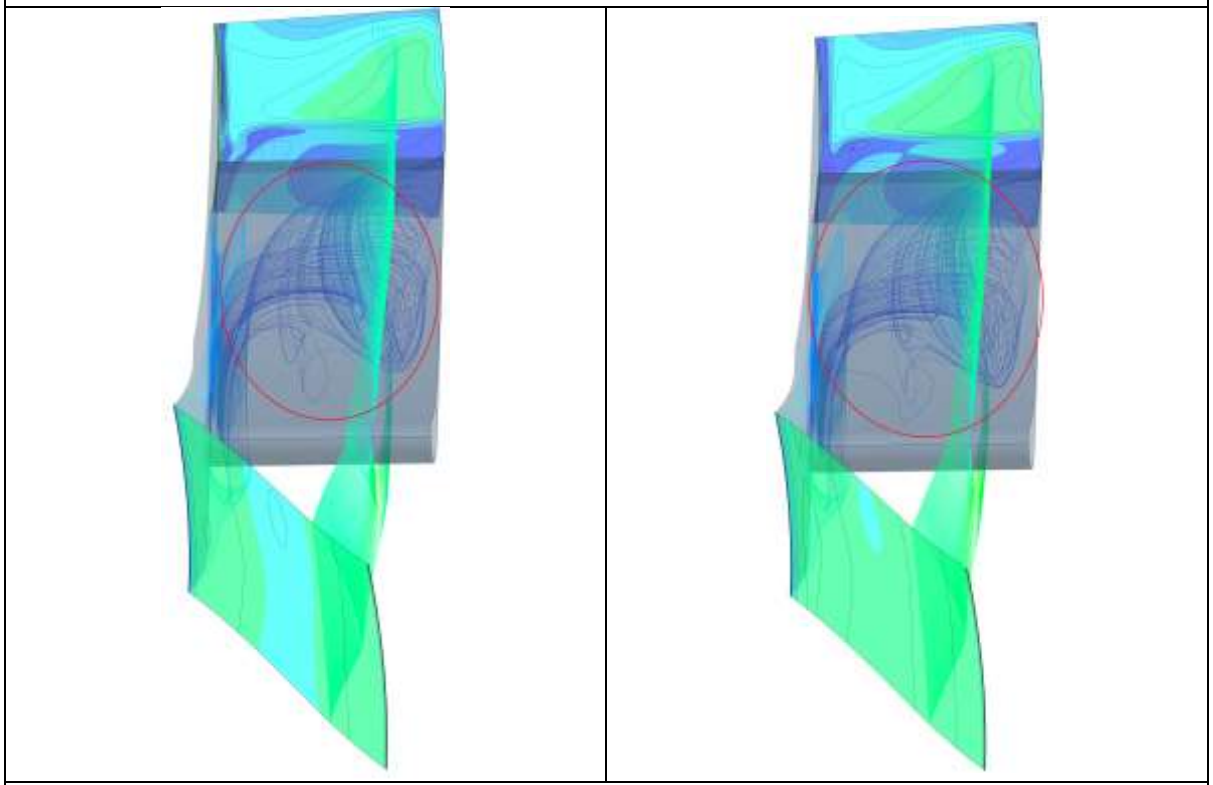

140 kRPM

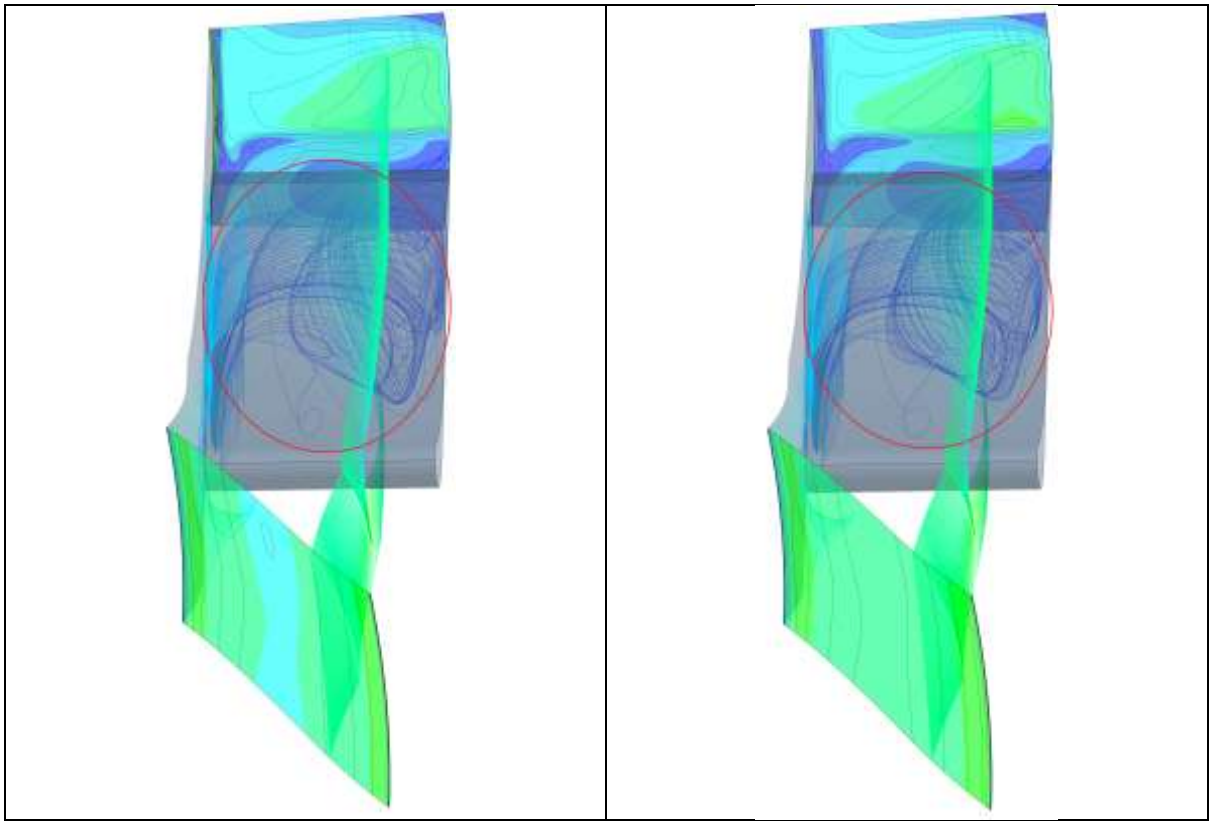

Table 6-4 depicts the pitch average view of the compressor with streamlines drawn from the inlet on the left to the outlet on the right. From this view, it is clear that two recirculation zones were present in the compressor. The first being behind the leading edge of the main impeller blade and the second at the trailing edge of the impeller. The streamlines for 120 kRPM and 140 kRPM are similar but differs at 80 kRPM. At the 80 kRPM, the vortex at the leading edge of the main impeller blade was larger for the global heat addition method than for the primary zone heating method. This indicates the initial stages of surge in the impeller due to the load on the impeller being too small. As the load on the impeller increased, the mass flow rate and pressure ratio also increased, as was the case for primary zone heating, resulting in the compressor operating point moving away from surge and the vortex reducing in size.

The Mach number iso-surfaces given in Table 6-5 strengthens the argument that the load on the impeller was too low for global heat addition at 80 kRPM, the reason being that the compressor is generally designed so that the flow at the impeller tip is sonic. This was, however, not the case for global heat addition, meaning that the load on the impeller was too low.

Table 6-4: Compressor pitch average streamlines coloured by velocity in $m.s^{-1}$.

Global heat addition	Primary zone heat addition
	
80 kRPM	
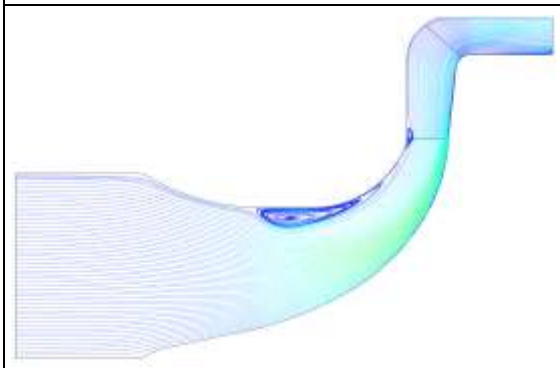	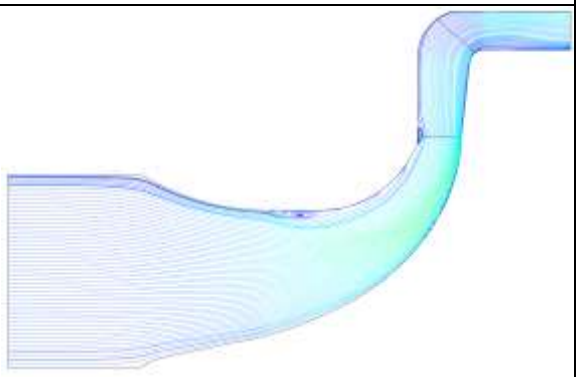
120 kRPM	
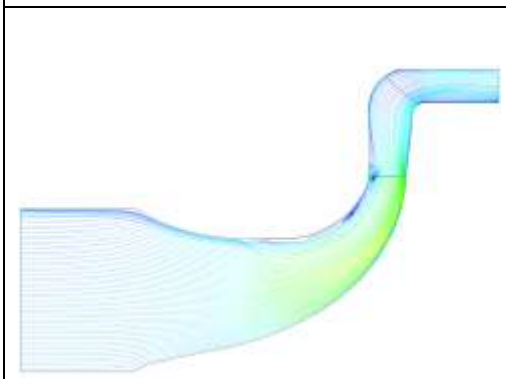	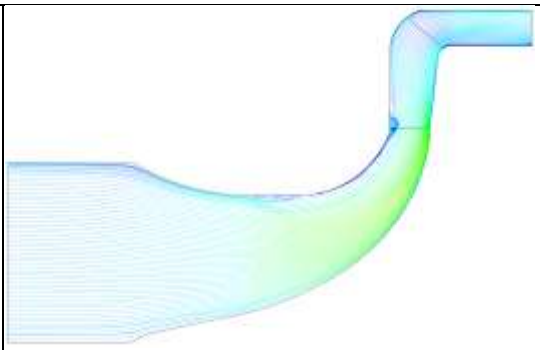
140 kRPM	
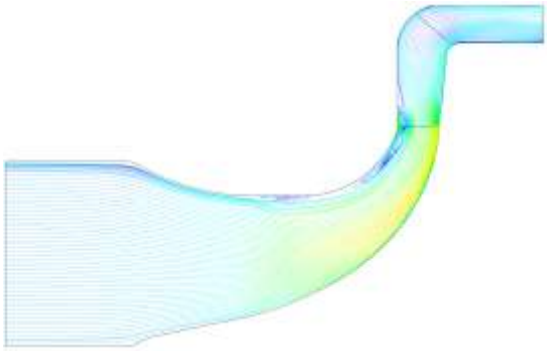	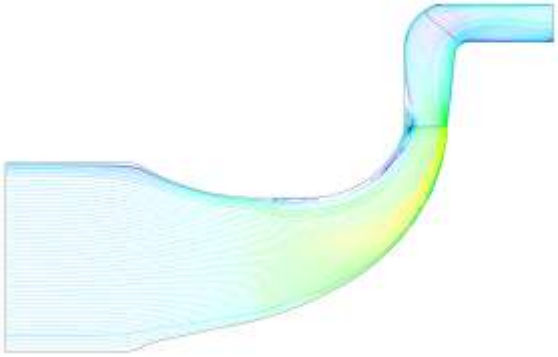

Table 6-5, Table 6-6 and Table 6-7 illustrate the Mach number iso-surfaces corresponding to sonic flow with a Mach number of 1. The flow inside the iso-surface has a Mach number higher than 1. It was found that the sonic region predicted by the primary zone heat addition model was larger for every rotational velocity and component. This is correct because the mass flow rate and thus also the velocity was higher for the primary zone heat addition

method which means that the Mach number would be larger (Eq. 3-2) if the temperature does not differ significantly between the two heat addition methods, which was the case.

Table 6-5 shows the iso-surfaces in the impeller when looking from the inlet downstream. Studying the impeller iso-surfaces given in Table 6-5 and Table 6-6, it is clear that as the rotational velocity and thus also the mass flow rate increased, the sonic region also increased. The sonic region does, however, not cover the entire domain from side to side and hub to shroud which means that the impeller was not choked and did not indicate a component mismatch. The reason for the sonic flow at the inlet was the small inlet flow area together with the blockage caused by the main impeller blade which further reduced the flow area and increased the fluid velocity. This was why splitter blades were used because if it was a full blade, the blockage may have caused the compressor to choke at the impeller inlet. The sonic flow near the shroud at the trailing edge of the impeller blades was a result of the high blade speed as the radius increased.

Table 6-5: Impeller Mach number iso-surface of M=1.

Global heat addition	Primary zone heat addition
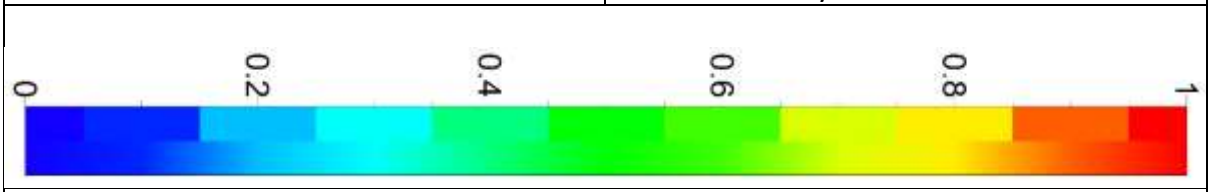	
80 kRPM	
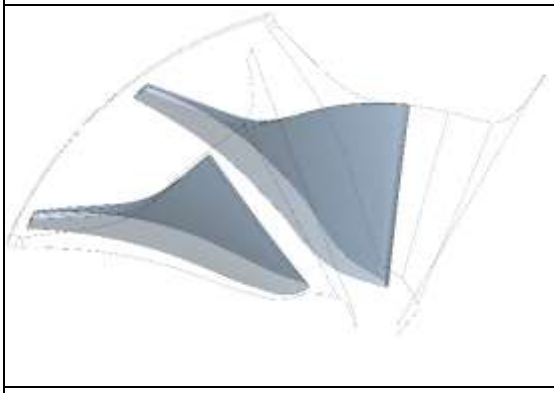	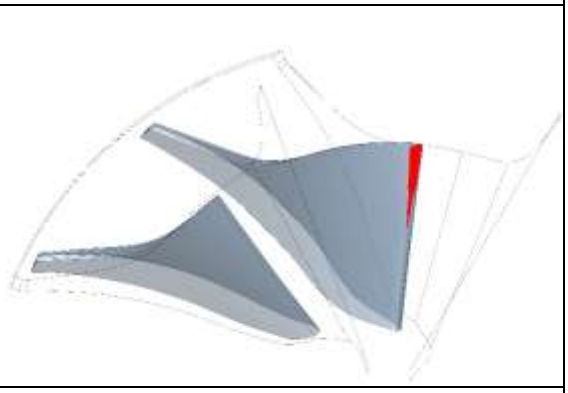
120 kRPM	
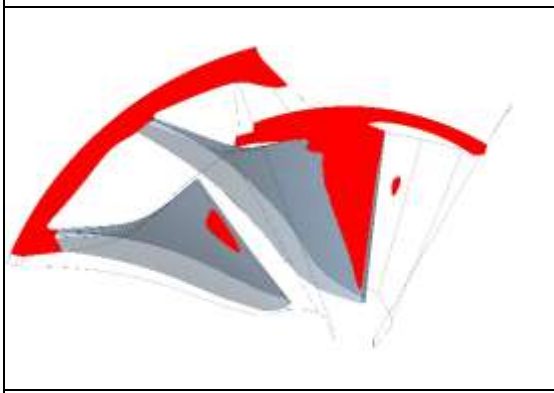	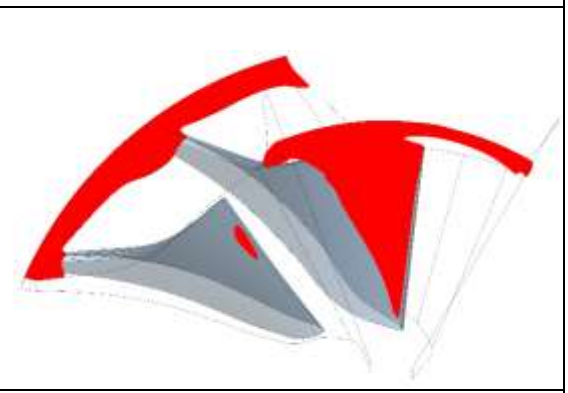
140 kRPM	

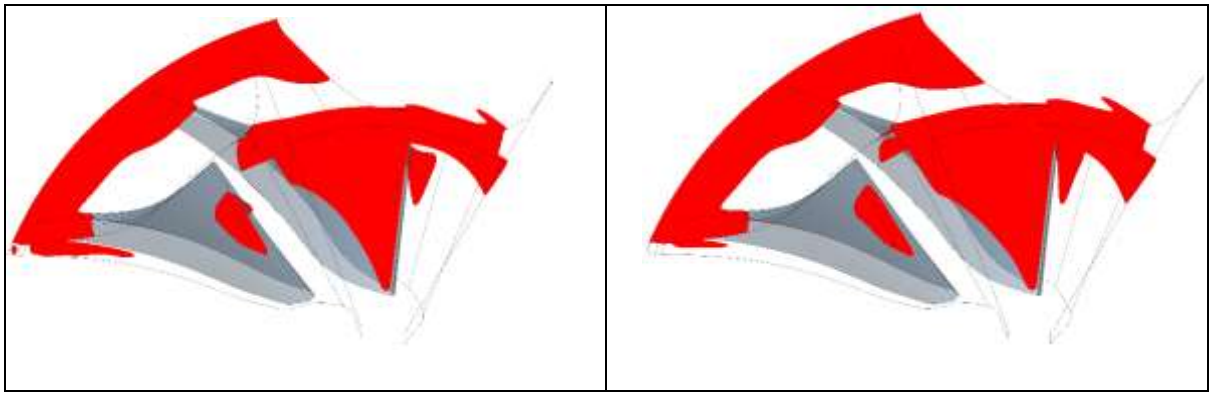

Table 6-6 shows the iso-surfaces on the impeller and wedge diffuser when looking perpendicular to the rotation axis with the leading edge of the wedge being the highest point on the diffuser. Studying the iso-surfaces on the wedge diffuser domain in Table 6-6 and Table 6-7 it is clear that the diffuser did not choke. The sonic flow in the wedge diffuser domain is located at the domain inlet because the inlet is at the smallest radius and thus had the smallest flow area and the highest velocities. The flow area increases as the fluid moves through the wedge diffuser domain which slows the fluid down in order to increase its pressure. The increase in the flow area is caused by the increase in the radius of the flow path while the increasing thickness of the wedge diffuser reduces the rate at which the flow area increases.

Table 6-6: Impeller and wedge diffuser Mach number iso-surface of M=1.

Global heat addition	Primary zone heat addition
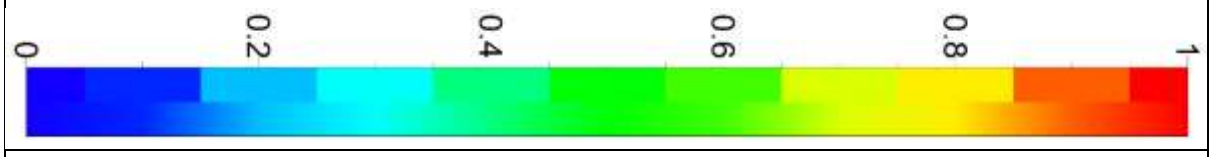	
80 kRPM	

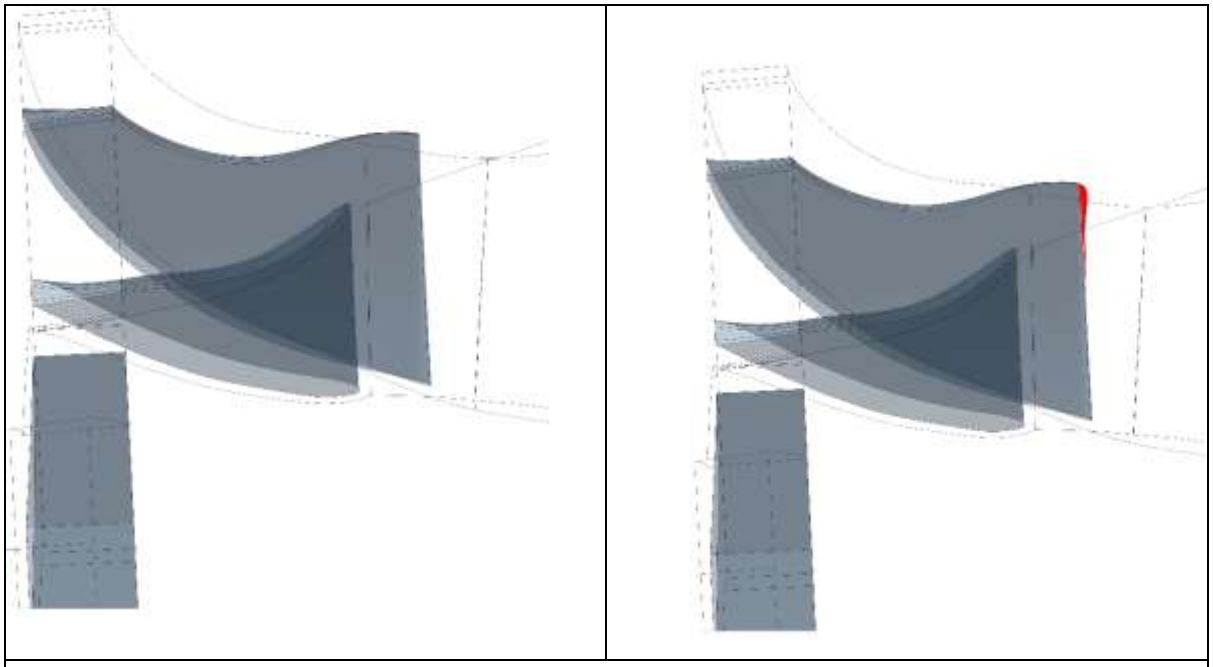

120 kRPM

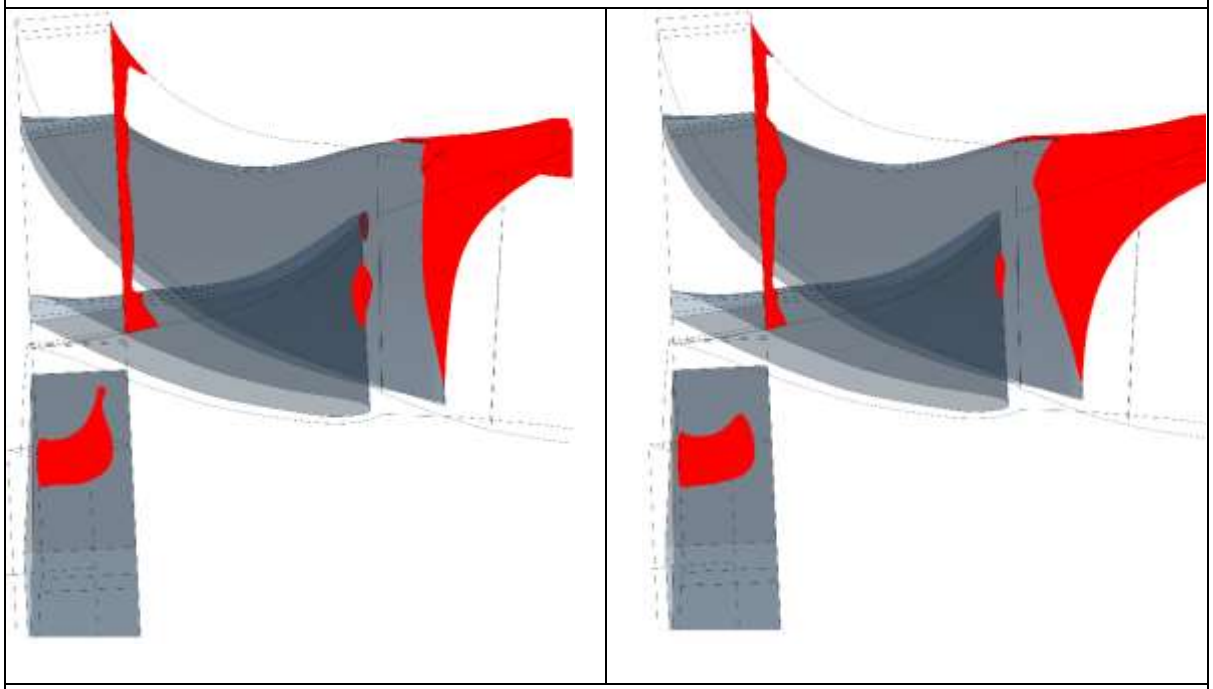

140 kRPM

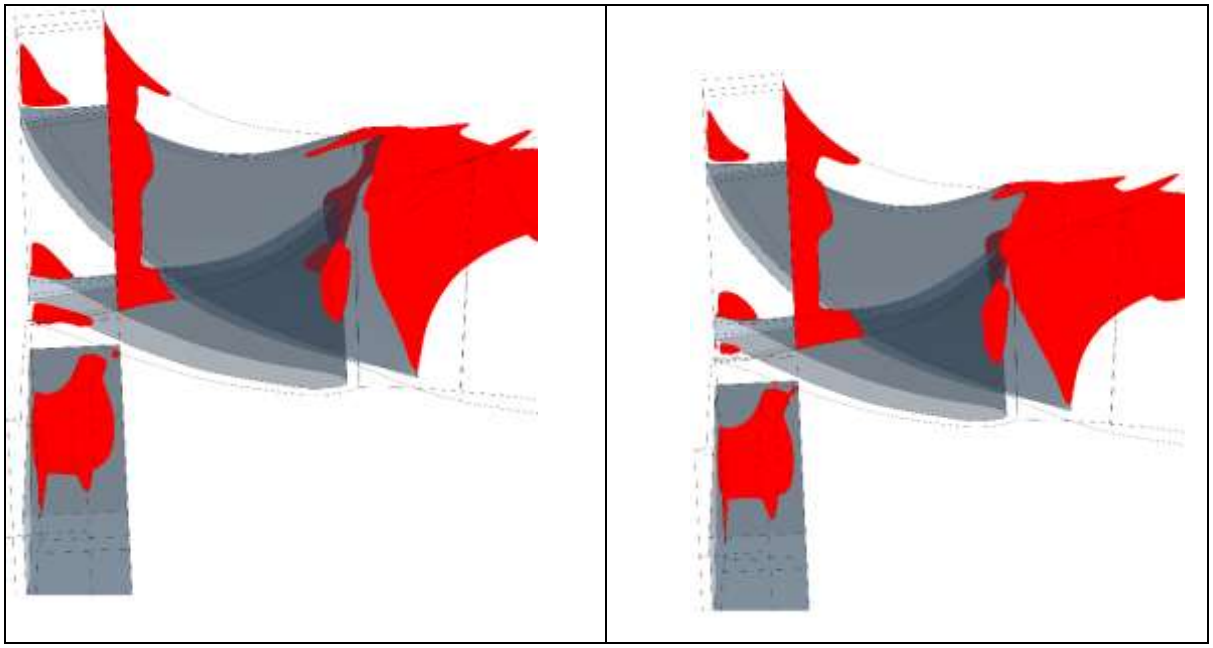

Table 6-7 shows the wedge diffuser and deswirler from above with the suction side of the deswirler and the blunt trailing edge of the wedge diffuser being closest to the viewer. The deswirler does not have any sonic flow because it has the largest radius and thus also the largest flow area. The domain of the deswirler can be choked when a bad design is used where the blockage of the blades is too large but, from the results given in Table 6-7, it is clear that the deswirler did not have this problem.

Table 6-7: Wedge diffuser and deswirler Mach number iso-surface of M=1.

Global heat addition	Primary zone heat addition
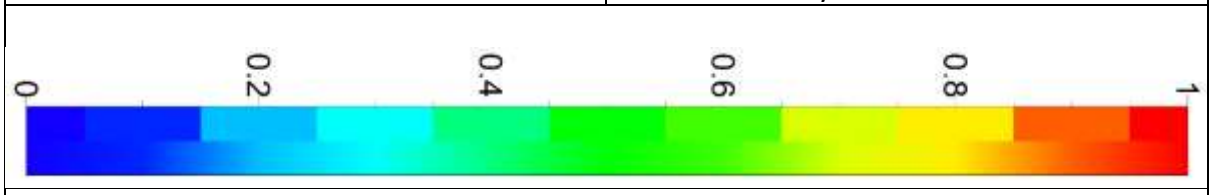	
80 kRPM	
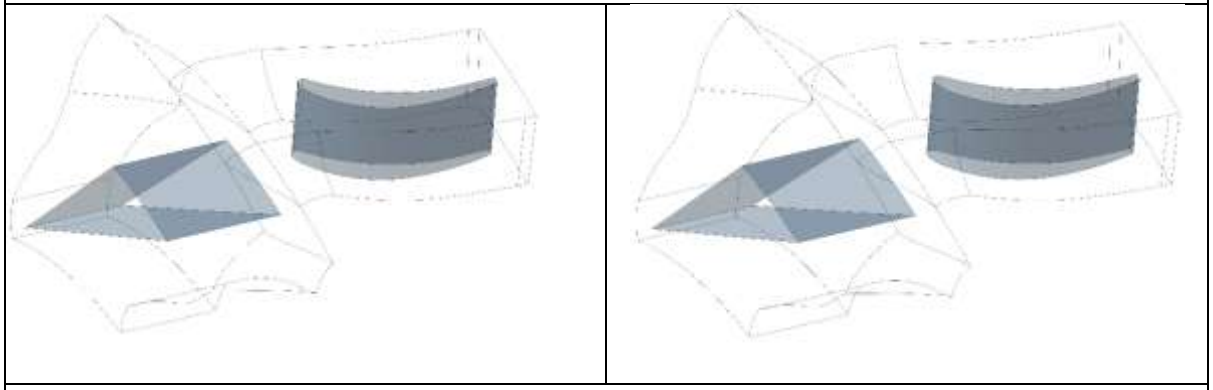	
120 kRPM	

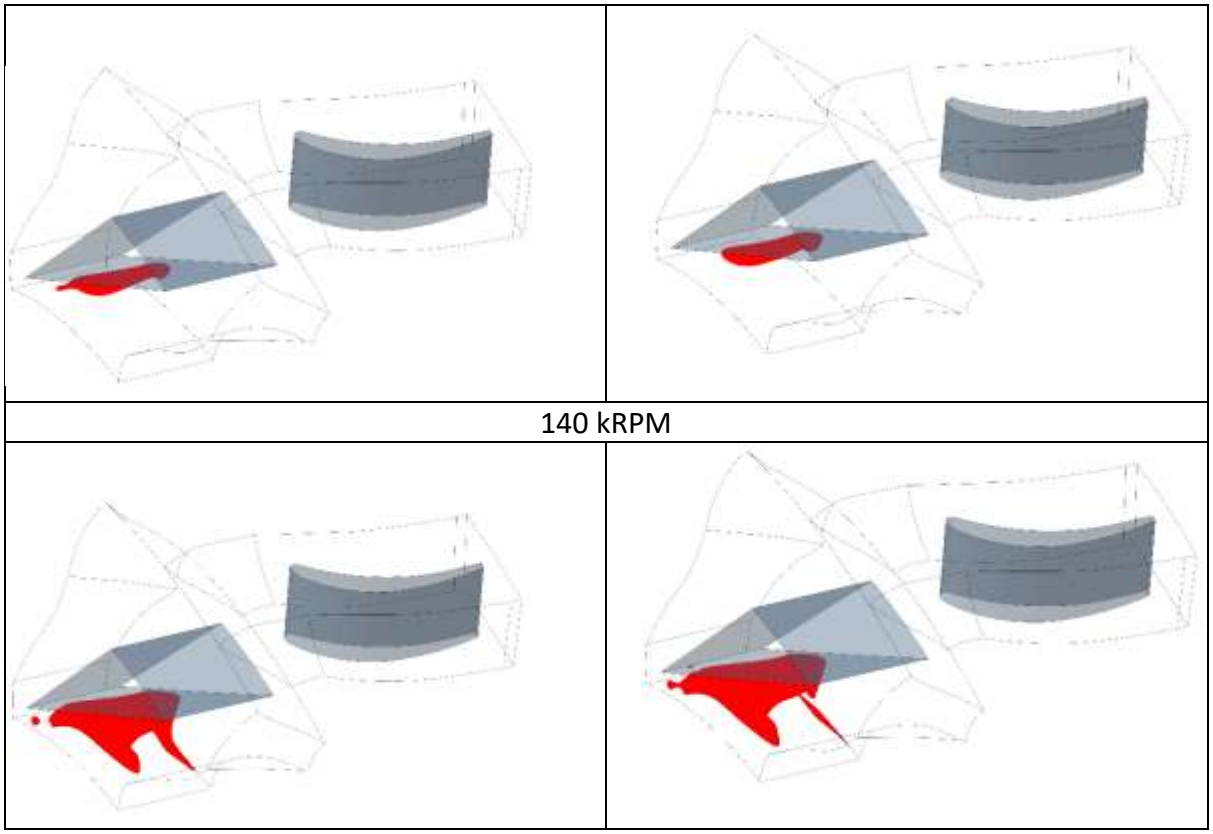

6.3 TURBINE FLOW

The turbine is downstream from the combustor and modelling the combustion process as a heat source would thus have a direct effect on the turbine results. Because of this, it was necessary to check the streamlines to determine if any unrealistic behaviour caused by the combustor could be observed.

Table 6-8 depicts the streamlines in the NGV flowing from right to left (when looking at the suction side of the NGV's leading edge) with the viewer being upstream and slightly higher than the NGV. It is clear that the streamlines did not have any sharp change in direction as expected from the accelerating flow in a turbine. It is noted that the only difference between the graphs is the velocity magnitude which increased as the rotational velocity increased. The vortex below the shroud at the domain inlet was a result of the inlet to the NGV not being smooth and is not related to the heat addition models. The approximately 90^0 corner at the shroud does not direct the flow smoothly into the NGV but allows fluid flowing in the axial and radial direction to enter the NGV. A vortex forms where the two perpendicular velocity vectors enter the NGV. It is clear that the hot fluid temperatures at the hub, as illustrated in Figure 5-5 and Figure 5-7, did not have a noticeable effect on the fluid streamlines through the NGV.

Table 6-8: NGV streamlines coloured by velocity in $m.s^{-1}$.

Global heat addition	Primary zone heat addition
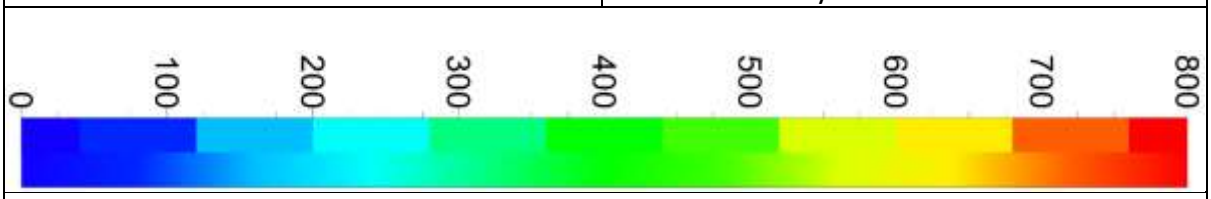	
80 kRPM	
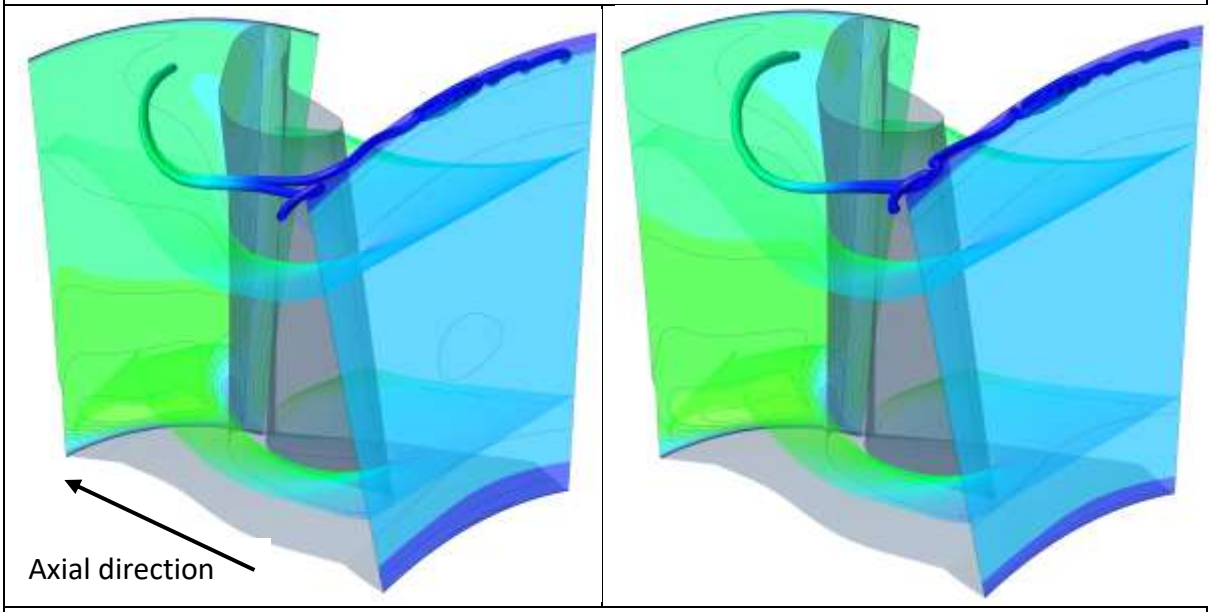	
120 kRPM	
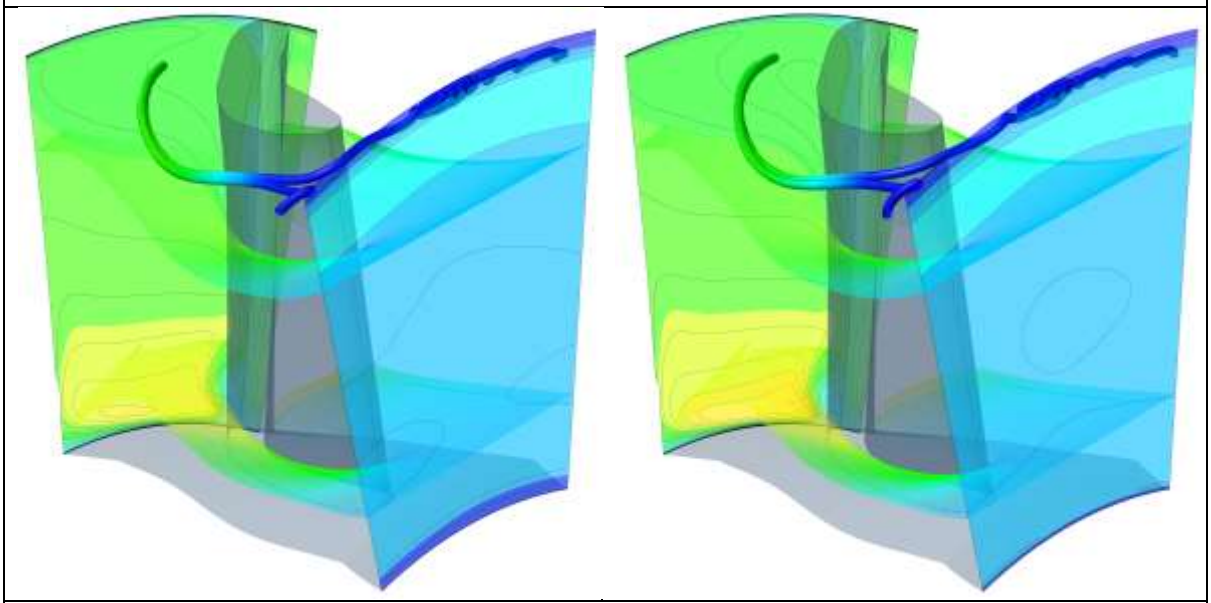	
140 kRPM	

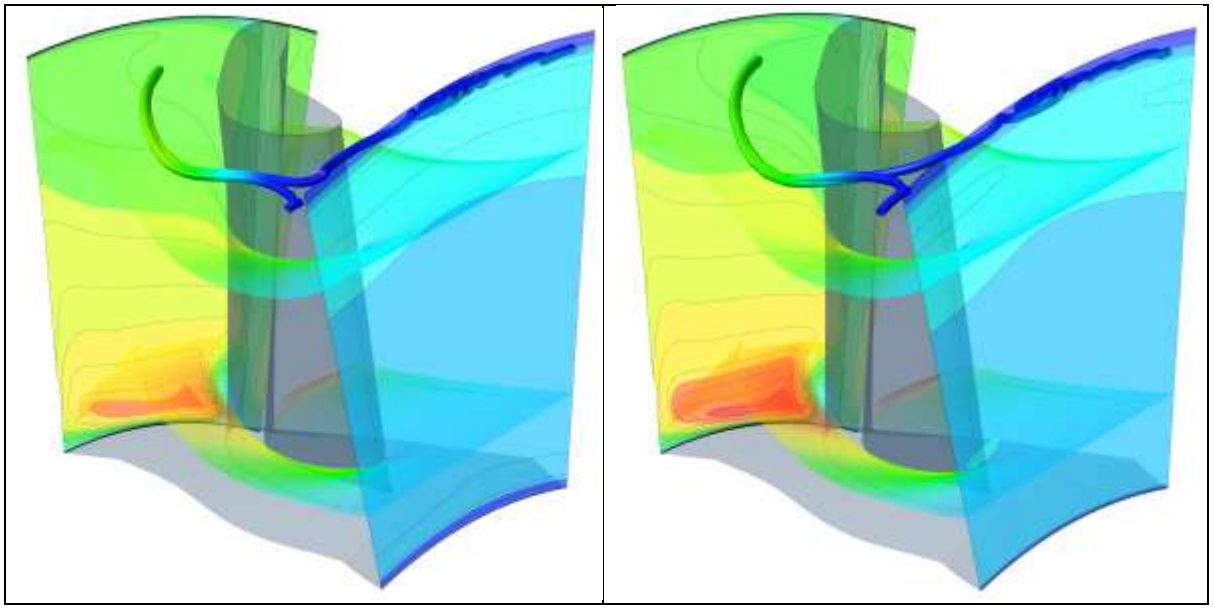

Table 6-9 illustrates the streamlines through the rotor when looking at the suction side of the rotor with the viewer being slightly upstream of the rotor. The streamlines did not present any sharp changes, as expected. The figures also illustrate the secondary flow originating in the tip gap between the rotor and shroud which formed a vortex on the suction side of the blade (Snedden, 2011). As expected, the velocity increased as the rotational velocity increased.

Table 6-9: Rotor streamlines coloured by velocity in $m.s^{-1}$.

Global heat addition	Primary zone heat addition
	
80 kRPM	

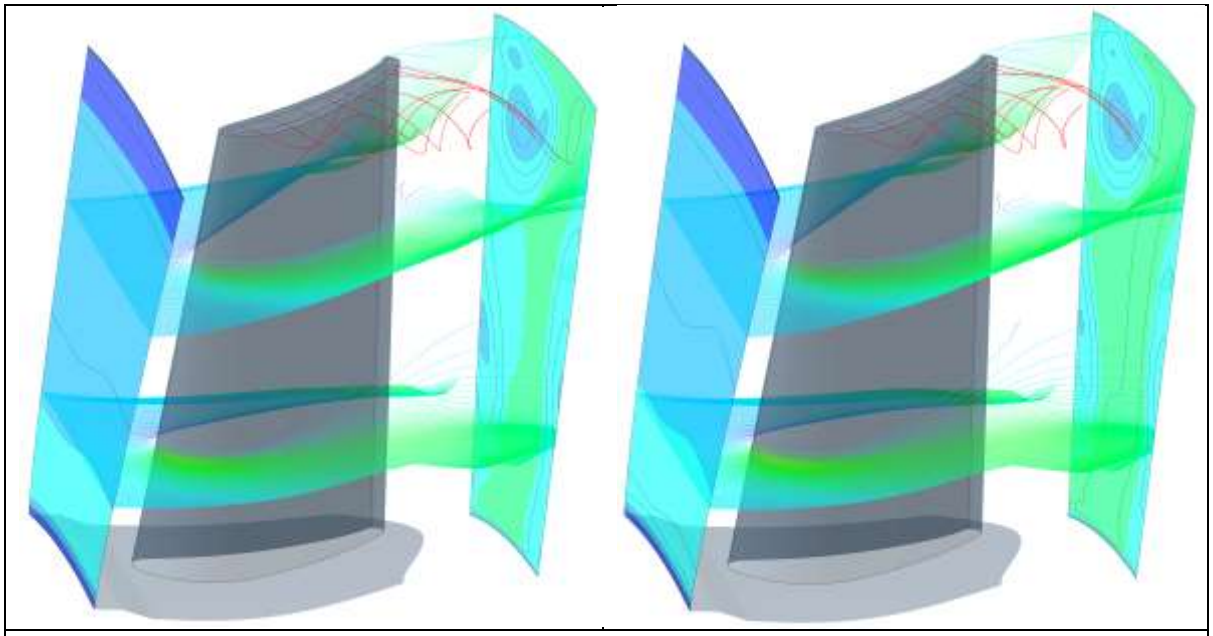

120 kRPM

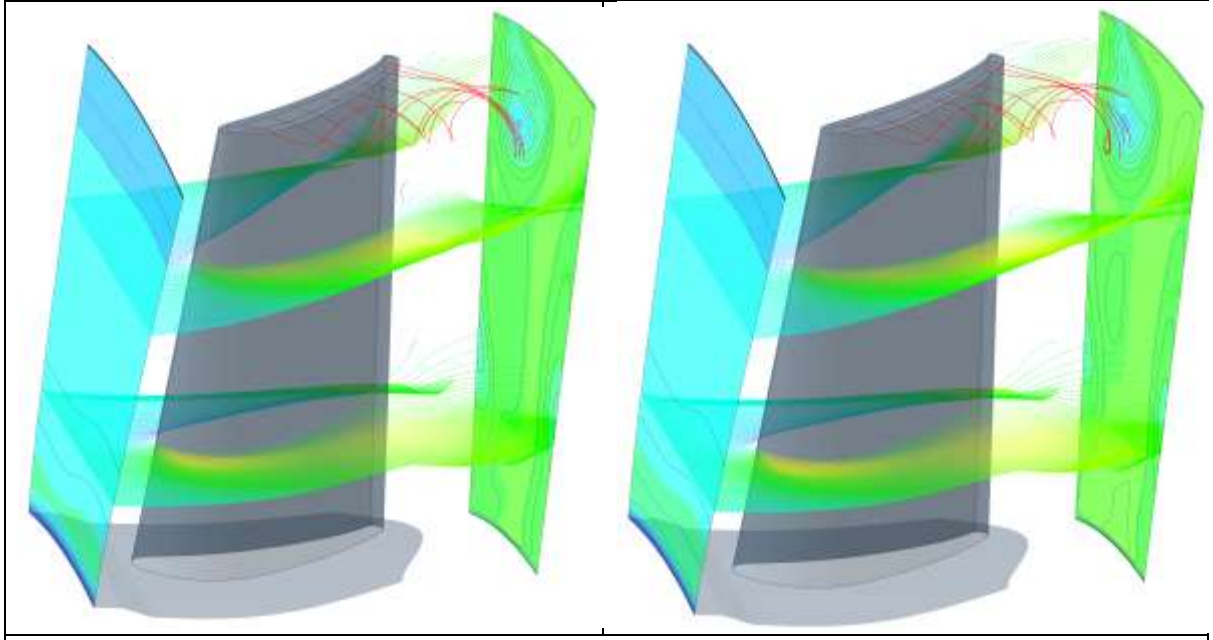

140 kRPM

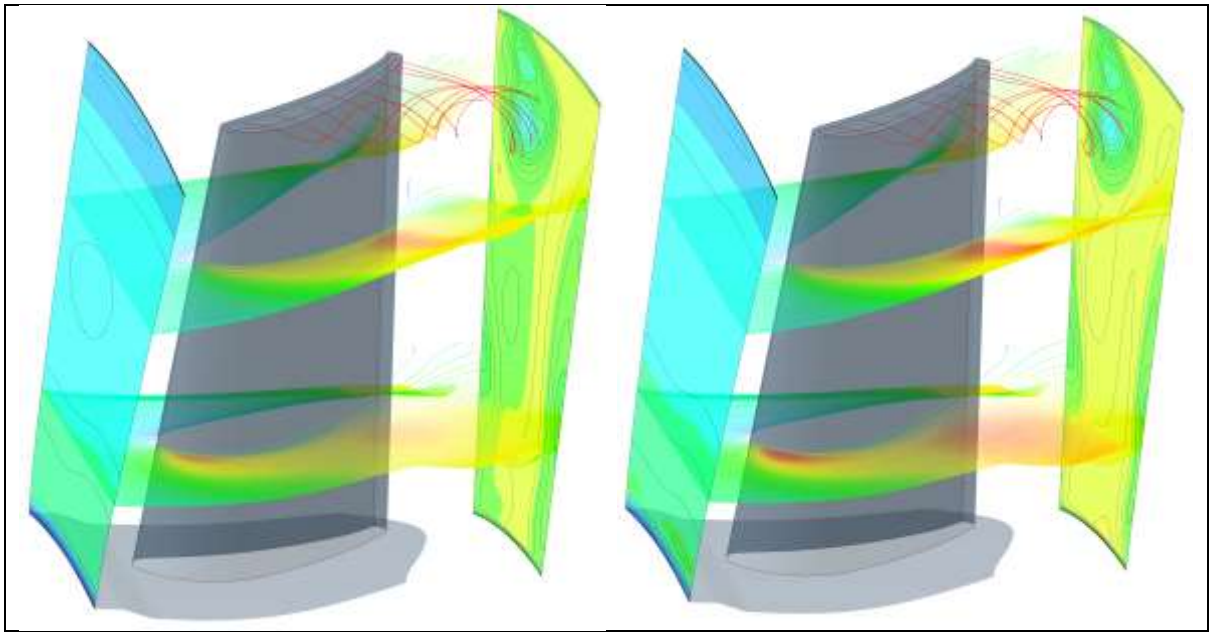

The iso-surfaces for a Mach number of 1 in the turbine is given in Table 6-10 with the views being from opposite sides of the turbine but both viewers are downstream of the turbine. Again it is noted that the sonic region grew as the rotational velocity increased, as expected. The flow was mostly sonic near the blade tip on the suction side of the rotor in the region of the trailing edge because of the following:

1. The blade speed increased with radius, therefore the fluid velocity also increased, causing the flow close to the tip of the blade to be sonic consequently moving down the blade as the rotational velocity increased.
2. The velocities on the suction surface of the blade are higher than on the pressure surface, resulting in the flow first reaching sonic velocities in a region on the suction surface.

The small sonic regions at the 120 kRPM and 140 kRPM speed line were a result of the blades having a highly curved profile around which the fluid had to flow, resulting in the fluid having to accelerate and becoming sonic at those locations.

Table 6-10: Turbine Mach number iso-surface of M=1.

Global heat addition	Primary zone heat addition
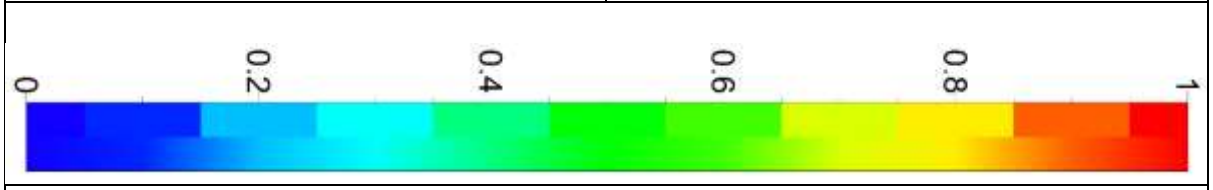	
80 kRPM	

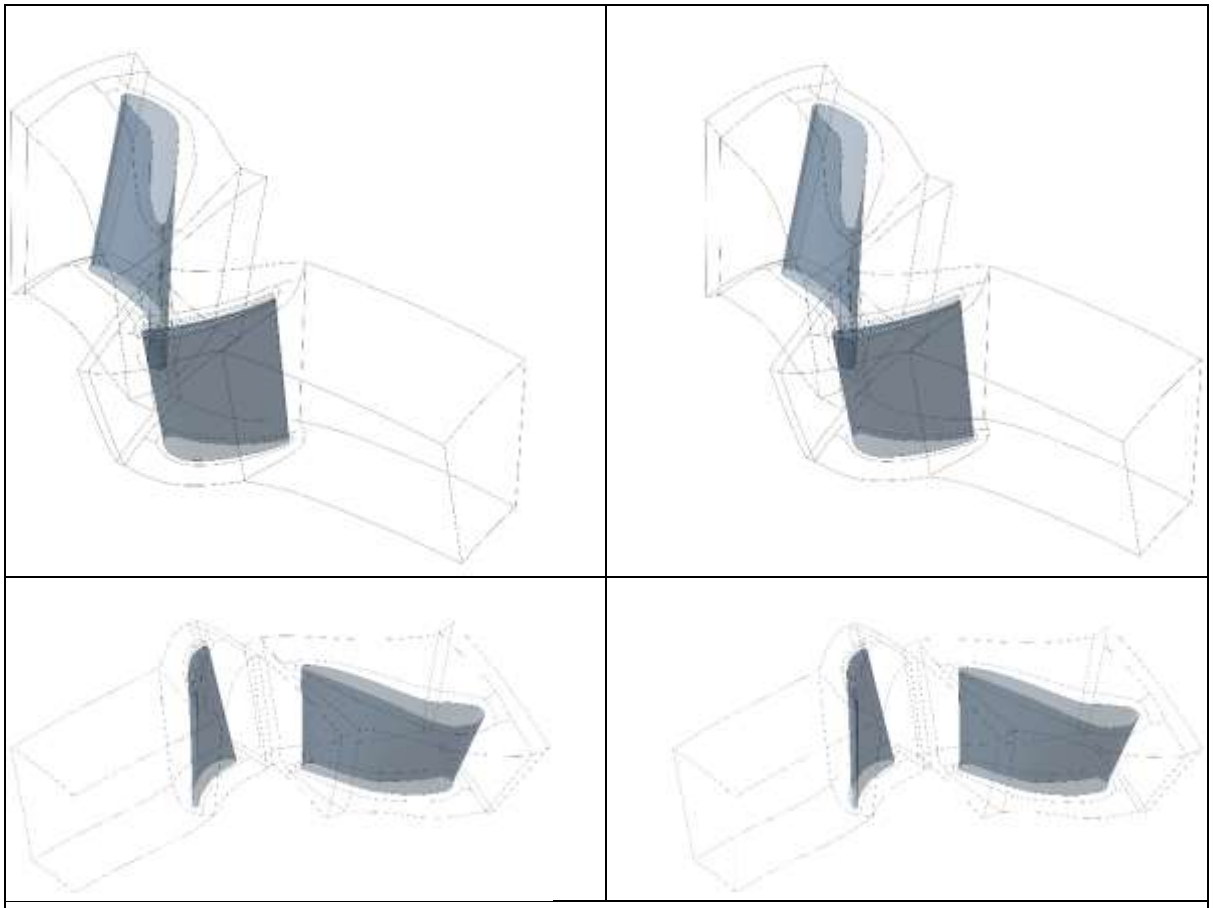

120 kRPM

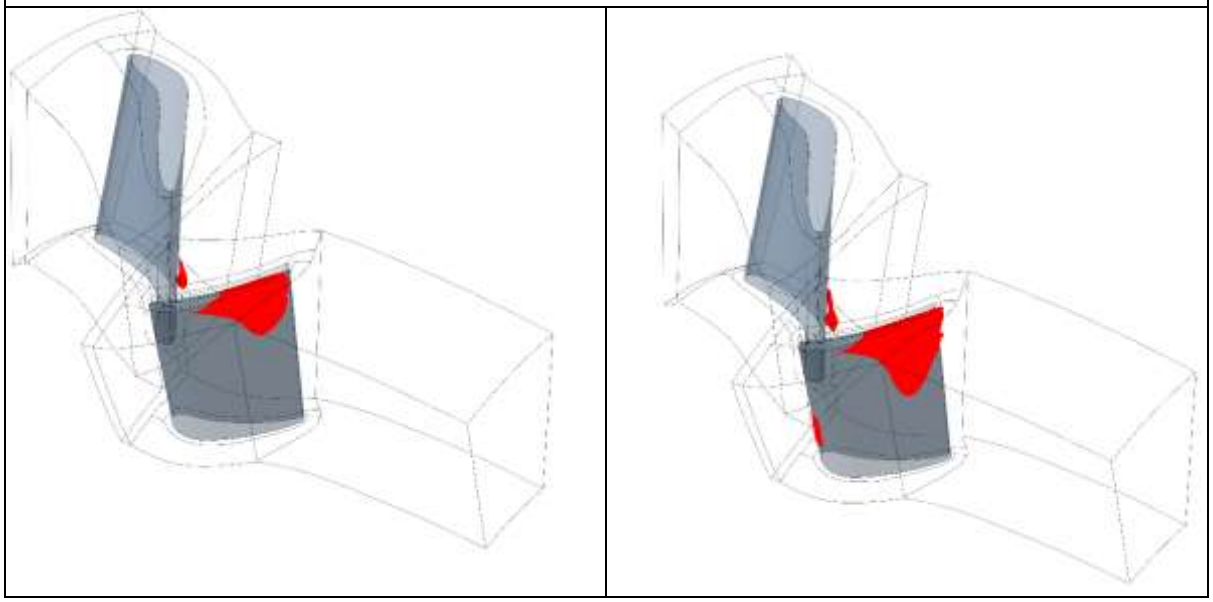

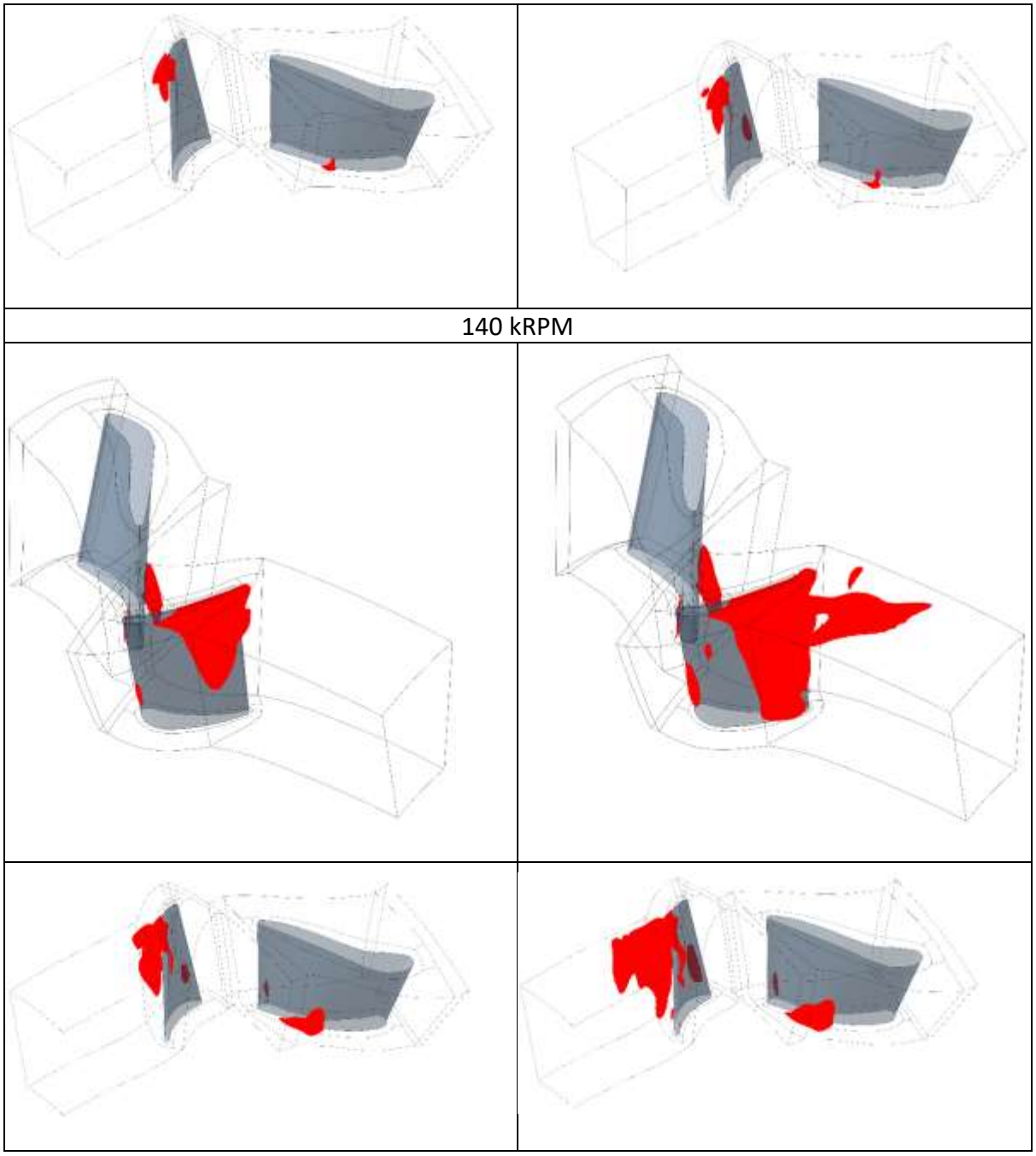

6.4 NOZZLE FLOW

The nozzle is downstream from the turbine and combustor and because there were no irregularities in the turbine caused by the heat addition method, it could be expected that the nozzle would also not present any irregularities.

Table 6-11 illustrates the streamlines through the nozzle entering the outlet domain and leaving through the outlet viewing the nozzle from an upstream location. The results show that the main jet flow did not interact with the wall boundary condition applied at the outer

circumference of the domain meaning that the radius of the outlet domain was large enough. It was also found that the fluid leaving the nozzle had residual swirl and will be discussed together with the results contained in Table 6-12.

Table 6-11: Nozzle streamlines coloured by velocity in m.s^{-1}.

Global heat addition	Primary zone heat addition
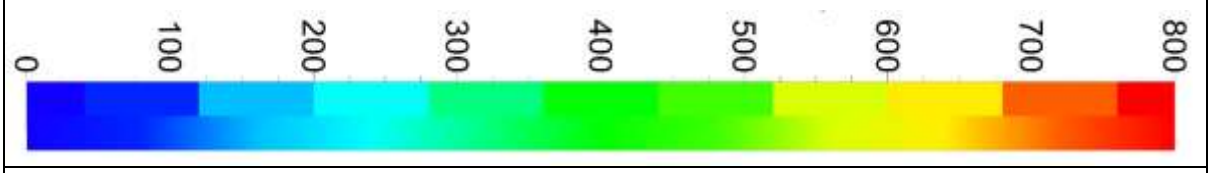	
80 kRPM	
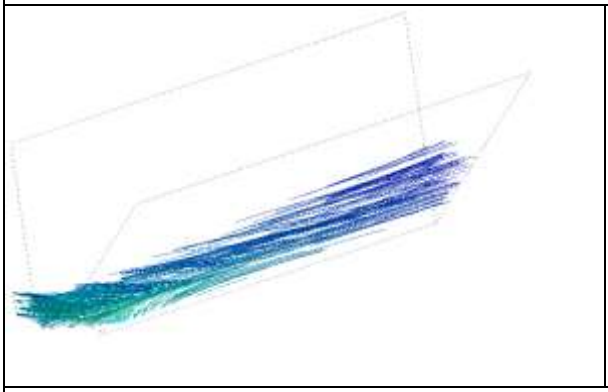	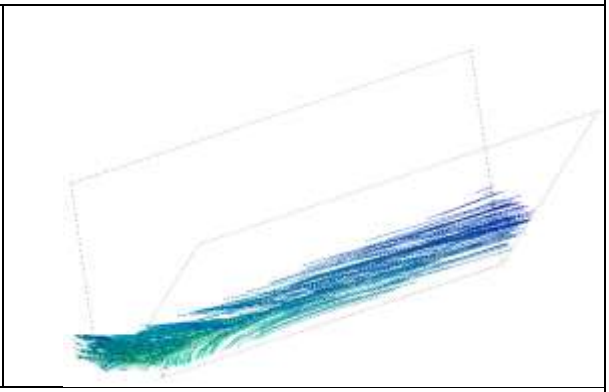
120 kRPM	
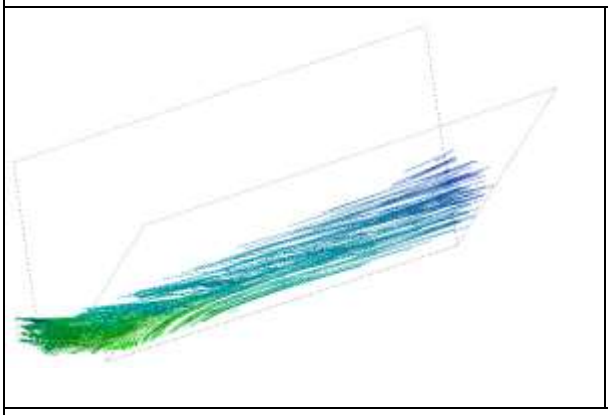	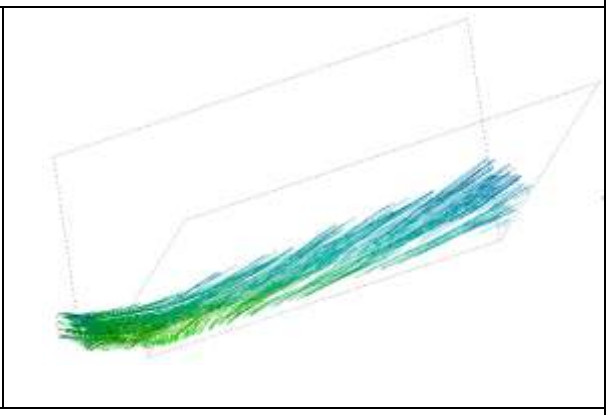
140 kRPM	
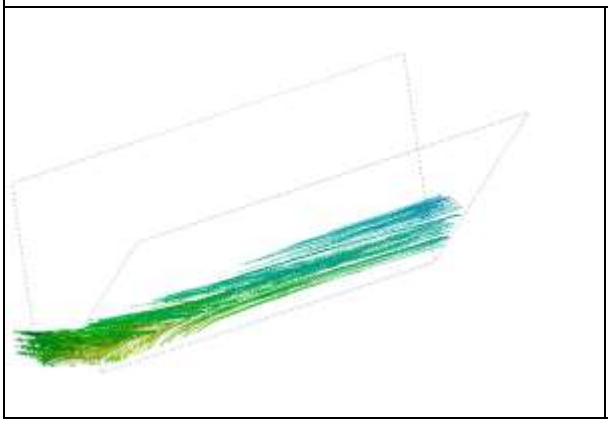	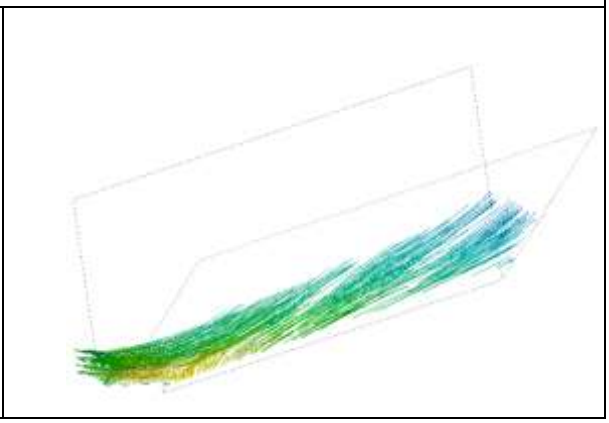

Table 6-12 illustrates the flow swirl angle leaving the turbine domain. The residual swirl differed for each rotational velocity and heat addition method. This was expected because the swirl in the nozzle is coupled to the geometry of the rotor and the mass flow rate. The rotor will generally be designed so that the swirl angle is below 10^0 at the design speed, in this case, 120 kRPM. Despite the uncertainty in the turbine blade geometry as pointed out in Section 3.2, the swirl angle at the pitch line was below 20^0 and close to the ideal value of 5^0 at 80 kRPM and 120 kRPM and means that the turbine has a good design with regards to swirl. The trailing edge blade angle of the simulated turbine was thus likely not significantly different from that of the actual geometry.

Table 6-12: Flow swirl angle in degrees leaving the turbine and entering the nozzle.

Global heat addition	Primary zone heat addition
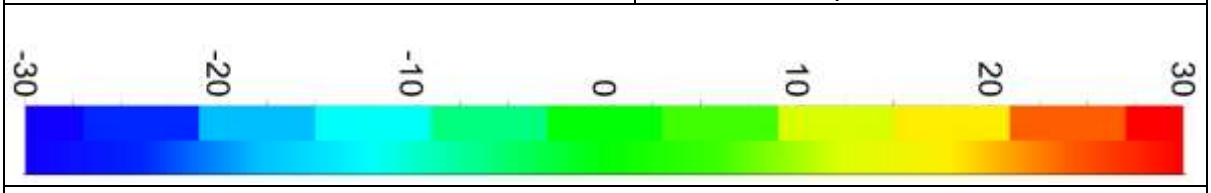	
80 kRPM	
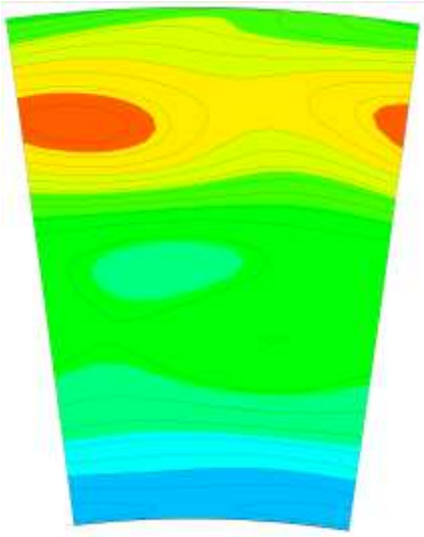	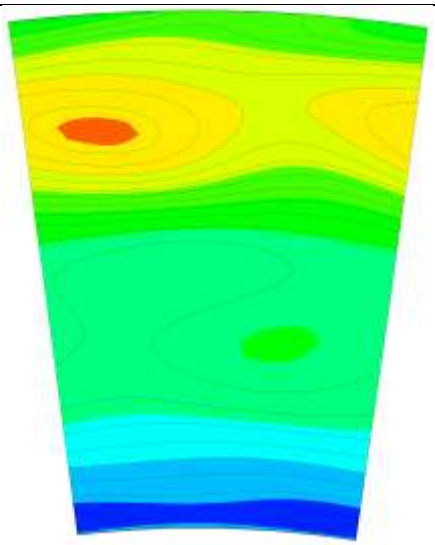
120 kRPM	
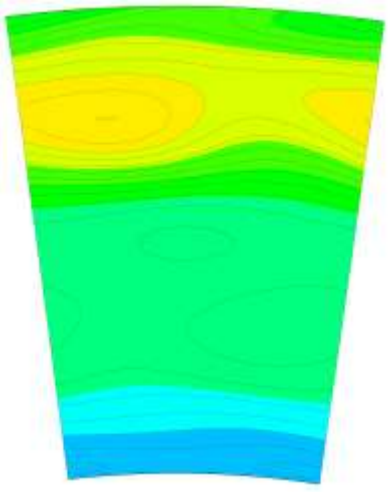	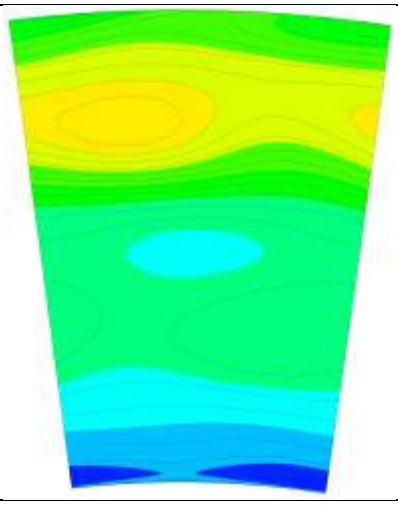
140 kRPM	

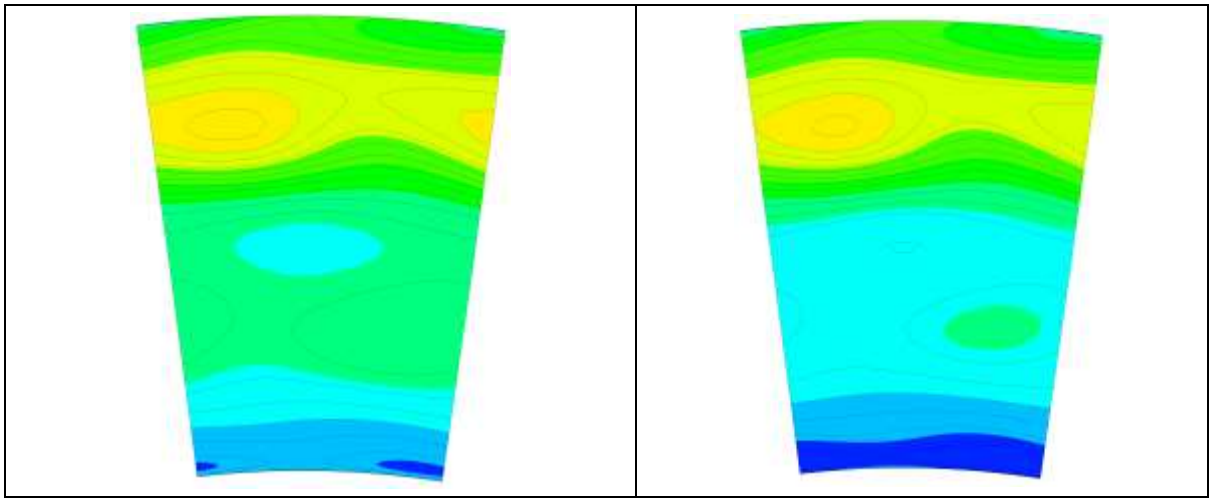

Table 6-13 illustrates the Mach number contours in the nozzle with the nozzle inlet on the left bottom corner of the figures and the outlet on the right. As in the case of the streamline results, the jet had no clear interaction with the top wall at the outer radius of the domain. The Mach number increased with the increase in mass flow rate, as expected, with none of the contours having sonic flow.

Table 6-13: Nozzle centre Mach number contour.

Global heat addition	Primary zone heat addition
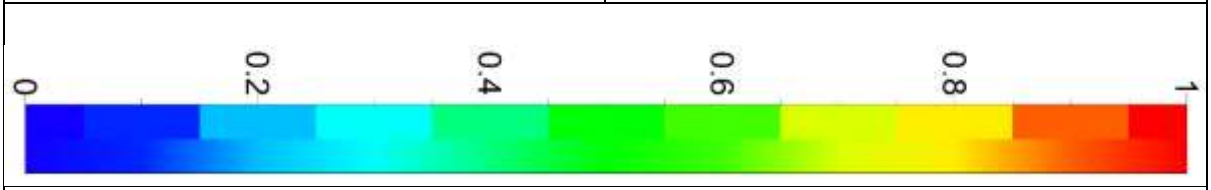	
80 kRPM	
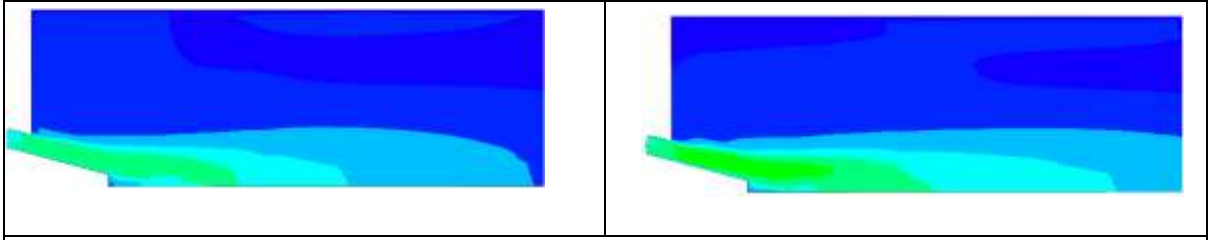	
120 kRPM	
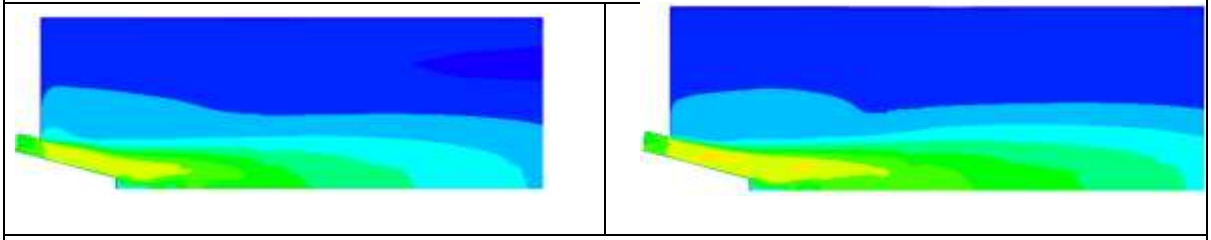	
140 kRPM	

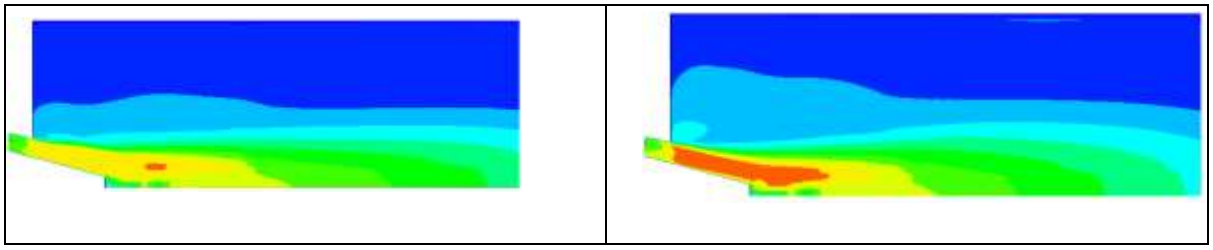

It is noted that the nozzle was nearly choked at 140 kRPM with a mass flow rate of 0.254 kg/s. The experimental mass flow rate at 120 kRPM was 0.288 kg/s and it is therefore clear that the nozzle in the experiments would be nearly choked when running at 120 kRPM. This means that the mass flow would be choked in the nozzle for rotational velocities higher than design speed meaning that the BMT 120 KS engine does not have a component mismatch related to choked flow when assuming the experimental mass flow results are correct.

6.5 SUMMARY

In conclusion, it is clear that the only difference between the global heating results and the primary zone heating results were those caused by the mass flow rate. These differences were visible when plotting the Mach number since the higher the mass flow rate was, the higher the Mach number. The combustor modelling approach did not introduce any irregularities into the flow which may cause the simulation results to differ significantly from the experimental results. Because of this, it can be concluded that if the Mach number plots are important for the outcome of the simulation, the primary zone heating model should be implemented. If this is not the case, the global heat method should be implemented because of its better simulation time.

Up to 140 kRPM no component mismatch was found as expected from an engine that operated successfully. It was expected that the nozzle would choke and limit the mass flow rate at rotational velocities higher than design speed if the experimental mass flow rate was correct.

The limiting factor that prevented the engine from operating up to 140 kRPM, was the TIT due to the addition of too much heat. Table 6-14 gives the TIT for the two heat addition methods at the three rotational velocities simulated.

Table 6-14: TIT for the different heat addition methods at 80, 120 and 140 kRPM

Rotational velocity [kRPM]	Global heat addition	Primary zone heat addition
80	964.7 K	939 K
120	1127 K	1121 K
140	1369 K	1408 K

Because the TIT at 140 kRPM was higher than 1150 K, the engine would not be able to operate at this rotational velocity because the material properties of the turbine would start to weaken due to the high TIT causing either the NGV to melt or the rotor to fail mechanically. Thus, 140 kRPM cannot be considered as a valid operating point and should be avoided.

CHAPTER 7 CONCLUSION

In this study, a heat source is proposed to model the combustion process in a micro gas turbine to reduce simulation time by reducing the number of equations that had to be solved. The simulation time was, however, dependent on the stability of the simulation when applying a heat source. This is because the heat addition methodology caused instability in the model which had to be damped by reducing the CFL number, consequently increasing the simulation times. This means that the possibility to reduce the simulation time of a complete micro gas turbine simulation is dependent on the stability of the model used to solve the combustion process and which heat addition method was used. If both simulations were equally stable, the heat addition simulations would solve the simulation faster.

With regards to the initial research objectives, it can be concluded that suitable boundary conditions were applied to the simulation domain to model the micro gas turbine. The combustion process was simplified by using a heat source.

Two methods were used to model combustion as a heat source, both comparing positively with the experimental results. The mass flow rate was the only variable whose accuracy was of a concern since it was underpredicted on average by 21%. This difference was found to most likely result from a combination of experimental and simulation errors including:

- The bell mouth inlet that was used to calculate the experimental mass flow rate from the pressure measurements, was not calibrated.
- Unrealistically high temperatures in the combustor as a result of excessive heat addition in recirculation zones.
- The interface between the compressor and combustor did not allow the compressor flow to develop.
- Inaccurate blade geometries used in the simulations as no better geometry was available.

The first method that was used to model combustion was to apply a heat source to the entire combustor domain. This method is referred to as the global heat addition method. The second method was to apply a local heat source to the primary combustion zone since this is where combustion takes place in the actual engine. The local heat source was cylindrical and referred to as the primary zone heat addition method. The key features of these two methods are:

1. Global heat addition solved more than six times faster than primary zone heat addition.
2. Primary zone heat addition was more accurate than global heat addition when compared to the experiments.
3. Primary zone heat addition produced temperature distribution in the combustor that could be used to scrutinize the combustor design as follows:

   a. It is able to predict that the combustor liner will be burnt because it has an accurate temperature distribution. This was found to be consistent with the experiments because the combustor liner was burnt during the experiments.
   b. The lack of swirl in the combustor.
   c. The faulty through-flow area ratio between the inner and outer combustor liner which caused the hot flow to attach to the inner combustor liner.
4. Primary zone heat addition is sensitive to recirculation zones which may easily cause unrealistic temperature distributions in the combustor. This means that a suitable location had to be selected for the heat source and this will take time.

Considering the pros and cons it made sense to rather use global heat addition than primary zone heat addition purely because of the time it would take to produce a result. If the results have to be as accurate as possible and a computer with a high number of cores (in the region of 24 cores) were available, primary zone heating would be suggested.

Both methods used to model combustion had no noticeable effect on the streamlines through the engine, but only on the size of the sonic regions. This was expected because the size of a sonic region was directly proportional to the mass flow rate and the two methods did not predict the same mass flow rate. Both methods also predicted that the engine would be able to operate at 80 kRPM and 120 kRPM as was the case in the experiments. It also showed that the engine would not be able to operate at 140 kRPM which was 20 kRPM higher than design speed because the TIT was too high and would cause the turbine to fail.

The simulation method used in this study has the following capabilities:

- It will give a good indication of the engine performance within and outside its operating range.
- The method identified the onset of surge in the compressor due to the mass flow through the compressor being to low.
- The method can predict, with reasonable accuracy, the performance implication of making changes to the engine.
- This method has the potential to identify component mismatches in a micro gas turbine depending on research into the mass flow deficit:
    - If the experimental mass flow rate was at fault, the method can be used to solve mismatches.
    - If the simulation mass flow rate was at fault, implementing the changes in the recommendations is expected to resolve the mass flow rate deficit allowing this method to solve mismatches.

If the mass flow deficit is resolved, the next step would be to investigate whether this method could be used to identify component mismatches by simulating a micro gas turbine with known problems. This simulation would be performed at the rotational velocity at which the engine suffered choke to determine if this method predicts a component mismatch as described in Section 6.1.

CHAPTER 8 RECOMMENDATIONS

This chapter includes recommendations which would be beneficial to add to the method used in this study. These recommendations, when implemented, are expected to reduce the simulation time and improve the simulation results so that it would fit the experimental results better. This chapter also recommends what should be done when the cause of the mass flow deficit is identified.

The most important recommendation would be to investigate the mass flow deficit by doing the following:

1. Calibrate the bell mount inlet.
2. Resolve the unrealistic high temperatures in the combustor.
3. Increase the distance between the deswirler trailing edge and the interface between the compressor and combustor domain. It can be done in several ways, the easiest being to move the compressor forward to create an extended flow passage allowing the flow to develop before it reaches the combustor.

The unrealistically high temperatures in the combustor can be resolved by using one of the following methods:

1. Write a boundary condition for the combustor domain that limits the temperature to 2500 K which is 100 K higher than the maximum flame temperature in the combustion models that was described in Subsection 5.2.1.
2. Experimentally determine the fluid properties of kerosene at high temperature and use it in the simulations.
3. Use the experimental fluid properties of air in the simulation.

The first method would be ideal because it would have a minimal effect on the stability of the simulation. Stability was a major concern for the fluid model since the exponential burnt air material model caused the flow solver to crash and forced the fluid model to have an asymptotic shape. Having an even larger gradient in the C_P vs Temperature values, as proposed by both 2. and 3. above, would worsen the convergence problems.

If limiting the maximum temperature in the combustor and moving the interface further from the deswirler does not improve the mass flow, the following numerical simulations could be performed. These simulations will help determine the cause of the mass flow deficit if it was a result of numerical inaccuracies:

1. Simulate the combustion process using the method described in Section 3.4.
2. Perform the simulations on a different simulation platform such as FloEFD.
3. Perform a Numeca simulation using the same setting that was used by Trebunskikh et al. for the BMT 120 KS geometry and boundary conditions.

The simulations mentioned in the literature correlates well with the experimental results, thus implementing the differences between the simulations in Section 2.6 and those ran in

this study should lead to simulation results that match the experimental results. Implementing the changes in the suggested order would result in systematically finding the cause of the mass flow deficit. If these steps do not declare the source of the problem, the cause may be related to the inaccurate geometrical files as mentioned in Section 3.2.

Another important recommendation is to couple the magnitude of the heat source with the power difference between the compressor and turbine. This essentially automates the simulation process so that every simulation gives a power matched result for a specified rotational velocity which can be compared to experimental results. By doing this, the simulation time would reduce significantly because on average 3 simulations at every rotational velocity was required to have the power in the engine matched. This will then allow the user to compare the simulation and experimental EGT to determine if they are matched.

Linked with the above recommendation would be to increase the accuracy of the simulation by changing the fuel mass flow rate based on the magnitude of the heat source and the heating value of the fuel. This is because, for the simulations in this study, the fuel mass flow rate was held constant at 0.005 kg/s for all simulations for simplicity reasons. The most efficient way to implement this would be to incorporate it into the boundary condition for the magnitude of the heat source as mentioned above. This means that as the heat source is changed to match the power, the fuel mass flow rate would be updated so that the power in the micro gas turbine is matched when all variables are converged. The fuel mass flow rate can be written as a function of the heat source's magnitude using Eq. 8-1:

$$\dot{Q} = \dot{m} \times HV \qquad \textit{Eq. 8-1}$$

With:

- $\dot{Q}$: Heat transfer rate (source or sink) [W].
- $\dot{m}$: Mass flow rate [kg/s].
- HV: The heating value of the fuel used which is approximately 42 MJ/kg for kerosene (Farokhi, 2014).

It is also recommended that further research is done on the effect of the shape of the heating zone when using primary zone heating. This includes using a rectangular doughnut shape heating zone which captures the entire primary heating zone.

It was demonstrated in Section 5.1 that neglecting the combustion process would not have a significant effect on the physics of the micro gas turbine related to component performances. The neglected effects that can be seen as critical for engine operation were linked to the mixing of fuel with air as well as burning the fuel-air mixture. However, because this project involves neglecting the chemistry of combustion to reduce the simulation time, these effects were discarded. If these effects have to be captured, another simulation method has to be used where the combustion process is solved. It is recommended that this method should consist of imposing the combustor inlet and outlet profiles solved in the complete micro gas turbine simulation as boundary conditions to a combustor component simulation. By using

this method, the component simulation would be very similar to simulating the complete engine while solving the combustion process.

Most of the small discrepancies between the simulated and experimental results were found to be as a result of the blades not flapping or smearing and the tip gaps not closing at high rotational velocities. It would not be recommended that these effects be included in the simulation because this would require meshing the solid parts and solving the fluid-structure interaction. In doing this, the simulation time would be increased drastically while the results can only improve by approximately 5% to be the same as the experimental results which does not justify the simulation time.

REFERENCES

Additive manufacturing revolution for gas turbines. 2016. Available: https://www.siemens.com/customer-magazine/en/home/energy/bringing-power-to-the-people/additive-manufacturing-revolution-for-gas-turbines.html [2017, September 07].

AMT Netherlands. n.d. Available: http://www.amtjets.com/ [2017, August 30].

Ando, Y. 2014. *Top 5 Benefits You Need to Know About Utilizing CFD Software » Simulating Reality, Delivering Certainty*. Available: http://simulatemore.mscsoftware.com/5-benefits-you-need-to-know-about-cfd-software/ [2017, October 03].

Banerjee, J. 2018. *What is the difference between single spool and two spool jet engine? - Quora*. Available: https://www.quora.com/What-is-the-difference-between-single-spool-and-two-spool-jet-engine [2019, March 28].

Best practice guidelines for turbomachinery CFD. 2015. Available: https://www.cfd-online.com/Wiki/Best_practice_guidelines_for_turbomachinery_CFD [2018, August 13].

Brasz, J.J. 1988. *Investigation into the Effect of Tip Clearance on Centrifugal Compressor Performance*. Available: https://proceedings.asmedigitalcollection.asme.org [2018, November 16].

Candel, S., Thévenin, D., Darabiha, N., Veynante, D. & Thevenin, D. 1999. Progress in Numerical Combustion. *Combustion Science and Technology*. 149:297–337. DOI: 10.1080/00102209908952110org/10.1080/00102209908952110.

Capitelli, M., Colonna, G., Gorse, C. & D'angola, A. 2000. *Transport properties of high temperature air in local thermodynamic equilibrium*. Available: https://link-springer-com.uplib.idm.oclc.org/content/pdf/10.1007%2Fs100530070094.pdf [2018, September 25].

Capstone Turbine Corporation (CPST). n.d. Available: https://www.capstoneturbine.com/ [2017, August 31].

ÇENGEL, Y.A. & GHAJAR, A.J. 2015. *Heat and Mass Transfer: Fundamentals & Applications*. 5th ed. McGraw-Hill Education.

Cole, K.D. 2003. *Boundary Condition Types.* Available: http://www.greensfunction.unl.edu/OrganizeGF/node1.html [2017, October 16].

"Combustion Modeling". n.d. Available: http://www.ansys.com/-/media/Ansys/corporate/resourcelibrary/brochure/ANSYS-Combustion-Brochure.pdf [2017, October 15].

Combustion Tools | ANSYS Combustion Simulation. n.d. Available: http://www.ansys.com/products/fluids/combustion-tools [2017, October 15].

Corbo, M.A., Stefanko, D.B. & Leishear, R.A. n.d. *PRACTICAL USE OF ROTORDYNAMIC ANALYSIS TO CORRECT A VERTICAL LONG SHAFT PUMP'S WHIRL PROBLEM*. Available: https://pdfs.semanticscholar.org/d88a/def04254cfafebaba294d53a50c5f5ede969.pdf [2018, November 15].

Dunham, J. & Meauze, G. 1998. Agard working group study of 3d navier-stokes codes applied to single turbomachinery blade rows. *ASME 98-GT-50*. 3.

Dunn, D., Snedden, G. & von Backstrom, T.W. 2009. Turbulence model comparison for a low pressure 1.5 test turbine. 1–7. Available: http://researchspace.csir.co.za/dspace/bitstream/10204/4538/1/Dunn_2009.pdf.

Engineering Toolbox. Air - Prandtl Number. 2018. Available: https://www.engineeringtoolbox.com/air-prandtl-number-viscosity-heat-capacity-thermal-conductivity-d_2009.html [2018, June 25].

Farokhi, S. 2014. *Aircraft Propulsion*. 2nd Edition ed. John Wiley & Sons. Available: https://app.knovel.com/web/toc.v/cid:kpAPE00015/viewerType:toc//root_slug:aircraft-propulsion-2nd/url_slug:engine-thrust-performance?&issue_id=kpAPE00015 [2018, September 25].

FLUENT 6.3 User's Guide - 15. Modeling Non-Premixed Combustion. n.d. Available: https://www.sharcnet.ca/Software/Fluent6/html/ug/node623.htm [2018, July 26].

FLUENT 6.3 User's Guide - 25.8.1 First-Order Accuracy vs. Second-Order Accuracy. 2006. Available: https://www.sharcnet.ca/Software/Fluent6/html/ug/node1015.htm [2018, September 04].

Follow the chemistry to better CFD combustion simulations - SAE International. n.d. Available: http://articles.sae.org/15182/ [2017, October 15].

Gas turbines - Power Generation - Siemens Global Website. n.d. Available: https://www.siemens.com/global/en/home/products/energy/power-generation/gas-turbines.html#!/ [2017, August 29].

Gilheany, S. 2003. *RAM is 100 Thousand Times Faster than Disk for Database Access*. Available: https://www.directionsmag.com/article/3794 [2018, July 02].

Gonzalez, C.A., Wong, K.C. & Armfield, S. 2007. *Computational study of a micro-turbine engine combustor using large eddy simulation and Reynolds averaged turbulence models*. Available: http://anziamj.austms.org.au/ojs/index.php/ANZIAMJ/article/view/ [2018, November 07].

Griffis, C., Wilson, T., Schneider, J. & Pierpont, P. 2009. Unmanned Aircraft System Propulsion Systems Technology Survey. Available: http://commons.erau.edu/publication [2017, October 13].

Grosshauser, R. 2016. *Turbines vs. Reciprocating Engines - Power Engineering*. Available: http://www.power-eng.com/articles/print/volume-120/issue-11/features/turbines-vs-reciprocating-engines.html [2017, October 03].

Haque, A., Ahmad, F., Yamada, S. & Chaudhry, S.R. 2007. Assessment of Turbulence Models for Turbulent Flow over Backward Facing Step. *World Congress on Engineering*. 2. Available: http://www.iaeng.org/publication/WCE2007/WCE2007_pp1340-1345.pdf [2018, December 13].

Heat Transfer Boundary Conditions. n.d. Available: http://help.autodesk.com/cloudhelp/2014/ITA/SimCFD/files/GUID-D39DB8C7-05C5-481B-8604-6EB0EF6E69A9.htm [2017, October 16].

Jaguar C-X75 Concept. 2010. Available: http://www.bladonjets.com/applications/automotive/jaguar-c-x75-concept-case-study/ [2017, October 13].

Jet Engine Diagram. n.d. Available: http://aliveandbloggin.com/jet-engine-diagram.html [2017, October 08].

Korpela, S.A. 2011. *Principles of Turbomachinery*. John Wiley & Sons. Available: http://www.wiley.com/go/permission. [2018, June 26].

Krige, D.S. 2013. Performance Evaluation of a Micro Gas Turbine Centrifugal Compressor Diffuser by. (March).

Lefebvre, A.H. & Ballal, D.R. 2010. *GAS Turbine Combustion Alternative Fuels and Emissions*. 3rd Edition ed. Taylor & Francis Group. Available: http://160592857366.free.fr/joe/ebooks/Automative engineering books/GAS Turbine Combustion Alternative Fuels and Emissions.pdf [2018, November 12].

Leniart, A. 2017. *Hard Drive vs RAM Drive Speed Comparisons. RAMDisk introduced!* Available: https://www.experts-exchange.com/articles/30459/Hard-Drive-vs-RAM-Drive-Speed-Comparisons-RAMDisk-introduced.html [2018, July 02].

Marcellan, A. 2015. An exploration into the potential of microturbine based propulsion systems for civil Unmanned Aerial Vehicles. Available: https://repository.tudelft.nl/islandora/object/uuid:db9e8daf-dede-4915-9425-df4bc9706c12/datastream/OBJ [2017, October 13].

Micro jet turbine-powered Jet Vest developers seek a Kickstart. n.d. Available: http://newatlas.com/jet-vest-micro-turbine-rocket-belt/25431/ [2017, August 30].

Microturbine - definition of Microturbine by The Free Dictionary. n.d. Available: http://www.thefreedictionary.com/Microturbine [2017, August 29].

Microturbines - What is a Microturbine? n.d. Available: http://physics.oregonstate.edu/~hetheriw/projects/energy/topics/doc/elec/natgas/micro/Microturbines - What is a Microturbine.htm [2017, August 29].

Microturbines | WBDG Whole Building Design Guide. n.d. Available: https://www.wbdg.org/resources/microturbines [2017, August 29].

Mini Gas Turbine Lab | Educational Gas Turbine Jet Engine. n.d. Available: http://www.turbinetechnologies.com/educational-lab-products/turbojet-engine-lab [2017, August 29].

Müller, B. 1990. Comparison of Upwind and Central Finite-Difference Methods for the Compressible Navier-Stokes Equations. In *Numerical Treatment of the Navier-Stokes Equations*. Wiesbaden: Vieweg+Teubner Verlag. 90–99. DOI: 10.1007/978-3-663-14004-7_9.

Nusca, M.J., Chen, C.-C. & McQuaid, M.J. 2010. Modeling the Combustion Chamber Dynamics of Selectable-Thrust Rocket Motors. In *2010 DoD High Performance Computing Modernization Program Users Group Conference*. IEEE. 177–183. DOI: 10.1109/HPCMP-UGC.2010.37.

Oppong, F. 2016. Micro Gas Turbine Performance Evaluation. Stellenbosch University.

Paquin, R. 2015. Saving Time and Reducing Costs Through Simulation Consolidation. Available: http://investors.ansys.com/~/media/Files/A/Ansys-IR/annual-reports/whitepapers/aberdeen-saving-time-and-reducing-costs.pdf [2017, October 03].

PBS - Aircraft Engines. n.d. Available: http://www.pbsvb.com/customer-industries/aerospace/aircraft-engines [2017, October 13].

PBS - TJ80 Turbojet Engine. n.d. Available: http://www.pbsvb.com/customer-industries/aerospace/aircraft-engines/turbojet-engine-tj80 [2017, August 30].

Reed, J.A., Turner, M.G., Norris, A. & Veres, J.P. 2003. Towards an Automated Full-Turbofan Engine Numerical Simulation. *NASA Technical Memorandum; XVI Int. Symposium on Air Breathing Engines 2003*. (August):1–16.

Roache, P.J. 1998. *Verification and Validation in Computational Science and Engineering*. Albuquerque, New Mexico.

Salim, S.M. & Cheah, S.C. 2009. Wall y + Strategy for Dealing with Wall-bounded Turbulent Flows. *International MultiConference of Engineers and Computer Scientists (IMECS)*. II:1–6. DOI: 10.1.1.149.722.

Schlüter, J., Apte, S., Kalitzin, G., Weide, E.V.D., Alonso, J.J. & Pitsch, D.H. 2005. Large-scale integrated LES-RANS simulations of a gas turbine engine. *Center for Turbulence Research Annual Research Briefs*. 10. Available: https://web.stanford.edu/group/ctr/ResBriefs05/schluter2.pdf [2017, October 10].

science in a can, Yves Rossy: A Modern-Day Daedalus Ovid's legendary... n.d. Available: http://sciencesoup.tumblr.com/post/36772837146/yves-rossy-a-modern-day-daedalus-ovids-legendary [2017, August 30].

Sideroff, C. n.d. *Multi-Block Structured Meshing and Pre-Processing for OpenFOAM Turbomachinery Analysis*. Available: http://www.personal.psu.edu/dab143/OFW6/Training/sideroff_slides.pdf [2018, August 13].

Slagter, W. 2011. Cutting Design Cost: How Industry Leaders Benefit from Fast and Reliable CFD. Available: http://www.ozeninc.com/wp-content/uploads/2015/10/wp-cfd-business-benefits.pdf [2017, October 03].

Snedden, G.C. 2011. The Application of Non-Axisymmetric Endwall Contouring in a 1.5 Stage, Rotating Turbine. Durham University. Available: http://etheses.dur.ac.uk [2018, August 15].

Sutherland's law. 2008. Available: https://www.cfd-online.com/Wiki/Sutherland%27s_law [2018, July 02].

Sutherland, W. 1893. LII. The Viscosity of Gases and Molecular Force. *Philosophical Magazine Series 5, 36:223*. 507–531. DOI: 10.1080/14786449308620508.

Swanson, R.C. & Turkel, E. 1990. *ON CENTRAL-DIFFERENCE AND UPWIND SCHEMES*. Available: http://www.dtic.mil/dtic/tr/fulltext/u2/a227206.pdf [2018, August 27].

"The use of Micro turbine generators in hybrid electric vehicles". 2000. Available: http://www.bioturbine.org/Publications/PDF/microturbine-01-HILTECH.pdf [2017, August

31].

Trebunskikh, T. V, Ivanov, A. V & Dumnov, G.E. n.d. *FloEFD simulation of micro-turbine engine*. Available: http://cadflo.com/fileadmin/user_upload/Trebunskikh__-FloEFD_simulation_of_micro-turbine_engine.pdf [2018, October 15].

Tu, J., Yeoh, G.H. & Liu, C. 2013. *Computational Fluid Dynamics : A Practical Approach*. Elsevier/Butterworth-Heinemann.

Turner, M.G., Reed, J. a, Ryder, R. & Veres, J.P. 2004. Multi-Fidelity Simulation of a Turbofan Engine With Results Zoomed Into Mini-Maps for a Zero-D Cycle Simulation. *Turbo Expo 2004*. 2(November):219–230. DOI: 10.1115/GT2004-53956.

"UAV Reliability Study". 2003. *Office of the U.S. Secretary of Defence, Washington, D.C.*

"Uninhabited Air Vehicles: Enabling Science for Advanced Military Systems". 2000. *National Research Council, Washington, D.C.*

"USERGUIDE FINE™/Open with OpenLabs™ 6.2". 2018. (EN201705041305).

Vick, M., Young, T., Kelly, M., Tuttle, S. & Hinnant, K. 2016. A Simple Recuperated Ceramic Microturbine: Design Concept, Cycle Analysis and Recuperator Component Prototype Tests. 1–14.

Villalpando, F., Reggio, M. & Ilinca, A. 2011. Assessment of Turbulence Models for Flow Simulation around a Wind Turbine Airfoil. *Modelling and Simulation in Engineering*. 2011:1–8. DOI: 10.1155/2011/714146.

Visavale, G. n.d. *Grid Generation for CFD Analysis of Turbomachinery*. Available: https://www.learncax.com/knowledge-base/blog/by-category/cfd/grid-generation-for-cfd-analysis-of-turbomachinery [2018, August 13].

Walsh, P.P. & Fletcher, P. 2004. *Gas Turbine Performance*. Oxford, UK: Blackwell Science Ltd. DOI: 10.1002/9780470774533.

Xu, G., Hanauer, C., Wright, Y.M. & Boulouchos, K. 2016. CFD-Simulation of Ignition and Combustion in Lean Burn Gas Engines. DOI: 10.4271/2016-01-0800.

APPENDIX A FLUID PROPERTY GRAPHS

Figure 0-1 below shows the specific heat of air plotted against temperature.

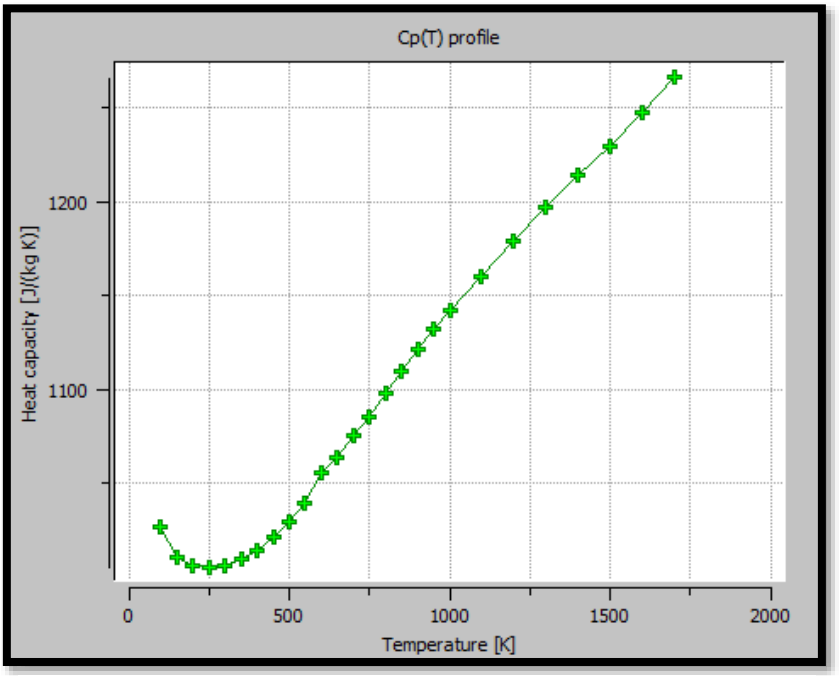

Figure 0-1: Specific heat plotted against temperature for air.

Figure 0-2 below shown the heat conductivity of air plotted against temperature.

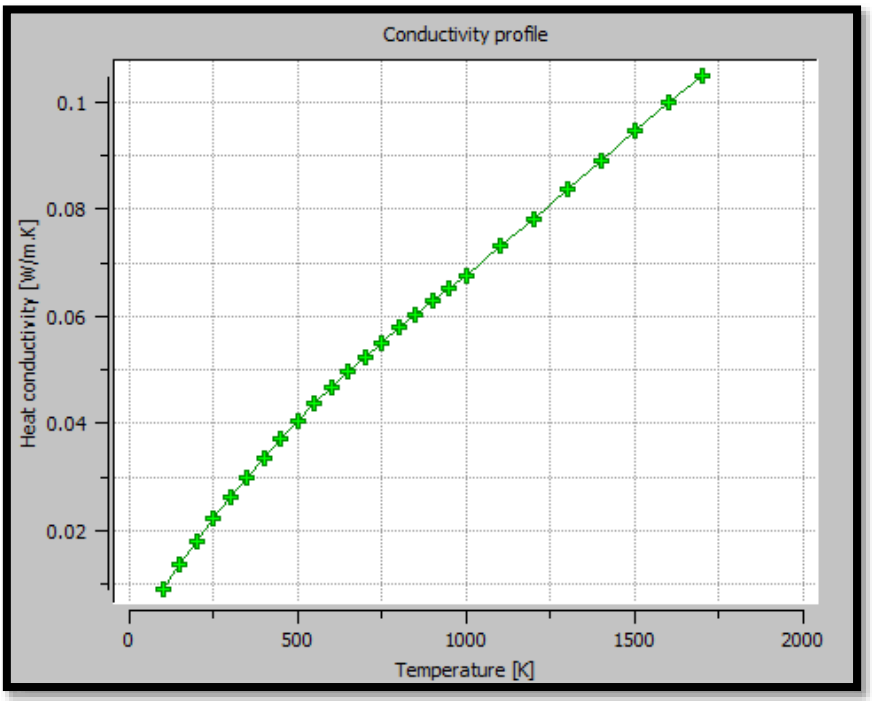

Figure 0-2: Thermal conductivity plotted against temperature for air.

Figure 0-3 below shown the dynamic viscosity of air plotted against temperature.

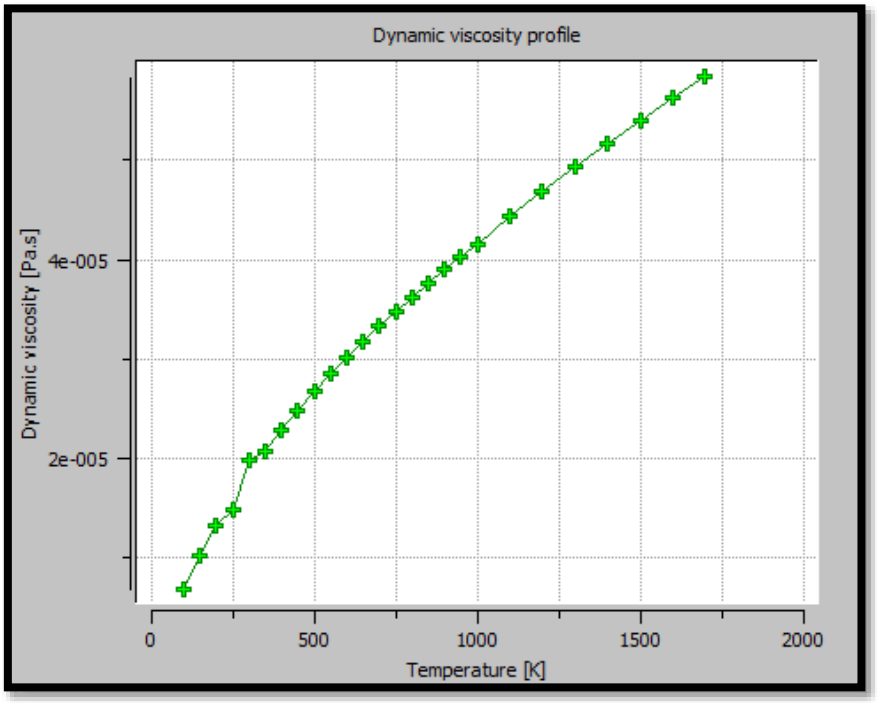

Figure 0-3: Dynamic viscosity plotted against temperature for air.